

Properties of the lowest-lying baryons in chiral perturbation theory

Jorge Martín Camalich

Departamento De Física Teórica



Universidad de Valencia

TESIS DOCTORAL

VALENCIA 2010

D. Manuel José Vicente Vacas, Profesor Titular de Física Teórica de la Universidad de Valencia,

CERTIFICA: Que la presente Memoria *Properties of the lowest-lying baryons in chiral perturbation theory* ha sido realizada bajo mi dirección en el Departamento de Física Teórica de la Universidad de Valencia por D. Jorge Martín Camalich como Tesis para obtener el grado de Doctor en Física.

Y para que así conste presenta la referida Memoria, firmando el presente certificado.

Fdo: Manuel José Vicente Vacas

A mis padres y mi hermano

Contents

Preface	ix
1 Introduction	1
1.1 Chiral symmetry of QCD	1
1.2 Foundations of χ PT	4
1.2.1 Leading chiral Lagrangian for pseudoscalar mesons	4
1.2.2 Loops, power counting and low-energy constants	6
1.2.3 Matrix elements and couplings to gauge fields	7
1.3 Baryon χ PT	9
1.3.1 Leading chiral Lagrangian with octet baryons	9
1.3.2 Loops and power counting in $B\chi$ PT	11
1.4 The decuplet resonances in $B\chi$ PT	14
1.4.1 Spin-3/2 fields and the consistency problem	15
1.4.2 Chiral Lagrangian containing decuplet fields	18
1.4.3 Power-counting with decuplet fields	18
2 Electromagnetic structure of the lowest-lying baryons	21
2.1 Magnetic moments of the baryon octet	21
2.1.1 Formalism	22
2.1.2 Results	24
2.1.3 Summary	33
2.2 Electromagnetic structure of the decuplet	35
2.2.1 Formalism	36
2.2.2 Results	39
2.2.3 Summary	46
3 Hyperon semileptonic decays	49
3.1 Formalism	50

3.1.1	Hyperon semileptonic decays	50
3.1.2	χ PT calculation of $f_1(0)$	52
3.2	Results	56
3.2.1	Octet-baryon contributions	56
3.2.2	Decuplet-baryon contributions	57
3.2.3	Full results and comparison with other approaches	58
3.2.4	Determination of V_{us}	60
3.3	Summary	61
4	Masses of the baryons	63
4.1	Formalism	64
4.2	Results	66
4.2.1	Experimental data	66
4.2.2	Analysis of lattice results	68
4.2.3	Phenomenological applications	72
4.3	Summary	77
5	Summary and Outlook	79
A	SU(3) algebra and Dirac matrices	85
B	Numerical value of the coupling constants	87
C	Tables and loop functions	89
C.1	Baryon-octet magnetic moments	91
C.2	Electromagnetic structure of the decuplet	93
C.3	Vector coupling $f_1(0)$	97
C.3.1	Tadpole diagrams	97
C.3.2	Wave-function renormalization diagrams	97
C.3.3	Sunset diagrams	99
C.4	Baryon masses	109
C.4.1	Loop functions and table of coefficients	109
C.4.2	Finite volume corrections	113
D	Lattice QCD results on the baryon masses	115
	Bibliography	117
	Resumen castellano	135
	Acknowledgments	141

Preface

The ground-state baryons are physical objects of great interest. Their properties and interactions are essential to understand those of the atomic nuclei or of more exotic kinds of systems like the strange matter, which is believed to play a role in the macroscopic properties of astrophysical objects, e.g. neutron stars. Besides that, baryon phenomenology allows to study the non-perturbative regime of Quantum Chromodynamics (QCD). Given its uniqueness and its success to explain high-energy phenomena, QCD is acknowledged to be the quantum field theory that underlies the strong properties and interactions of mesons and baryons. However, at the low-energy regime where these hadrons are the relevant degrees of freedom, QCD is non-perturbative and it is impossible to solve in a straightforward manner. It is a great scientific endeavor to understand the extremely rich structure of hadrons and, in particular, of baryons directly from the few parameters of QCD, namely the strong coupling constant and quark masses. Additionally, their weak decays and reactions provide information on the flavor structure of the electroweak interactions that eventually may point out departures from the Standard Model predictions.

Experimental information on the properties, decays and reactions involving baryons has accumulated since the advent of the first accelerators. These issues still are among the main topics of research in many facilities. Experiments are currently taking place or are scheduled in Laboratories like CERN-SPS (Europe) with hadron beams (COMPASS), TJNAF (USA) in photoproduction reactions (CLAS) and parity-violating electron scattering (Q-weak), GSI (Germany) in $p p$ collisions (HADES), LNF (Italy) in kaonic atoms (SIDHARTA), MAMI (Germany) in parity-violating electron scattering (A2), etc. Further experiments are planned in centers like CERN-SPS (NA-62), J-PARC or GSI (pion beam). Moreover, the last few years have witnessed an impressive development in the lattice QCD description of several observables and realistic results on baryon structure are starting to appear.

This thesis describes the research project which I have been committed to during the last years and presents results that have been published in a series of papers [1, 2, 3, 4, 5]. The main goal of this project has been to ad-

vance in the development of a model-independent and systematic approach to the properties and low-energy interactions of the lowest-lying octet and decuplet baryons in a unified manner within a $SU(3)$ -flavor formulation of chiral perturbation theory. Although important progress has been made using non-perturbative methods based in the unitarization of the scattering amplitudes (see e.g. Refs. [6, 7, 8, 9, 10, 11, 12, 13] and references therein), the perturbative approach has been stacked for almost two decades because the convergence of the chiral series appears to be spoiled by the relatively heavy strange quark and the non-perturbative effects of the low-lying resonances. With the experimental data collected for years and the progress being reported by the lattice QCD community, we think it is timely to try to establish a reliable and perturbative effective field theory approach to the baryonic sector of QCD.

Our findings show that the scheme proposed in this thesis, based in a Lorentz covariant Lagrangian and in the explicit inclusion of decuplet degrees of freedom, is quite promising and shows a clear advance in the right direction. Indeed, some of the longstanding problems afflicting baryon chiral perturbation theory, such as the poor convergence is overcome for quantities like the baryon magnetic moments [1, 2] or the quark-mass dependence of their masses [5]. Moreover, we have contributed to the understanding of the nature of the chiral expansion for baryons discussing the differences among the various approaches. It is fair to acknowledge at this point the *FeynCalc* [14] and *FORM* [15] programming systems that have been essential for the efficient performance of the heavy symbolic calculations described in this thesis. Other applications that have been worked out during these years on finite nuclear density [16], $SU(2)_F$ -B χ PT [17, 18, 19] or heavy-light systems [20] have not been included for the sake of consistency.

We hope that the approach to baryon chiral perturbation theory presented in this thesis, illustrated with examples spanning from the electromagnetic structure of baryons to the extraction of parameters of the Standard Model or the analysis of lattice results, will be helpful to process in an unified manner the data on baryon structure and interactions that will be coming soon from both experimental facilities and lattice calculations.

Introduction

In this chapter our aim is to present a brief but comprehensive introduction to the theoretical framework and methods used in this thesis. More detailed information on these issues can be found in many reviews [21, 22, 23, 24, 25, 26] and text books [27, 28, 29, 30, 31]. In Sec. 1.1 we address the idea of chiral symmetry and its breaking in QCD as the starting point to build up an effective field theory of QCD at low energies with hadrons as basic degrees of freedom. This program is called *chiral perturbation theory* (χ PT) and it is outlined in Sec. 1.2 for the case of the pseudoscalar octet of mesons. The central aspects of χ PT as the construction of the chiral Lagrangian, the power-counting scheme or the inclusion of external sources are discussed there. In Sec. 1.3, we present the extension of the χ PT methods to describe the properties of the baryons and their low-energy interaction with pseudoscalar mesons, i.e. baryon chiral perturbation theory (B χ PT). The power-counting problem and the different solutions circumventing it that have been proposed so far are discussed with some detail there. Finally, in Sec. 1.4 we introduce the formalism covering the inclusion of the spin-3/2 decuplet resonances in B χ PT.

1.1 Chiral symmetry of QCD

The portion of the Standard Model (SM) that describes the strong interaction is Quantum Chromodynamics (QCD) [32, 33, 34, 31] which Lagrangian density reads

$$\mathcal{L}_{QCD} = -\frac{1}{4}G_A^{\mu\nu}G_{\mu\nu}^A + \bar{q}(i\not{D} - \mathcal{M})q, \quad (1.1)$$

where q is the N_f -multiplet containing N_f flavors of spin-1/2 quark fields and $\mathcal{M}=\text{diag}(m_u, m_d, m_s, \dots)$ the corresponding mass matrix. The operator D_μ is the $SU(3)$ -color covariant derivative introducing the coupling g of the

quarks to the gluons and $G_A^{\mu\nu}$ is the gluon strength field tensor with the color index A [31]. Among the six quark flavors present in the SM, the u , d and s have masses $\ll 1$ GeV and are called *light quarks* in opposition to the *heavy quarks* c , b and t with masses above 1 GeV. The analysis of the *running* of the strong coupling constant given by the renormalization group equation leads to the fact that QCD is a theory with a weak coupling at high energies (*asymptotic freedom*) [32] and with a strong one at low-energies [35]. In this non-perturbative regime QCD appears to be confining. This is supported by the experimental evidence that the asymptotically free strong interacting particles at these energies are not quarks and gluons but clusters of them organized in color singlets called *hadrons*.

In order to treat the strong dynamics at the non-perturbative regime it is useful to analyze the global symmetries of QCD. In fact, rewriting the quark part of the Lagrangian of Eq. (1.1) in terms of their right-hand, $q_R = (1 + \gamma_5)q/2$, and left-hand, $q_L = (1 - \gamma_5)q/2$, components

$$\mathcal{L}_{QCD}^q = i\bar{q}_L \not{D} q_L + i\bar{q}_R \not{D} q_R - \bar{q}_L \mathcal{M} q_R - \bar{q}_R \mathcal{M} q_L, \quad (1.2)$$

one sees that besides the $SU(3)$ -color gauge and C , P , T symmetries, the QCD Lagrangian fulfills vector and axial $U(1)$ symmetries related to the invariance with respect to global phase transformations of the left- and right-hand components of the quark fields. The vector symmetry leads to a classification of the hadron spectrum according to the corresponding conserved quantum number B (*baryon number*) into *mesons* ($B = 0$) and *baryons* ($B \geq 1$), whereas the latter is broken at the quantum level by the axial anomaly. Equivalent considerations applied to independent phase transformations on the different quark flavors lead to the conserved *flavor numbers*.

Moreover, the Lagrangian of Eq. (1.2) has a $SU(N_f)_L \otimes SU(N_f)_R$ chiral symmetry in the limit of vanishing quark masses ($m_q \rightarrow 0$) that is then called the *chiral limit*. In the physical world, one shall expect chiral symmetry to be approximately realized for the light quarks and, for this case, it makes sense to explore its breaking perturbatively [36]. We then have 16 (approximately) conserved currents

$$R_a^\mu = \bar{q}_R \gamma^\mu \frac{\lambda_a}{2} q_R, \quad L_a^\mu = \bar{q}_L \gamma^\mu \frac{\lambda_a}{2} q_L, \quad (1.3)$$

where λ^a are the Gell-Mann matrices, which can be found in the Appendix A, and $a = 1, \dots, 8$ is a chiral $SU(3)$ -flavor index. The associated conserved charges $Q_{L,R}$ satisfy a chiral algebra

$$\begin{aligned} [Q_X^a, Q_Y^b] &= i\delta_{XY} f_{abc} Q_X^c, \\ (X = L, R; \quad f_{abc} &= \text{chiral-}SU(3) \text{ structure constants}) \end{aligned} \quad (1.4)$$

that is the keystone of the *current-algebra* approach to the strong interaction developed in the sixties [37, 38]. Taking sums and differences we can rewrite Eqs. (1.3) in terms of the axial and vector currents

$$V_a^\mu = \bar{q}\gamma^\mu\frac{\lambda_a}{2}q, \quad A_a^\mu = \bar{q}\gamma^\mu\gamma_5\frac{\lambda_a}{2}q, \quad (1.5)$$

which have the following divergences with the explicit symmetry breaking structure given by the quark masses

$$\partial_\mu V_a^\mu = \frac{1}{2}i\bar{q}[\mathcal{M}, \lambda_a]q, \quad \partial_\mu A_a^\mu = \frac{1}{2}\bar{q}\{\mathcal{M}, \lambda_a\}\gamma_5q. \quad (1.6)$$

Both currents are conserved in the chiral limit. The vector current is also trivially conserved if the quarks have the same mass. However, the axial current is not conserved and its divergence is proportional to a pseudoscalar piece. This last relation, fulfilled by the QCD axial currents, can be interpreted as the microscopic basis for the success of the partially conserved axial current (PCAC) methods [39, 40, 38] that were developed in partnership with the current algebra. The approximate conservation of the currents Eq. (1.5) should be manifest in the structure of the hadron spectrum [41] and couplings. In fact, one realizes that low-lying baryons and mesons sharing the same quantum numbers and approximately the same mass can be grouped into irreducible representations of $SU(3)$ [42].

On the other hand, the parity partners of these multiplets do not appear in the spectrum with approximately the same mass. This fact suggests that in the non-perturbative regime the axial part of the chiral symmetry is hidden, i.e. the QCD vacuum is not invariant under the chiral transformations. Chiral symmetry is then said to be *spontaneously broken* [39] and there exists a continuum of degenerate vacua connected by an octet of (approximately) massless pseudoscalar quanta called *Goldstone bosons* [43]. An inspection of the hadron spectrum reveals that such an octet shall correspond to the one containing the pions (π), kaons (K) and eta (η) mesons. It then makes sense to tackle the non-perturbative QCD dynamics at low-energies by treating the pseudoscalar mesons as the relevant degrees of freedom within a Lagrangian formulation. Such program in terms of a non-linear realization of chiral symmetry can be called generically as a *chiral dynamics* [44] approach and lies in the foundations of the *effective field theory* (EFT) of QCD at very low-energies, namely the χ PT [36, 45, 46, 47].

1.2 Foundations of χ PT

In this section, we pretend to give a brief introduction to χ PT and its foundations and we address the interested reader to any of the nice reviews [21, 22, 23, 25] for a more complete treatment of the topic.

1.2.1 Leading chiral Lagrangian for pseudoscalar mesons

A convenient way to describe the pseudoscalar mesons is in terms of a non-linear function of the local fields $\pi(x)$, $K(x)$ and $\eta(x)$ [44, 48, 49, 50] given by the unitary 3×3 matrix $U(x)$

$$U(x) = \exp\left(i\frac{\phi(x)}{v}\right), \quad (1.7)$$

where v is a parameter to be fixed and with

$$\phi = \lambda^a \phi^a = \begin{pmatrix} \pi^0 + \frac{1}{\sqrt{3}}\eta_8 & \sqrt{2}\pi^+ & \sqrt{2}K^+ \\ \sqrt{2}\pi^- & \pi^0 + \frac{1}{\sqrt{3}}\eta_8 & \sqrt{2}K^0 \\ \sqrt{2}K^- & \sqrt{2}K^0 & -\frac{2}{\sqrt{3}}\eta_8 \end{pmatrix}. \quad (1.8)$$

Under chiral transformations $(L, R) \in SU(3)_L \otimes SU(3)_R$, U transforms like [48]

$$U \rightarrow LUR^\dagger. \quad (1.9)$$

The chiral invariant Lagrangian containing the minimum number of derivatives on the pseudoscalar fields is then

$$\mathcal{L}_{\chi S}^{(2)} = \frac{v^2}{4} \langle \partial_\mu U \partial^\mu U \rangle, \quad (1.10)$$

where $\langle \dots \rangle$ denotes trace in flavor space. The meaning of the super-index (2), for the moment, corresponds to the number of derivatives in the Lagrangian term. One completes the latter Lagrangian with the simplest piece obtained including the explicit chiral symmetry breaking that is given by the non-vanishing light quark masses. We take the case with isospin symmetry ($m \equiv m_u = m_d$) that we denote as $N_f = 2 + 1$ with the corresponding mass matrix in Eq. (1.1) as \mathcal{M}_{2+1} ,

$$\mathcal{L}_{\chi SB}^{(2)} = \frac{v^2 B_0}{2} \langle \mathcal{M}_{2+1} U^\dagger + U \mathcal{M}_{2+1}^\dagger \rangle, \quad (1.11)$$

where the constant B_0 can be related with the quark condensate $\langle \bar{q}q \rangle = \langle \bar{u}u + \bar{d}d + \bar{s}s \rangle$, through $B_0 = -\langle \bar{q}q \rangle / 3v^2$, and the super-index (2) now means twice the number of quark mass insertions in the Lagrangian piece.

The Lagrangian of Eqs.(1.10) and (1.11) provides a model for pseudoscalar meson self-interactions that incorporates the features of chiral symmetry of the low-energy QCD and which depends on the parameters v and B_0 . It can be expanded in a Taylor series of the pseudoscalar-meson fields such that

$$\begin{aligned} \mathcal{L}^{(2)} \equiv \mathcal{L}_{\chi S}^{(2)} + \mathcal{L}_{\chi SB}^{(2)} &= \frac{1}{2} \left(\partial_\mu \pi^0 \partial^\mu \pi^0 + m_\pi^2 \pi^{0^2} \right) + \frac{1}{2} (2\partial_\mu \pi^+ \partial^\mu \pi^- + 2m_\pi^2 \pi^- \pi^+) \\ &+ \frac{1}{2} (2\partial_\mu K^+ \partial^\mu K^- + 2m_K^2 K^+ K^-) + \frac{1}{2} (2\partial_\mu K^0 \partial^\mu \bar{K}^0 + 2m_K^2 \bar{K}^0 K^0) \\ &+ \frac{1}{2} (\partial_\mu \eta \partial^\mu \eta + m_\eta^2 \eta^2) + \mathcal{L}_I^{(2)}, \end{aligned} \quad (1.12)$$

where we have identified the pseudoscalar quadratic masses as linear functions of the quark masses

$$\begin{aligned} m_\pi^2 &= 2B_0 m, \\ m_K^2 &= B_0(m + m_s), \\ m_\eta^2 &= \frac{2}{3} B_0(m + 2m_s). \end{aligned} \quad (1.13)$$

These results, together with the equation for B_0 introduced above, are known as the Gell-Mann-Renner-Oakes relations [51] and they imply the Gell-Mann-Okubo mass formula for mesons [52, 53]

$$4m_K^2 = m_\pi^2 + 3m_\eta^2. \quad (1.14)$$

The part \mathcal{L}_I contains terms with derivative couplings among an even number of pseudoscalar mesons, all related by just a single parameter v . This is connected to the pseudoscalar meson decay constant F_ϕ taking the proper matrix element of the axial current determined from the Lagrangian (1.10)

$$A_a^\mu = -v \partial^\mu \phi_a + \mathcal{O}(\phi^2) \quad ; \quad \langle 0 | A_a^\mu | \phi_b(p) \rangle = -i v p^\mu \delta_{ab} \implies v \equiv F_\phi. \quad (1.15)$$

At tree-level, one obtains from the Lagrangian \mathcal{L}_I an interaction term among 4 mesons

$$\mathcal{L}_I \simeq \frac{1}{24F_\phi^2} (\langle [\phi, \partial_\mu \phi] \phi \partial_\mu \phi + B_0 \langle \mathcal{M}_{2+1} \phi^4 \rangle) + \mathcal{O}(\phi^6), \quad (1.16)$$

that (for on-shell pions) leads to the celebrated $\pi\pi$ scattering lengths obtained in the sixties by Weinberg using current algebra methods [54]. Those corresponding to πK , KK , $\pi\eta$, etc, and predictions for the scattering amplitudes of an even number of pseudoscalar mesons also follow trivially from \mathcal{L}_I .

1.2.2 Loops, power counting and low-energy constants

Besides that the Lagrangian approach expresses in a dynamical and compact form the physical content of the chiral algebra and PCAC, it allows to straightforwardly extend their results by including the effects of loops as computed in quantum field theory. This is, in fact, a necessary step in order to elaborate a realistic theory of strong interactions, since the loops provide the imaginary parts of the amplitudes which are related with the physical thresholds and required by unitarity. However, their inclusion is troubled by the non-renormalizable nature of the theory given by $\mathcal{L}^{(2)}$. Indeed, the n -loop-integrals are related with ultraviolet divergences which are to be regularized with the inclusion in the Lagrangian of counterterms $\delta\mathcal{L}^{(2n)}$ with n quark mass insertions or which are chiral invariant and contain $2n$ derivatives. The infinite number of contributions to a particular Green function that arise when accounting for the loop effects can be organized by a *power-counting* scheme valid for very low-momenta q and light quark masses m_q . A Feynman diagram consisting of V_{2n} vertices from Lagrangian pieces with $2n$ derivatives or n quark mass insertions and with L loops is of order $\mathcal{O}(p^D)$ where p will generically denote from now on the two low scales (q and m_q) and D is the order in the counting scheme [45],

$$D = 2 + 2L + \sum_n (2n - 2)V_{2n}. \quad (1.17)$$

Therefore, $\mathcal{L}^{(2)}$ provides the leading-order (LO) contribution at $D = 2$ and the loop effects start to contribute at $D = 4$ or next-to-leading order (NLO). At $D = 4$, one has further Lagrangian terms or pieces $\mathcal{L}^{(4)}$, containing a finite number of operators accompanied by parameters or *low-energy constants* (LECs) which allow for a complete renormalization of these loops. From $\mathcal{L}^{(4)}$ (and from $\mathcal{L}^{(2)}$ at the two-loop level), one obtains loop contributions with $D = 6$ or next-to-leading-order (NNLO), which renormalize the LECs of the Lagrangian $\mathcal{L}^{(6)}$. This structure in the counting of tree-level and loop contributions continues to higher orders. The final Lagrangian is

$$\mathcal{L} = \mathcal{L}^{(2)} + \mathcal{L}^{(4)} + \mathcal{L}^{(6)} + \dots, \quad (1.18)$$

and the resulting theory can account for the loop-contributions provided that the renormalization of the LECs can be performed systematically order-by-order in the counting. When we refer to low energy, momenta or quark masses one should more precisely tell the scale to which we are comparing. An answer arises from the loop graphs, since a suppression factor $(p^2/(\Lambda_{\chi SB})^2)$ appears, with $\Lambda_{\chi SB} \sim 4\pi F_\phi \sim 1$ GeV the so-called chiral symmetry breaking scale. This agrees with the characteristic scale for the emergence of the first vector

resonances (the $\rho(770)$ meson) and it represents the range over which our low-energy perturbative expansion remains valid.

The organization provided by the power-counting scheme only applies in the regime where a description of strong interactions in terms of hadrons makes sense. A natural question to be answered at this point concerns the relation between this theory and the underlying QCD. It is obvious that some connection should exist, given that the global symmetry structure of both theories is the same. In fact, it has been first conjectured [45] and then later demonstrated [55] that if any of the portions of Eq. (1.18), $\mathcal{L}^{(2n)}$, is exhaustive in the sense that contains *all* the terms allowed by the symmetries, then \mathcal{L} yields the most general S -matrix consistent with these symmetries and with the fundamental principles of quantum field theory (unitarity, analyticity and the cluster decomposition principle). Therefore, the theory developed from \mathcal{L} should give the same S -matrix elements as QCD order-by-order in a perturbative expansion on q and m_q .

The quantum field theory developed from Eq. (1.18) is called χ PT and represents the low-energy EFT of QCD. At a given order, all strong-interacting phenomena involving just pseudoscalar mesons can be related to a finite number of LECs containing the information on the non-perturbative QCD dynamics that has been integrated out. A noteworthy remark is that the LECs appear in the chiral Lagrangian as bare constants *to be renormalized at the chiral-limit* that is the point we are perturbing about. To calculate their values directly from QCD is not straightforward, and they are, in practice, fixed using experimental data or the quark mass dependence of LQCD simulations. The leading order Lagrangian $\mathcal{L}^{(2)}$ depends only on F_ϕ , whereas $\mathcal{L}^{(4)}$ and $\mathcal{L}^{(6)}$ contain 12 [47] and 90 LECs respectively [56]. We notice that the number of independent Lagrangian operators one may construct rapidly increases with the chiral order so that, at some point, χ PT becomes impractical.

Finally, it is worth to remark that the tree-level contributions appear as polynomial expansions on the external momenta q and quark masses m_q and their contributions to Green functions are hence called *analytical*. On the other hand, *non-analytical* structures like $\log(q^2/m_\phi^2)$ are the clear signature of the corrections given by the chiral loops.

1.2.3 Matrix elements and couplings to gauge fields

One can generalize the Lagrangian (1.1) to include external sources with different parity and Lorentz transformation properties and arbitrary flavor struc-

ture [46, 47]

$$\tilde{\mathcal{L}}_{QCD} = \mathcal{L}_{QCD} - \bar{q}_L \gamma^\mu l_\mu q_L - \bar{q}_R \gamma^\mu r_\mu q_R - \bar{q}_R (s + ih) q_L - \bar{q}_L (s - ih) q_R, \quad (1.19)$$

where in the $SU(3)$ -flavor theory, $l_\mu = l_\mu^0 + \lambda^a l_\mu^a$, $r_\mu = r_\mu^0 + \lambda^a r_\mu^a$, $s = s^0 + \lambda^a s^a$ and $h = h^0 + \lambda^a h^a$. One then recovers the original QCD Lagrangian with $l_\mu = r_\mu = h = 0$ and $s = \mathcal{M}_{2+1}$. The Lagrangian (1.19) is invariant under *local* $SU(3)$ chiral transformations if we demand the sources to transform like gauge fields

$$\begin{aligned} q_L &\rightarrow L(x)q_L, & q_R &\rightarrow R(x)q_R, \\ l_\mu &\rightarrow L(x)l_\mu L^\dagger(x) + i\partial_\mu L(x)L^\dagger(x), \\ r_\mu &\rightarrow R(x)r_\mu R^\dagger(x) + i\partial_\mu R(x)R^\dagger(x), \\ (s + ih) &\rightarrow L(x)(s + ih)L^\dagger(x), \\ (s - ih) &\rightarrow R(x)(s - ih)R^\dagger(x). \end{aligned} \quad (1.20)$$

The effective chiral Lagrangian can also be made invariant under the local transformations if one introduces covariant derivatives on the meson fields and replace the quark mass insertions

$$\partial_\mu U \rightarrow \partial_\mu U + il_\mu U - iU r_\mu, \quad \mathcal{M}_{2+1} \rightarrow \chi \equiv 2B_0 (s + ih). \quad (1.21)$$

In this form, it is easy to obtain the matrix elements of an arbitrary current by derivation of the generating functionals with respect to the source fields and we can then relate the ones appearing at the effective level with those corresponding to the QCD Lagrangian. Demanding the symmetries to be local, as in Eqs. (1.20), also allows us to introduce the coupling to external gauge fields in a natural way. For example, the electromagnetic interaction is included choosing $l_\mu = r_\mu = eQ A_\mu$ where $Q = (\lambda_3 + \lambda_8/\sqrt{3})/2$ is the quark electric charge operator in units of e and A_μ is the photon field¹. Besides the minimal coupling introduced in the covariant derivatives, one shall construct the most general locally invariant couplings to the effective hadronic fields. This can be done defining the strength tensor fields

$$L_{\mu\nu} = \partial_\mu l_\nu - \partial_\nu l_\mu + i[l_\mu, l_\nu], \quad R_{\mu\nu} = \partial_\mu r_\nu - \partial_\nu r_\mu + i[r_\mu, r_\nu], \quad (1.22)$$

which, under local chiral transformations, respond like

$$L_{\mu\nu} \rightarrow L(x)L_{\mu\nu}L^\dagger(x), \quad R_{\mu\nu} \rightarrow R(x)R_{\mu\nu}R^\dagger(x). \quad (1.23)$$

¹We use the convention $e > 0$ so that the electron has an electric charge of $-e$. The Gell-Mann matrices are displayed in Appendix A

The power counting must be extended to account for Lagrangian terms containing the external source and tensor fields. We will assume that the minimal coupling is of the same order as the derivative on the meson field $U(x)$ such that $D_\mu U(x) \sim \mathcal{O}(p)$. The couplings to the external strength tensor fields contain derivatives on the sources and, in the low-energy limit, it makes sense to consider $L_{\mu\nu} \sim R_{\mu\nu} \sim \mathcal{O}(p^2)$.

1.3 Baryon χ PT

1.3.1 Leading chiral Lagrangian with octet baryons

The methods of χ PT can be extended to describe the low-energy interaction of pseudoscalar mesons with heavy matter fields [44, 48, 49, 50, 57]. We first study the inclusion of the lowest-lying $J^P = 1/2^+$ baryon octet using a traceless 3×3 complex matrix

$$B = \sum_{a=1}^8 \frac{\lambda^a B^a}{\sqrt{2}} = \begin{pmatrix} \frac{1}{\sqrt{2}}\Sigma^0 + \frac{1}{\sqrt{6}}\Lambda & & \Sigma^+ & p \\ & \Sigma^- & -\frac{1}{\sqrt{2}}\Sigma^0 + \frac{1}{\sqrt{6}}\Lambda & n \\ & \Xi^- & \Xi^0 & -\frac{2}{\sqrt{6}}\Lambda \end{pmatrix}, \quad (1.24)$$

whereas the pseudoscalar meson fields are now realized with $u = \sqrt{U}$. Under local chiral transformations (we omit from now on the explicit dependence on x)

$$u \rightarrow LuK^\dagger = KuR^\dagger, \quad B \rightarrow KBK^{-1}, \quad (1.25)$$

where

$$K \equiv K(L, R, U) = \left(\sqrt{UL^\dagger} \right)^{-1} \left(\sqrt{RU} \right), \quad (1.26)$$

is the so-called *compensator field*. For a vector transformation $L = R = V$ one can easily see from Eqs. (1.26) and (1.9) that $K = V$, responding the baryons B linearly as an octet under the $SU(3)_V$ subgroup of the chiral group. For the case $R \neq L$ the function K depends non-linearly on U so that the corresponding axial part of the transformation relates baryon states with different number of pseudoscalar mesons.

One introduces a Lorentz vector called *vielbein*

$$u^\mu = \frac{i}{2} \left(u^\dagger (\partial^\mu - ir^\mu) u - u (\partial^\mu - il^\mu) u^\dagger \right), \quad u^\mu \rightarrow Ku^\mu K^\dagger. \quad (1.27)$$

We redefine the scalar and pseudoscalar sources in Eq.(1.21)

$$\chi_\pm = u^\dagger \chi u^\dagger \pm u \chi^\dagger u, \quad \chi_\pm \rightarrow K \chi_\pm K^\dagger. \quad (1.28)$$

and the strength field tensors in Eq. (1.22)

$$F_{\pm}^{\mu\nu} = uL^{\mu\nu}u^\dagger \pm u^\dagger R^{\mu\nu}u, \quad F_{\pm}^{\mu\nu} \rightarrow KF_{\pm}^{\mu\nu}K^\dagger. \quad (1.29)$$

A covariant derivative that transforms in a simple way with K can be defined with a *connection* Γ^μ

$$\begin{aligned} \Gamma_\mu &= \frac{1}{2} \left(u^\dagger (\partial_\mu - ir_\mu) u + u (\partial_\mu - il_\mu) u^\dagger \right), \\ D_\mu X &= \partial_\mu X + [\Gamma_\mu, X] - iv_\mu^0 X, \quad D_\mu X \rightarrow KD_\mu X, \end{aligned} \quad (1.30)$$

where v_μ^0 is the singlet part of an external vector current, $v_\mu^0 = (l_\mu^0 + r_\mu^0)/2$ (Sec. 1.2.3). With the help of the compensator field, we are then able to elaborate the B χ PT that keeps the $SU(3)_V$ - flavor symmetry ($SU(3)_F$ from now on) for the baryon fields at the same time as the chiral invariance on the couplings with the pseudoscalar mesons. Given the simple transformation rules of the fields introduced above, they can be used as building blocks for the construction of the baryon chiral Lagrangian. In order to assign a power counting to the Lagrangian operators constructed thereof one takes

$$D_\mu B, \bar{B}, B \sim \mathcal{O}(1), \quad u_\mu \sim \mathcal{O}(p), \quad \chi_\pm, F_{\pm}^{\mu,\nu} \sim \mathcal{O}(p^2). \quad (1.31)$$

Covariant derivatives over u_μ , χ_\pm or $F_{\pm}^{\mu,\nu}$ increase by 1 the order in the counting. With these ingredients one obtains the leading chiral Lagrangian containing octet baryons

$$\mathcal{L}_{\phi B}^{(1)} = \langle \bar{B} (i\mathcal{D} - M_{B0}) B \rangle + D/F \langle \bar{B} \gamma^\mu \gamma_5 [u_\mu, B]_{\pm} \rangle, \quad (1.32)$$

where we have assumed that $(i\mathcal{D} - M_{B0}) B \sim \mathcal{O}(p)$, being M_{B0} a mass in the chiral limit that is the same for all the octet baryons. The term $\bar{B}B$ is the only $SU(3)_F$ singlet that can be made with the B fields alone and the baryon-octet mass splittings in B χ PT necessarily arise due to $SU(3)_F$ -breaking of the pseudoscalar meson masses. This flavor-breaking structure is general for any matrix element calculated in $SU(3)_F$ -B χ PT. Finally, in a spin-1/2 field theory derivatives can be contracted with Lorentz indices of spinorial objects so that the chiral order in the baryon theory counts one-by-one. Expanding the Lagrangian (1.32) in the meson fields we get

$$\begin{aligned} \mathcal{L}_{\phi B}^{(1)} &\simeq \langle \bar{B} (i\mathcal{D} - M_{B0}) B \rangle \\ &+ \frac{i}{8F_\phi^2} \langle \bar{B} [[\phi, \not{\partial}\phi], B] \rangle + \langle \bar{B} [\not{\phi}, B] \rangle + \frac{i}{2F_\phi} \langle \bar{B} [[\phi, \not{\phi}], B] \rangle \\ &- D/F \langle \bar{B} \gamma^\mu \gamma_5 \left[\left(\frac{\partial_\mu \phi}{2F_\phi} - a_\mu \right), B \right]_{\pm} \rangle - \frac{iD/F}{2F_\phi} \langle \bar{B} \gamma^\mu \gamma_5 [[\phi, v_\mu], B]_{\pm} \rangle + \dots, \end{aligned} \quad (1.33)$$

where we have rewritten the external left- and right-handed sources with their vector and axial components, $v_\mu = (r_\mu + l_\mu)/2$ and $a_\mu = (r_\mu - l_\mu)/2$. The first line is the free-Lagrangian for the baryon fields. In the second line of Eq. (1.33) we find the interactions generated by the covariant derivative; the first term yields the so-called $\pi\pi NN$ Weinberg-Tomozawa contact interaction [54, 58] and the second attaches an external vector source (e.g. the photon) to the baryons. The third line of Eq. (1.33) comes from the Lagrangian proportional to D or F , and its first term is written in a way that the coupling to a external axial (weak) field is automatically related with the strong ϕBB interaction couplings. Indeed, defining $g_A = D + F$, $M_{B0} \rightarrow M_N$ and $F_\phi \rightarrow F_\pi$, this term encloses a generalized version of the Goldberger-Treiman relation discovered for the πNN interaction [59, 60]

$$g_{\pi N} = \frac{g_A M_N}{F_\pi}, \quad (1.34)$$

where g_A can be obtained from the neutron beta decay, and $g_{\pi N}$ from pion nucleon scattering or the nucleon-nucleon interaction. This connection between the weak and the strong interaction is known to be fulfilled experimentally at the percent level. Finally, the last term in the third line leads to the Kroll-Ruderman low-energy theorem for the photo-production of pseudoscalar mesons off the nucleon [61].

1.3.2 Loops and power counting in $B\chi$ PT

At tree-level, the leading chiral Lagrangian for baryons (1.32) embodies a set of well known and successful low-energy results obtained with the current algebra and PCAC methods. The Lagrangian formulation gives us the chance to improve them including loop corrections systematically in perturbation theory. The idea is, as in the case of the pseudoscalar mesons, to introduce a power counting scheme valid at low momenta and light-quark masses and to organize the infinite contributions to a particular Green-function in a cascade of decreasing importance. The fulfillment of the same chiral Ward identities at the fundamental and effective sides ensures, perturbatively in p , the connection of the $B\chi$ PT with the underlying QCD. However, the power counting in this case is blurred due to the presence of a new parameter, the baryon mass M_{B0} , that is finite (does not vanish) in the chiral limit and which interpretation in terms of the underlying quarks and gluons is subtle [57]. Moreover, M_{B0} is of the same order as the chiral symmetry breaking scale and loop graphs containing baryon propagators yield contributions of order $M_{B0}/\Lambda_{\chi SB} \sim \mathcal{O}(1)$.

A consistent power counting for baryons can be settled considering them as non-relativistic fields [62]; for processes with $B = 1$, a Feynman diagram

with L loops, N_M meson propagators, N_B baryon propagators and V_k vertices of k th order Lagrangian scales as $\mathcal{O}(p^D)$ where

$$D = 4L - 2N_M - N_B + \sum_k kV_k. \quad (1.35)$$

The non-relativistic treatment of the baryon fields has been implemented in a systematic fashion within the heavy-baryon (HB) χ PT formalism [63]. This approach exploits that in the regime of validity of χ PT the baryons can only be slightly off-shell as compared with their masses and it proposes a two-fold expansion in powers of $p/M_{B_0} \sim p/\Lambda_{\chi SB}$. Namely, one defines the baryon momentum as $P_\mu = M_{B_0}\xi_\mu + k_\mu$ and assumes that $\xi^2 = 1$ and $k \cdot \xi \sim \mathcal{O}(p)$. Then, the baryon fields are redefined, $B_\xi(x) = \exp(iM_{B_0}\xi_\mu k^\mu)$ so that they obey a massless Dirac equation $\not{\partial}B_\xi = 0$ and their propagators are $i/(\xi \cdot k)$. With these new fields one casts B χ PT as an expansion in powers of k instead of $P \sim M_{B_0}$ that explicitly fulfills the power counting of Eq. (1.35). As in the theory for mesons, the renormalization of the LECs in HB χ PT can be completed order by order.

On the other hand, relativistic corrections of the type k/M_{B_0} have to be considered in calculations beyond leading loop order. The fact that these may be large, questions the applicability of the HB expansion in some parts of the low-energy region. A remarkable example concerns the $SU(3)_F$ phenomenology which the HB formalism has failed to describe in a comprehensive and precise way [64]. This is undoubtedly due to the large relativistic corrections induced by the K and η meson masses. Besides that, at leading loop order the HB approach misses anomalous threshold contributions in triangular graphs and leads to a poor convergence in form factor calculations [22, 65].

The convergence problems of the HB scheme have renewed the interest on the covariant formulation of B χ PT and have motivated the advent of different methods to organize the perturbative series in order to satisfy the formula Eq. (1.35) [57, 66, 67, 68, 65, 69, 70]. To better understand the power-counting structure of the loop contributions that follow from the Lagrangian (1.32) we have included the Fig. 1.1, where in the horizontal axis is the number of loops L and in the vertical one the power-counting D . The left-hand plot represents the counting in conventional χ PT for pseudoscalar mesons in dimensional regularization. The loops generated from $\mathcal{L}^{(2)}$ give contributions at 4th, 6th, ... orders for $L = 1, 2, \dots$ respectively so that there is a one-by-one relation between D and L . Loop diagrams generated from the higher order Lagrangians $\mathcal{L}^{(4)}$, $\mathcal{L}^{(6)}$, ... have the same form. In the right-hand side of the Fig. 1.1, it is displayed the counting obtained in dimensional regularization (\overline{MS} scheme) for graphs arising from the leading baryon Lagrangian of Eq. (1.32). The black dots are the expected D given by the power-counting formula (1.35)

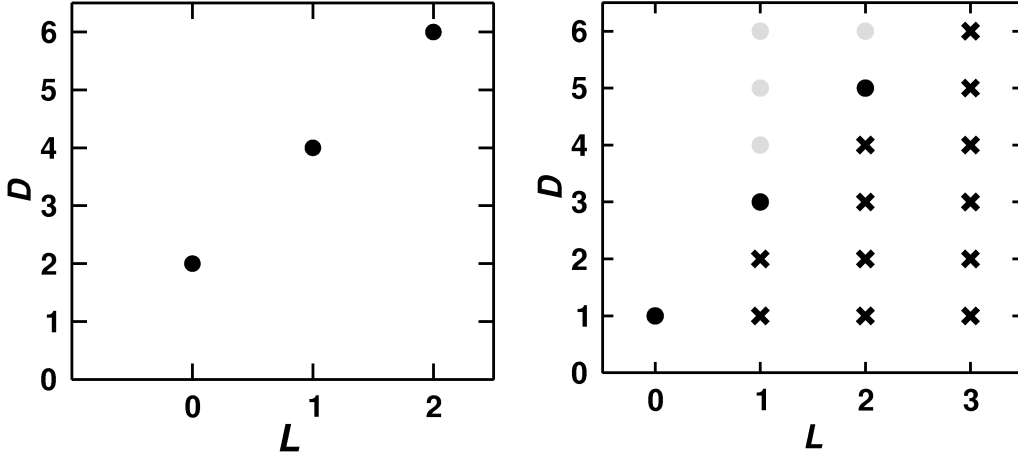


Figure 1.1: Diagram of the structure of the power-counting of the loops in conventional χ PT (left) and B χ PT (right).

and it is the pattern obeyed by the loops in the HB formulation for which the same conclusions as in the purely mesonic sector follow. The grey dots are contributions that are higher-order in the p/M_{B_0} expansion and represent, from the HB viewpoint, a resummation of relativistic corrections. Finally, the crosses are contributions that are below the order dictated by Eq. (1.35) and therefore they break the power counting. These latter terms appearing from the baryonic graphs are indeed the ones that jeopardize the applicability of a systematic perturbative approach to covariant B χ PT, i.e. graphs with an arbitrarily high number of loops contribute to all the low orders.

A consistent organization of the counting in covariant B χ PT arises from the following crucial observation: *The leading infrared divergent (non-analytical) behavior of the baryonic loop graphs obeys the power-counting formula (1.35) and agrees with the one given by HB [57, 67, 65, 69].* This means that all the terms breaking the counting (the crosses in left hand diagram of Fig. 1.1) are analytical and, consequently, of the same type as those given at tree-level by the most general chiral Lagrangian. For instance, one could define an extension of the \overline{MS} scheme in dimensional regularization in order to absorb systematically the power-counting breaking terms into the LECs. In fact, this is a proposal called the extended-on-mass-shell (EOMS) renormalization scheme [69, 70] in which one recovers the counting by a redefinition of the finite set of LECs available up to certain order at the same time as includes relativistic (analytical and non-analytical) corrections to the HB result. The EOMS scheme has been extensively applied in the $SU(2)$ -flavor sector of B χ PT in calculations of nucleon and $\Delta(1232)$ form-factors [71, 72, 73, 74, 75, 76, 77, 17], masses [78],

or Compton scattering off the proton [79, 80].

Another covariant approach is the infrared (IR)B χ PT [65] that is rather more subtle. Given a covariant loop integral in the Feynman parameterization, the IR scheme proposes to separate it in the so-called infrared (I) and regular (R) parts that are obtained manipulating the Feynman integral limits

$$H = \frac{1}{ab} = \int_0^1 \frac{dz}{(1-z)a + zb} = \int_0^\infty \dots + \int_\infty^1 \dots \equiv I + R, \quad (1.36)$$

where a includes only low-scales and b all the heavy ones. It is shown, that the I part contains all the infrared divergent parts of the loop graph, i.e. contains its non-analytical structure, but at the same time it fulfills the power-counting formula of Eq. (1.35). On the other hand, R appears in the low energy region as a polynomial expansion in p that contains the power-counting breaking terms. The IR *ansatz* is then to *renormalize* B χ PT keeping only the I part of any computed loop function and absorbing the R part in the LECs of the most general (and *infinite*) chiral Lagrangian. Obviously, the EOMS can be obtained from IR just truncating the regular part at (non-including) the order we calculate so that both prescriptions are equivalent up to higher orders. Nevertheless, the representation of the loop-function H in terms of its I and R parts is not valid in the whole energy region because the IR prescription is known to introduce un-physical cuts at high energies and heavy quark masses [65, 81, 1]. In principle, this should not affect the description at low-energies where the chiral expansion is valid although it has been detected that the tail of these cuts already appears at relatively low-quark masses and energies as the ones involved in $SU(3)_F$ -B χ PT [1] or chiral extrapolations [81].

1.4 The decuplet resonances in B χ PT

The lowest-lying decuplet of $J^P = 3/2^+$ resonances plays a very important role in low-energy baryon phenomenology due to the closeness of its average physical mass M_T with respect to the one of the baryon octet M_B and to the relatively large strength of the octet-decuplet P -wave coupling. A very well known example of its importance is the dominance of the $\Delta(1232)$ resonance in the cross section of πN scattering at relatively low-energies. The effects of the decuplet resonances are included in B χ PT perturbatively through the LECs and when one attempts to extend the range of applicability to large enough external momenta or quark masses one shall include their effects non-perturbatively. This is indeed the case with three flavors ($N_f = 2 + 1$) since the typical scale for the onset for the decuplet resonances $M_T - M_B \equiv \delta \sim 0.3$ GeV is well below the values of our expansion parameters m_K or m_η . To

account for the decuplet effects we introduce them as basic degrees of freedom and consider their virtual corrections in the same footing as those given by the octet baryons [82, 24, 26].

1.4.1 Spin-3/2 fields and the consistency problem

We introduce the flavored vector-spinor T_μ^{abc} where the tensor indices abc are completely symmetrized to form the decuplet,

$$\begin{aligned}
 T^{111} &= \Delta^{++}, & T^{112} &= \frac{\Delta^+}{\sqrt{3}}, & T^{122} &= \frac{\Delta^0}{\sqrt{3}}, \\
 T^{222} &= \Delta^-, & T^{113} &= \frac{\Sigma^{*+}}{\sqrt{3}}, & T^{123} &= \frac{\Sigma^{*0}}{\sqrt{6}}, \\
 T^{223} &= \frac{\Sigma^{*-}}{\sqrt{3}}, & T^{133} &= \frac{\Xi^{*0}}{\sqrt{3}}, & T^{233} &= \frac{\Xi^{*-}}{\sqrt{3}}, \\
 & & T^{333} &= \Omega^-, & &
 \end{aligned} \tag{1.37}$$

matching the physical free-fields described by a Rarita-Schwinger [83] flavor-singlet Lagrangian

$$\mathcal{L}_T^f = \bar{T}_\mu^{abc} (i\gamma^{\mu\nu\alpha} \partial_\alpha - M_{T0} \gamma^{\mu\nu}) T_\nu^{abc}. \tag{1.38}$$

In the last equation, M_{T0} is an average decuplet mass in the chiral limit, $\gamma^{\mu\nu\alpha}$, $\gamma^{\mu\nu}$ are the antisymmetric products of gamma matrices (see Appendix A) and repeated flavor indices $abc \dots$ are summed over.

The vector-spinor, or Rarita-Schwinger field, T_μ (we do not consider the flavor structure in the following discussion) is an object with 16 components (4 of the spinor times 4 of the Lorentz index) of which only 8 (4 in case of a massless field) correspond to the physical spin-3/2 particle and antiparticle [84, 85, 86]. The Dirac equation of motion,

$$i(\not{\partial} - M_{T0})T_\mu = 0, \tag{1.39}$$

and the two *constraints* derived also from the Euler-Lagrange equations of Eq. (1.38),

$$\partial \cdot T = 0, \tag{1.40}$$

$$\gamma \cdot T = 0, \tag{1.41}$$

guarantee, in the free case, that the independent components of the vector-spinor field are those corresponding to the physical degrees of freedom. To introduce interactions that do not spoil these constraints and do not activate the

spurious degrees of freedom is the so-called *consistency* problem. Theories with unconstrained spin-3/2 fields (not *consistent*) lead to well-known pathologies as non-positive definite commutators or acausal propagation [87, 88, 89, 90, 84].

A way to treat the consistency problem arises after noticing that the massless Rarita-Schwinger Lagrangian obeys an invariance against

$$T_\mu \rightarrow T_\mu + \partial_\mu \epsilon, \quad (1.42)$$

where ϵ is a spinor field. The application of the Dirac's Hamiltonian analysis of the constraints [91] shows that, in the massless case, this symmetry reduces the dynamical degrees of freedom to the 4 physical ones, whereas the mass term in Eq. (1.38) breaks the symmetry in a correct way, activating the 4 other physical components of the massive spin-3/2 field [84, 85]. Thus, consistent spin-3/2 theories can be built demanding that the interactions terms fulfill the symmetry of the massless Rarita-Schwinger Lagrangian, Eq. (1.42) [85, 92]. We will call these interactions *consistent* interactions or couplings.

The Rarita-Schwinger propagator is the d -dimensional inverse operator of Eq. (1.38),

$$S_{\mu\nu}(p) = -\frac{\not{p} + M_{T0}}{p^2 - M_{T0}^2 + i\epsilon} \left[g_{\mu\nu} - \frac{1}{d-1} \gamma_\mu \gamma_\nu - \frac{1}{(d-1)M_{T0}} (\gamma_\mu p_\nu - \gamma_\nu p_\mu) - \frac{d-2}{(d-1)M_{T0}^2} p_\mu p_\nu \right]. \quad (1.43)$$

The spin-1/2 content of this propagator can be made explicit decomposing it in terms of the spin projectors [26, 86],

$$S_{\mu\nu}(p) = -\frac{\not{p} + M_{T0}}{p^2 - M_{T0}^2 + i\epsilon} (P^{\frac{3}{2}})_{\mu\nu} + \frac{d-2}{(d-1)M_{T0}^2} (\not{p} + M_{T0}) (P^{\frac{1}{2}})_{\mu\nu} - \frac{1}{\sqrt{d-1}M_{T0}} \left((P^{\frac{1}{2}})_{12} - (P^{\frac{1}{2}})_{21} \right), \quad (1.44)$$

where

$$(P^{\frac{3}{2}})_{\mu\nu} = g_{\mu\nu} - \frac{1}{d-1} \gamma_\mu \gamma_\nu - \frac{1}{(d-1)p^2} (\not{p} \gamma_\mu + p_\mu \gamma_\nu \not{p}) - \frac{d-4}{d-1} \frac{p_\mu p_\nu}{p^2}, \quad (1.45)$$

$$(P^{\frac{1}{2}})_{\mu\nu} = \frac{1}{(d-1)p^2} (-p_\mu p_\nu + \not{p} (\gamma_\mu p_\nu - \gamma_\nu p_\mu)) + \frac{1}{(d-1)} \gamma_\mu \gamma_\nu, \quad (1.46)$$

$$(P_{22}^{\frac{1}{2}})_{\mu\nu} = \frac{p_\mu p_\nu}{p^2}, \quad (1.47)$$

$$(P_{12}^{\frac{1}{2}})_{\mu\nu} = \frac{1}{\sqrt{d-1}p^2} (p_\mu p_\nu - \not{p}\gamma_\mu p_\nu), \quad (1.48)$$

$$(P_{21}^{\frac{1}{2}})_{\mu\nu} = \frac{1}{\sqrt{d-1}p^2} (\not{p}p_\mu\gamma_\nu - p_\mu p_\nu), \quad (1.49)$$

which verify the orthogonality relations,

$$(P_{ij}^I)_{\mu\rho}(P_{kl}^J)^{\rho\nu} = \delta^{IJ}\delta_{jk}(P_{il}^I)_{\nu}^{\mu}, \quad I, J = \frac{3}{2}, \frac{1}{2}, \quad i, j, k, l = 1, 2. \quad (1.50)$$

The operators $(P_{22}^{\frac{3}{2}})_{\mu\nu}$ and $(P_{ij}^{\frac{1}{2}})_{\mu\nu}$ project the Rarita-Schwinger spinors into their spin-3/2 and spin-1/2 states respectively, and it is clear that the spurious degrees of freedom will, in general, contribute to physical processes containing virtual relativistic spin-3/2 fields.

However, in the case of a theory with consistent interactions these unphysical contributions will decouple. A vertex derived using Feynman rules from a consistent coupling $\Gamma^\mu(p, \dots)$ verifies the transversality condition

$$p_\mu \Gamma^\mu(p, \dots) = 0, \quad (1.51)$$

such that,

$$\Gamma^\mu(p, \dots) S_{\mu\nu} \Gamma^\nu(p, \dots) = -\Gamma^\mu(p, \dots) \frac{\not{p} + M_{T0}}{p^2 - M_{T0}^2 + i\epsilon} (P_{22}^{\frac{3}{2}})_{\mu\nu} \Gamma^\nu(p, \dots). \quad (1.52)$$

Namely, in the physical processes with virtual spin-3/2 fields described by a consistent theory only the physical degrees of freedom are dynamical and contribute to the matrix elements. It is important to stress that this is a consequence of the symmetry in Eq. (1.42) imposed at the Lagrangian level. The deletion by hand of the spin-1/2 structures of the propagator in Eq. (1.44) may destroy symmetries of the theory [26] or develop unphysical infrared singularities [93].

Nevertheless, the contributions of the spin-1/2 components to physical observables are equivalent to those given by a finite set of local operators [94, 92, 93, 26]. In the context of the EFTs (in particular of χPT), a proper treatment of the consistency problem may lead to a better convergence of the perturbative (chiral) expansion (see e.g. Sec. 2.1 for the particular case of the baryon octet magnetic moments in $SU(3)_F$ - $B\chi PT$ [2]).

1.4.2 Chiral Lagrangian containing decuplet fields

The chiral Lagrangian of the decuplet baryons is constructed introducing them as heavy matter fields [82]. In terms of the compensator field K , the decuplet field changes under a local chiral transformation as²

$$T_\mu^{abc} \rightarrow K_d^a K_e^b K_f^c T_\mu^{def}, \quad (1.53)$$

and the first step to build the chiral Lagrangian is to replace the partial derivative in Eq. (1.38) by a chiral covariant derivative

$$\mathcal{D}_\rho = \partial_\rho T_\nu^{abc} + (\Gamma_\rho)_d^a T_\nu^{dbc} + (\Gamma_\rho)_d^b T_\nu^{adc} + (\Gamma_\rho)_d^c T_\nu^{abd}. \quad (1.54)$$

The decuplet leading chiral Lagrangian $\mathcal{L}_T^{(1)}$ is completed with two more terms that will be written in terms of derivatives of the vector-spinor fields

$$\mathcal{L}_{\phi BT}^{(1)} = \frac{i\mathcal{C}}{M_{T0}} \varepsilon^{abc} (\mathcal{D}_\rho \bar{T}_\mu^{ade}) \gamma^{\rho\mu\nu} (u_\nu)_b^d B_c^e + \text{h.c.}, \quad (1.55)$$

$$\mathcal{L}_{\phi T}^{(1)} = \frac{i\mathcal{H}}{M_{T0}} \bar{T}_\mu^{abc} \gamma^{\mu\nu\rho\sigma} \gamma_5 (u_\sigma)_d^c (\mathcal{D}_\rho T_\nu^{abd}), \quad (1.56)$$

$$\mathcal{L}_T^{(1)} = \mathcal{L}_T^f + \mathcal{L}_{\phi BT}^{(1)} + \mathcal{L}_{\phi T}^{(1)}, \quad (1.57)$$

In this form, the ϕBT and ϕTT couplings appearing at leading order in the expansion in the pseudoscalar fields of the corresponding Lagrangian terms are consistent. These are equivalent to more conventional chiral couplings [89, 94, 95], which are not consistent, via the equivalence theorem [96] and a redefinition of the decuplet fields [92, 26]. The difference between both sets of couplings are higher-order contact operators with LECs that encloses the spurious spin-1/2 contributions [92]. Nonetheless, a full consistent treatment for electromagnetic or weak processes is not possible since we are still lacking a general and consistent gauge theory coupled to the spin-3/2 fields³ [97, 98].

1.4.3 Power-counting with decuplet fields

As in the case of the baryon octet fields, the inclusion of the heavy scale M_{T0} in the theory complicates the assignment of a power-counting order to the loop graphs. Moreover, $M_{T0} - M_{B0} \sim \delta$ is comparable to the size of our expansion parameters so that one may define an additional expansion on $\delta/\Lambda_{\chi SB}$. In fact, two different power-counting schemes have been proposed,

²We are denoting $(X)_b^a$ as the element of row a and column b of the matrix representation of X .

³More precisely on the couplings of the gauge fields to the virtual spin-3/2 fields .

first the so-called small-scale expansion (SSE) where $\delta \sim p$ [24] and second the δ -expansion that depends on the kinematical region where one performs the expansion [99]. In the Lorentz covariant calculations presented in this thesis, we do not perform any additional expansion in δ but we choose to keep M_{B0} and M_{T0} as independent parameters both scaling as of $\sim \mathcal{O}(1)$. The diagrams with decuplet resonances also follow the power-counting formula Eq. (1.35) and the terms breaking it now appear as complicated functions of M_{B0} and M_{T0} that we absorb into the LECs within an extension of the EOMS scheme. More precisely, *we subtract from the covariant loop functions including decuplet fields their contribution at the chiral limit ensuring the fulfillment of the power counting of Eq. (1.35) as well as to recover the HB limit, i.e. in the SSE scheme* [2].

Finally, the Rarita-Schwinger propagator, Eq. (1.43), has a problematic high-energy behavior [100]. It appears obvious from Eq. (1.43) that in the loop graphs including virtual spin-3/2 fields there is a mismatch between the power-counting and the power of divergence of the loop. In the context of an EFT, this is responsible for the appearance of $d-4$ singularities of a chiral order higher than the one naively expected using the power counting [2]. These infinities would be absorbed by the proper counter-terms to be included at higher orders. However, we do not include these terms explicitly but perform a \overline{MS} -subtraction on them and study the residual regularization-scale dependence.

In the following, we present the description of some baryonic observables using $SU(3)_F$ - $B\chi$ PT up to $\mathcal{O}(p^3)$ and $\mathcal{O}(p^4)$ accuracies (one-loop order). We focus in the application of the covariant formalism in the EOMS scheme and in the inclusion of the decuplet resonances as explicit degrees of freedom. In all the considered cases, we recover the corresponding HB results in the $1/M_{B0}$ expansion and they are compared with the full-relativistic results. In Chap. 2, we study the electromagnetic structure of the lowest-lying baryons, namely, of those belonging to the respective octet and decuplet $SU(3)_F$ -multiplets. In Sec. 2.1, the analysis of the baryon octet magnetic moments is used to discuss in detail the differences among various approaches to $B\chi$ PT. The comparison

between the HB and the covariant formalisms, and within the latter, between the EOMS and IR schemes on one hand and between different methods to treat the spin-3/2 fields on the other, motivates the establishment of the preferred framework that is used in the rest of this thesis. This approach is then applied, in Sec. 2.2, to predict the static electromagnetic structure of the decuplet resonances, namely their magnetic dipole, electric quadrupole and magnetic octupole moments as well as their charge radii. In Chap. 3, we illustrate the applications that $SU(3)_F$ -B χ PT may have in SM phenomenology predicting the $SU(3)_F$ -breaking of the hyperon vector coupling $f_1(0)$. Indeed, this coupling and its breaking are essential to understand the semileptonic hyperon decay data and to eventually extract the Cabibbo-Kobayashi-Maskawa matrix element V_{us} . Last but not least, in Chap. 4, we explore the potential of the covariant $SU(3)_F$ -B χ PT formalism to describe $N_f = 2 + 1$ LQCD results exploring those recently reported on the lowest-lying baryon spectrum. We close there the presentation of the results compiled in this thesis emphasizing the phenomenological applications that a successful combination of LQCD and χ PT may have in the future with the prediction of the baryonic sigma terms.

The leading loop corrections in $SU(3)_F$ -B χ PT depend only on relatively well known couplings and masses. The values for the parameters that have been used in the thesis are listed in Table B.1 of Appendix B.

Chapter 2

Electromagnetic structure of the lowest-lying baryons

In this chapter, we study the low-energy electromagnetic structure of the lowest-lying octet and decuplet baryons in B χ PT. The first part, Sec. 2.1, is devoted to the description of the baryon-octet magnetic moments and contains a detailed exposition of the differences obtained in various approaches like HB, EOMS and IR, or using different ways to include the spin-3/2 decuplet resonances. The second part, Sec. 2.2, concerns the structure of the coupling of the photon to the decuplet resonances, which, at low energies, can be cast in terms of the electric and magnetic moments and radii. We give predictions for the structure of the decuplet, and in particular of the $\Delta(1232)$, using the experimental data and recent LQCD results on the respective properties for the Ω^- baryon.

2.1 Magnetic moments of the baryon octet

The magnetic moments of the baryons are of the utmost importance since they contain information on the internal structure as read by electromagnetic probes or photons. A starting point in the understanding of the magnetic moments of the octet is the $SU(3)_F$ -symmetric model of Coleman and Glashow (CG from now on) [101]

$$\begin{aligned} \mu_{\Sigma^+} &= \mu_p, & \mu_{\Lambda} &= \frac{1}{2}\mu_n, & \mu_{\Xi^0} &= \mu_n, \\ \mu_{\Sigma^-} &= -(\mu_n + \mu_p), & \mu_{\Xi^-} &= \mu_{\Sigma^-}, & \mu_{\Lambda\Sigma^0} &= -\frac{\sqrt{3}}{2}\mu_n, \end{aligned} \quad (2.1)$$

and the isospin relation

$$\mu_{\Sigma^0} = \frac{1}{2}(\mu_{\Sigma^+} + \mu_{\Sigma^-}), \quad (2.2)$$

that describes the eight magnetic moments and the $\Lambda\Sigma_0$ transition moment in terms of two parameters. The CG approach is recovered at LO in χ PT so that the $SU(3)_F$ -breaking corrections to the baryon magnetic moments can be addressed in a systematic and model-independent fashion at NLO in the chiral expansion. However, since the first non-relativistic calculation in the mid-seventies [102], it has been realized that the chiral corrections are large and tend to worsen the description given by Eqs. (2.1) and (2.2). This result, that is also obtained in the HB χ PT formulation at NLO [103], makes it necessary to go up to NNLO of accuracy to find a good description of the magnetic moments data [104, 105, 106], although at the price of the predictive power since the number of not-constrained LECs is approximately equal to the number of experimental points [105]. The role of the relativistic corrections in the chiral series of the magnetic moments was explored in the IR scheme [107] and the description obtained at NLO was even worse than the one in HB. In this chapter, we will show how the situation is radically improved when the NLO corrections are calculated within a covariant scheme that resums the infinite tower of relativistic corrections in accordance to analyticity (EOMS scheme) [1]. Moreover, we have found that this improvement remains when the decuplet resonances are explicitly included in the covariant framework [2]. The comparison among the various approaches suggests the importance that the relativistic corrections and the analyticity properties of the loop-functions have in $SU(3)_F$ -B χ PT [1]. The relevance of filtering the spurious degrees of freedom from the spin-3/2 relativistic field is also highlighted.

2.1.1 Formalism

The structure of the baryons, as probed by photons, is encoded into the electromagnetic form factors

$$\langle B(p') | J^\mu | B(p) \rangle = e \bar{u}(p') \left\{ \gamma^\mu F_1(t) + \frac{i\sigma^{\mu\nu} q_\nu}{2M_B} F_2(t) \right\} u(p), \quad (2.3)$$

where $\sigma^{\mu\nu} = i[\gamma^\mu, \gamma^\nu]/2$, $t = (p' - p)^2$, $J^\mu = eQA^\mu$ is the electromagnetic quark vector current (see Sec 1.2.3), B characterizes the field of a octet-baryon, $u(p)$ its Dirac spinor and M_B is the corresponding mass. The functions $F_1(t)$ and $F_2(t)$ are called Dirac and Pauli form factors respectively and they have a definite physical meaning at $t = 0$ (interaction with real photons). Namely, $F_1(0) = Q_B$ the electric charge of the baryon, and $F_2(0) = \kappa_B$ the anomalous

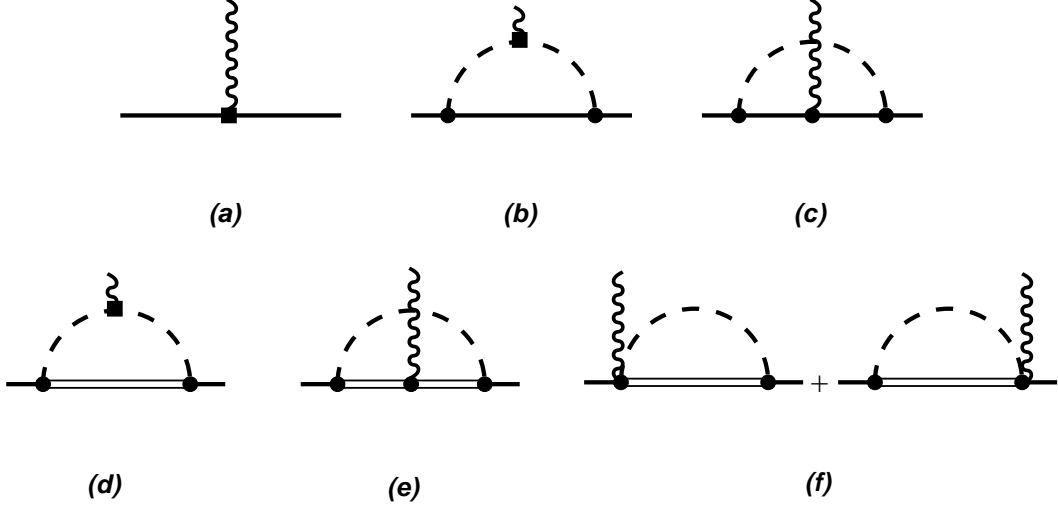


Figure 2.1: Feynman diagrams contributing to the octet-baryons magnetic moments up to $\mathcal{O}(p^3)$ in χ PT. The solid lines correspond to octet-baryons, double lines to decuplet-baryons and dashed lines to mesons. The black dots indicate 1^{st} -order couplings while boxes, 2^{nd} -order couplings.

magnetic moment of the baryon. The magnetic moment μ_B is then related to the sum of the Dirac and Pauli form factors at $t = 0$ through

$$\mu_B = (Q_B + \kappa_B) \frac{e}{2M_B}. \quad (2.4)$$

For the case of the $\Lambda\Sigma^0$ transition, the previous parameterization is generalized and the t -dependent $\Lambda\Sigma^0\gamma$ vertex can be written as

$$\begin{aligned} \langle \Sigma^0(p') | J^\mu | \Lambda(p) \rangle = \\ e \bar{u}(p') \left\{ \left(\gamma^\mu - \frac{M_{\Sigma^0} - M_\Lambda}{t} q^\mu \right) F_1^{\Sigma^0\Lambda}(t) + \frac{i\sigma^{\mu\nu} q_\nu}{M_{\Sigma^0} + M_\Lambda} F_2^{\Sigma^0\Lambda}(t) \right\} u(p). \end{aligned} \quad (2.5)$$

This form reduces to (2.3) for $M_{\Sigma^0} \rightarrow M_\Lambda$.

The chiral contributions to the baryon-octet anomalous magnetic moments up to NLO are represented in terms of Feynman graphs as in Fig. 2.1. The LO at $\mathcal{O}(p^2)$ is the tree-level contribution **(a)** given by the following terms in the chiral Lagrangian

$$\mathcal{L}_{\gamma B}^{(2)} = \frac{b_6^D}{8M_{B0}} \langle \bar{B} \sigma_{\mu\nu} \{ F_+^{\mu\nu}, B \} \rangle + \frac{b_6^F}{8M_{B0}} \langle \bar{B} \sigma_{\mu\nu} [F_+^{\mu\nu}, B] \rangle, \quad (2.6)$$

where, $F_+^{\mu\nu} = 2eQF^{\mu\nu}$ is the tensor field constructed out of the electromagnetic external source, i.e. Eq. (1.29), and $F_{\mu\nu} = \partial_\mu A_\nu - \partial_\nu A_\mu$ is the electromagnetic strength tensor. The contribution of the LECs b_6^D and b_6^F to the anomalous magnetic moments are

$$\kappa_B^{(2)} = \alpha_B b_6^D + \beta_B b_6^F, \quad (2.7)$$

where the coefficients α_B and β_B for each of the baryons in the octet are listed in Table C.1 of the Appendix C.1. This LO contribution is nothing else but the $SU(3)_F$ -symmetric prediction leading to the CG relations of Eqs. (2.1).

The $\mathcal{O}(p^3)$ diagrams **(b)**-**(f)** account for the leading $SU(3)_F$ -breaking corrections that are induced by the corresponding breaking in the masses of the pseudoscalar meson octet. Their contributions to the anomalous magnetic moment of a given member of the octet B can be written as

$$\kappa_B^{(3)} = \frac{1}{8\pi^2 F_\phi^2} \sum_{\substack{\phi=\pi,K,\eta \\ \alpha=b,\dots,f}} \xi_{BM}^{(\alpha)} H^{(\alpha)}(m_\phi) \quad (2.8)$$

where the coefficients $\xi_{BM}^{(\alpha)}$ are in Table C.1 of Appendix C.1. The loop functions $H^{(\alpha)}(m)$ for $\alpha = b, \dots, f$, expressed in terms of Feynman parameter integrals, the EOMS-renormalized LECs and the HB limits are also presented in the Appendix C.1. The loop functions only depend in the relatively well known couplings D , F , \mathcal{C} and F_ϕ and (1.15), the baryon masses and the pseudoscalar meson masses. The numerical values for these parameters used in the thesis can be found in Appendix B. In Eq. (2.8) we are implicitly using that the $SU(3)_F$ -breaking corrections to the baryon-masses start to contribute to the magnetic moments at NNLO. In the present calculation, the electromagnetic gauge invariance has been checked. We have computed the loop-contributions (Fig. 2.1) to the electric charge of any octet-baryon δQ_B and have verified that they are canceled by the wave-function renormalization Σ'_B of the minimal photon coupling: $\delta Q_B + Q_B \Sigma'_B = 0$.

2.1.2 Results

The magnetic moments of the baryon-octet have been often used as an example of the lack of convergence of the chiral series in $SU(3)_F$ -B χ PT. It is particularly interesting to compare the results obtained in the various approaches commonly used in the literature and to investigate the origin of their differences. We first focus on the contributions given by the octet diagrams **(b)** and **(c)** obtained at NLO in the HB, IR and EOMS approaches and discuss afterwards the contributions of the decuplet through the diagrams **(d)**, **(e)** and **(f)**.

Graphs with virtual octet-baryons

It is illustrative to solve the Feynman parameter integrals of the loop functions $H^{(b)}$ and $H^{(c)}$ shown in the Appendix C.1

$$\begin{aligned}
 H^{(b)}(m) &= -M_{B_0}^2 + 2m^2 + \frac{m^2}{M_{B_0}^2}(2M_{B_0}^2 - m^2) \log\left(\frac{m^2}{M_{B_0}^2}\right) \\
 &\quad + \frac{2m(m^4 - 4m^2M_{B_0}^2 + 2M_{B_0}^4)}{M_{B_0}^2\sqrt{4M_{B_0}^2 - m^2}} \arccos\left(\frac{m}{2M_{B_0}}\right), \\
 H^{(c)}(m) &= M_{B_0}^2 + 2m^2 + \frac{m^2}{M_{B_0}^2}(M_{B_0}^2 - m^2) \log\left(\frac{m^2}{M_{B_0}^2}\right) \\
 &\quad + \frac{2m^3(m^2 - 3M_{B_0}^2)}{M_{B_0}^2\sqrt{4M_{B_0}^2 - m^2}} \arccos\left(\frac{m}{2M_{B_0}}\right), \tag{2.9}
 \end{aligned}$$

where the ultraviolet divergences in Eqs. (C.2) and (C.3) vanish after the integration. One can clearly distinguish in Eq. (2.9) the terms $\sim M_{B_0}^2$ that contribute at $\mathcal{O}(p^2)$ to the magnetic moments, breaking the power counting.

In order to get rid of the power counting breaking problem we first follow the EOMS scheme, by which these pieces are absorbed into the available LECs, b_6^D and b_6^F . This is equivalent to redefining these two as

$$\tilde{b}_6^D = b_6^D + \frac{3DFM_{B_0}^2}{2\pi^2F_\phi^2}, \quad \tilde{b}_6^F = b_6^F,$$

so that

$$\tilde{H}^{(b)} = H^{(b)} + M_{B_0}^2, \quad \tilde{H}^{(c)} = H^{(c)} - M_{B_0}^2. \tag{2.10}$$

In this way, we have obtained the NLO relativistic contribution to the magnetic moments starting from $\mathcal{O}(p^3)$. Furthermore, one is able to recover the NLO quantum correction in the HB formalism by setting $M_{B_0} \sim \Lambda_{\chi\text{SB}}$

$$\tilde{H}^{(b)}(m) \simeq \pi m M_{B_0} + \mathcal{O}(p^2), \quad \tilde{H}^{(c)}(m) \simeq \mathcal{O}(p^2). \tag{2.11}$$

When added to the tree-level terms, this result completes the $\mathcal{O}(p^3)$ estimation of the baryon magnetic moments in the HB approach [103, 104]. The IR amplitudes have been calculated in Refs. [107]. They can be obtained subtracting from the full loop-functions (2.9) the corresponding regular parts, which can be expressed around the chiral limit as

$$\begin{aligned}
 R^{(b)}(m) &= -M_{B_0}^2 + \frac{19m^4}{6M_{B_0}^2} - \frac{2m^6}{5M_{B_0}^4} + \dots, \\
 R^{(c)}(m) &= M_{B_0}^2 + 2m^2 + \frac{5m^4}{2M_{B_0}^2} - \frac{m^6}{2M_{B_0}^4} + \dots, \tag{2.12}
 \end{aligned}$$

Table 2.1: Numerical results of the fits of \tilde{b}_6^D and \tilde{b}_6^F to the experimental values of baryon-octet magnetic moments up to $\mathcal{O}(p^3)$ in different χ PT approaches. The experimental values with the corresponding errors [108] are also displayed in the last row. All the values for the magnetic moments are expressed in units of nuclear magnetons, while \tilde{b}_6^D and \tilde{b}_6^F are dimensionless.

	CG	HB	IR	EOMS	Expt.
p	2.56	3.01	2.25	2.60	2.793(0)
n	-1.60	-2.67	-2.74	-2.16	-1.913(0)
Λ	-0.80	-0.42	-0.61	-0.64	-0.613(4)
Σ^-	-0.97	-1.35	-1.15	-1.12	-1.160(25)
Σ^+	2.56	2.18	2.38	2.41	2.458(10)
Σ^0	0.80	0.42	0.61	0.64	—
Ξ^-	-0.97	-0.52	-1.12	-0.93	-0.651(3)
Ξ^0	-1.60	-0.70	-1.28	-1.23	-1.250(14)
$\Lambda\Sigma^0$	1.38	1.68	1.86	1.58	$\pm 1.61(8)$
b_6^D	2.40	4.71	4.70	3.92	
b_6^F	0.77	2.48	0.43	1.28	
$\tilde{\chi}^2$	0.46	1.01	1.30	0.18	

where one can see that the power-counting breaking terms are removed in addition to an infinite chain of terms analytic in the quark masses. As it has been already pointed out in the Sec. 1.3.2, the IR representation is not valid in the whole energy region. In the particular case of the magnetic moments, the infrared and regular parts have unphysical cuts at $m = 2M_{B0}$.

In Table 2.1 we show numerical results for the baryon magnetic moments obtained by minimizing $\tilde{\chi}^2 = \sum(\mu_{th} - \mu_{exp})^2$ as a function of \tilde{b}_6^D and \tilde{b}_6^F . The $\Lambda\Sigma^0$ transition moment is not included in the fit and it is a prediction to be confronted with the experimental value. The $\tilde{\chi}^2$ is an estimator that has not absolute statistical meaning but allow us to asses the quality of the different approaches. We compare the CG result with the $\mathcal{O}(p^3)$ loop results given by the three different χ PT schemes discussed above, namely, the HB of the Eq. (2.11) and the covariant of the Eq. (2.9), within the EOMS of the Eq. (2.10) or the IR of the Eq. (2.12). The experimental values of the magnetic moments are also displayed for comparison.

The HB results show the longstanding problem of the poor convergence of $SU(3)_F$ -B χ PT for the baryon magnetic moments. The loop correction

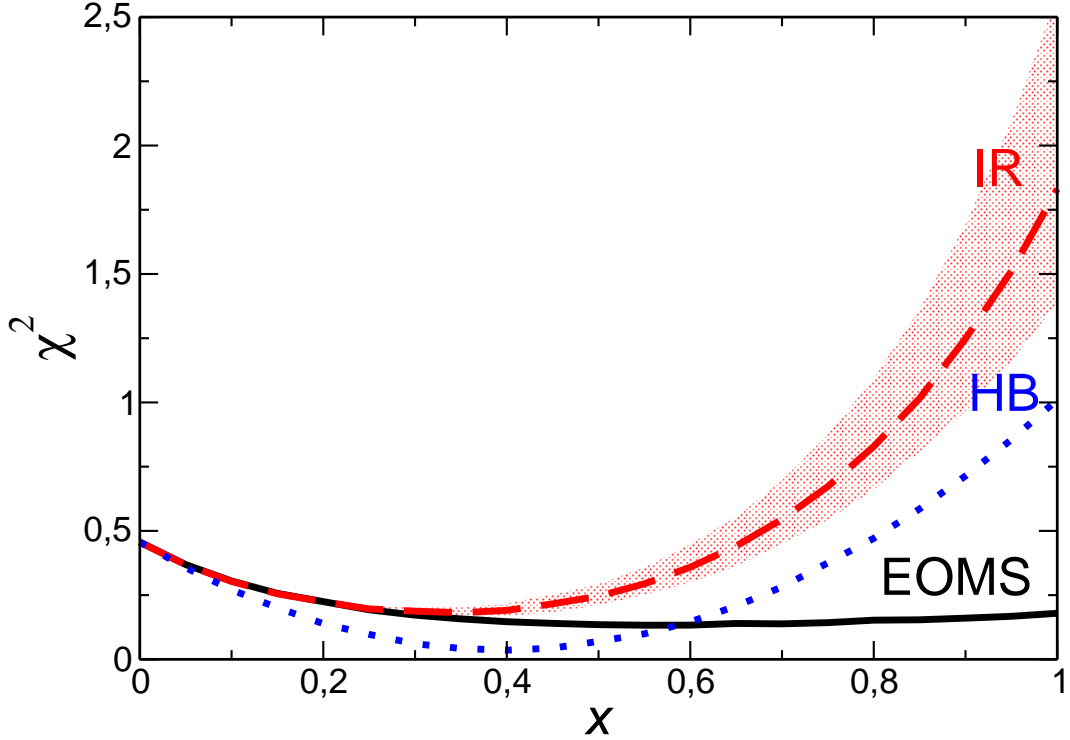


Figure 2.2: $SU(3)_F$ -breaking evolution (see text for details) of the minimal $\tilde{\chi}^2$ in χ PT up to $\mathcal{O}(p^3)$ in the different approaches with only dynamical octet-baryons reported in this work. We also show the shaded areas produced by the uncertainty in M_{B_0} when varying from 0.8 GeV to 1.1 GeV and choosing as central value $M_{B_0} = 0.94$ GeV [1]. This effect lies within the line thickness in the EOMS case, while the HB is independent of it.

amounts up to 80% of the leading contribution for some of the baryons. In this approach, it is necessary to come up to $\mathcal{O}(p^4)$ or NNLO to achieve a reasonable convergence, although the role of the loop contributions is not clear in a scenario where one has the same number of parameters as of experimental values to fit [105]. One expects that the covariant theory, with the proper higher-order chiral terms, should overcome the problem of convergence. However, the IR results are even worse than those obtained in HB and the inclusion of NNLO is also required to achieve a successful description of the experimental data [107].

On the other hand, the EOMS results presented here show a NLO improvement over the CG description. Indeed, the $\tilde{\chi}^2$ in this approach is better than the $SU(3)_F$ -symmetric description and much better than those obtained with

HB and IR. Moreover, we find that the NLO term represents, at most, half of the leading contribution

$$\begin{aligned}\mu_p &= 3.47 (1 - 0.257), \quad \mu_n = -2.55 (1 - 0.175), \\ \mu_\Lambda &= -1.27 (1 - 0.482), \quad \mu_{\Sigma^-} = -0.93 (1 + 0.187), \\ \mu_{\Sigma^+} &= 3.47 (1 - 0.300), \quad \mu_{\Sigma^0} = 1.27 (1 - 0.482), \\ \mu_{\Xi^-} &= -0.93 (1 + 0.025), \quad \mu_{\Xi^0} = -2.55 (1 - 0.501), \\ \mu_{\Lambda\Sigma^0} &= 2.21 (1 - 0.284).\end{aligned}$$

This is consistent with a maximal correction of about $m_\eta/\Lambda_{\chi\text{SB}}$ expected in $SU(3)_F$ -B χ PT. Remarkably, we predict a value for $\mu_{\Lambda\Sigma^0}$ that is very close to the experimental one assuming a positive sign.

In order to understand the differences between the three B χ PT formulations, we study the evolution of the minimal $\tilde{\chi}^2$ as we *switch-on* the $SU(3)_F$ -breaking effects, by introducing the parameter $x = m_\phi/m_{\phi,\text{phys}}$ (where $\phi = \pi, K, \eta$) and varying it between zero and one. As seen in Fig.4.2 [1], the three approaches coincide in the vicinity of the chiral limit. The EOMS and IR results stay very close up to $x \sim 0.4$. As x increases further, the HB and IR description of data get worse while, on the contrary, the EOMS result lies well below the $SU(3)_F$ -symmetric one. We interpret the rapid growth of the IR result as a manifestation of the change of the analytical structure of the theory made in this formulation, that already produces large spurious effects for the K and η physical masses.

Graphs with virtual decuplet-baryons

We now investigate the contributions of the diagrams **(d)**-**(f)** of Fig. 2.1 in the covariant formulation of B χ PT and in the HB limit. As explained in the Sec. 1.4, the description of spin-3/2 particles in relativistic quantum field theory is known to be problematic because of the presence of unphysical spin-1/2 components. The fulfillment of the consistency condition of Eq. (1.42) guarantees these spurious degrees of freedom to be constrained. Indeed, the chiral Lagrangians of Eqs. (1.55) and (1.56) provide such consistent ϕBT and ϕTT couplings to be used in the leading-order-loop graphs involving decuplet resonances. In this section we will analyze the decuplet contribution to the baryon octet magnetic moments and will also investigate the role that the unphysical components of the spin-3/2 fields may have in covariant B χ PT. More precisely, we will compare the results obtained for the diagrams **(d)**-**(f)** of Fig. 2.1 using the consistent Lagrangian Eq. (1.55) with those obtained with

the conventional chiral Lagrangian

$$\tilde{\mathcal{L}}_{\phi BT}^{(1)} = \frac{\mathcal{C}}{F_\phi} \varepsilon^{abc} \bar{T}_\mu^{ade} (g^{\mu\nu} + z\gamma^\mu \gamma^\nu) B_c^e \partial_\nu \phi_b^d + \text{h.c.}, \quad (2.13)$$

where z is a so-called off-shell parameter. An analysis of the constraint structure of the interacting theory of Eqs. (1.38) and (2.13) yields $z = -1$ [109]. Nevertheless, the resulting interaction still leads to well-known problems afflicting the relativistic quantum field theory of 3/2 spinors like non-positive definite commutators or acausal propagation [89, 90, 84].

A pertinent observation is that both Lagrangians, Eq. (1.55) and Eq. (2.13), are related via a field redefinition [92]

$$\tilde{\mathcal{L}}_{\phi BT}^{(1)} = \mathcal{L}_{\phi BT}^{(1)} + \tilde{\mathcal{L}}_{\phi\phi BB}^{(2)}, \quad (2.14)$$

where the second-order $\phi\phi BB$ contact term is [2]

$$\begin{aligned} \tilde{\mathcal{L}}_{\phi\phi BB}^{(2)} = & \frac{\mathcal{C}^2}{12M_{T0}^2 F_\phi^2} \left(3\langle \bar{B} \{ [\partial_\mu \phi, \partial_\nu \phi], (R^{\mu\nu} B) \} \rangle \right. \\ & \left. + \langle \bar{B} [[\partial_\mu \phi, \partial_\nu \phi], (R^{\mu\nu} B)] \rangle - 6\langle \bar{B} \partial_\mu \phi \rangle \langle \partial_\nu \phi (R^{\mu\nu} B) \rangle \right), \end{aligned} \quad (2.15)$$

with $R^{\mu\nu} = i\gamma^{\mu\nu\alpha} \partial_\alpha + M_{T0} \gamma^{\mu\nu}$. The latter Lagrangian is then interpreted as carrying the spin-1/2 content of the Lagrangian (2.13) and is eliminated by absorbing it into suitable higher-order LECs. The loop functions $H^{(\alpha)}$ corresponding to the diagrams **(d)**-**(f)** in Eq. (2.8) can be found in the Appendix C.1 in terms of Feynman-parameter integrals. The additional character that appears in the loop-functions of the diagram **(f)** indicates whether the seagull-diagram comes from the minimal substitution performed in the derivative of the meson fields (*I*) or of decuplet fields (*II*) in the consistent approach.

The loop divergent integrals are first regularized in the \overline{MS} -prescription. In this case, one finds the higher-order divergences discussed in Sec. 1.4. We use a value $\mu = 1$ GeV and analyze below our results with respect to a moderate variation around this value. In order to recover the power counting, we apply the EOMS-scheme on top of the \overline{MS} . From the EOMS-renormalized loop-functions $\hat{H}^{(\alpha)}$ one can then obtain the non-analytical pieces of the HB results in the SSE counting (see Sec. 1.4) assuming $M_{T0} = M_{B0} + \delta$ and applying that $M_B \sim \Lambda_{\chi SB}$ [103]. We also display the HB formulas in the Appendix C.1. In addition, one obtains the decoupling of the decuplet resonances for the limit where $M_{T0} \rightarrow \infty$. Indeed, one finds that the EOMS-renormalized loop-functions verify $\lim_{M_{T0} \rightarrow \infty} \hat{H}^{(\alpha)} = 0$.

We have also done the calculation using the conventional couplings of Eq. (2.13) with the choice $z = -1$. We found that the results of the seagull **(f)** of type *I* are the same in both approaches, whereas the diagram **(e)** with conventional couplings equals the same diagram **(e)** minus the seagull **(f)** of type *II* in the case of consistent couplings. The only difference between both calculations comes from diagram **(d)**. If we subtract the corresponding loop-function obtained using consistent couplings $H^{(d)}$ from the one obtained with the conventional couplings $H'^{(d)}$ we find

$$\delta H^{(d)}(m, \mu) = H'^{(d)}(m, \mu) - H^{(d)}(m, \mu) = \frac{3M_{B0}(M_{B0} + M_{T0})}{2M_{T0}^2} m^2 \left(1 - \log \left(\frac{m^2}{\mu^2} \right) \right). \quad (2.16)$$

One can check that this is the contribution given by a tadpole diagram where the $\phi\phi BB$ vertex is the one obtained from Eq. (2.15). Therefore, Eq. (2.16) is the higher-order contribution to the anomalous magnetic moments of the octet-baryons that is removed when using consistent couplings and interpreted as coming from unphysical degrees of freedom. Indeed, the difference between both approaches comes from diagram **(d)** for which the consistent couplings eliminate completely the spurious spin-1/2 components. On the other hand, both schemes include the non-consistent minimal γTT coupling. In this regard, we observe that the loop-contribution with this coupling gives the same result in both frameworks. Finally, we can also notice that the difference between the two schemes vanishes when the decuplet mass goes to infinity (decoupling limit), $\lim_{M_{T0} \rightarrow \infty} \delta H^{(d)} = 0$.

In Table 2.2 we show the numerical results for the baryon magnetic moments in $B\chi$ PT up to $\mathcal{O}(p^3)$ with the explicit inclusion of the decuplet contributions. We compare the $SU(3)_F$ -symmetric description with the different NLO χ PT calculations discussed above. Namely, we display the HB and the covariant-EOMS results both with $(B + T)$ and without (B) the inclusion of dynamical decuplets. In the covariant case we show the numerical results obtained using the consistent couplings $(B + T^*)$ and the conventional couplings with $z = -1$ $(B + T)$.

For the HB approach, one sees how the corrections of the dynamical baryon -octet and -decuplet go in the same direction and are of equivalent size. Consequently, the description obtained with only the baryon-octet, that already overestimated the $SU(3)_F$ -breaking corrections, gets much worsened. In the covariant case we obtain two quite different results depending on whether we use the consistent or the conventional ($z = -1$) couplings. For the latter, we find that in general the corrections given by the decuplet resonances are quite large and tend to spoil the NLO improvement over the Coleman-Glashow description.

Table 2.2: Baryon octet magnetic moments in $B\chi\text{PT}$ up to $\mathcal{O}(p^3)$ with the explicit inclusion of the decuplet contributions. We compare the $SU(3)_F$ -symmetric description with the different NLO χPT calculations discussed in the text. Namely, we display the Heavy Baryon and the covariant-EOMS results both with ($B+T$) and without (B) the inclusion of dynamical decuplets. In the covariant case we show the numerical results obtained using the consistent couplings ($B+T^*$) and the conventional couplings with $z = -1$ ($B+T$). We also include the experimental values from reference [108].

	CG	Heavy Baryon		Covariant EOMS			Expt.
		B	$B+T$	B	$B+T$	$B+T^*$	
p	2.56	3.01	3.47	2.60	3.18	2.61	2.793(0)
n	-1.60	-2.62	-2.84	-2.16	-2.51	-2.23	-1.913(0)
Λ	-0.80	-0.42	-0.17	-0.64	-0.29	-0.60	-0.613(4)
Σ^-	-0.97	-1.35	-1.42	-1.12	-1.26	-1.17	-1.160(25)
Σ^+	2.56	2.18	1.77	2.41	1.84	2.37	2.458(10)
Σ^0	0.80	0.42	0.17	0.64	0.29	0.60	...
Ξ^-	-1.60	-0.70	-0.41	-0.93	-0.78	-0.92	-0.651(3)
Ξ^0	-0.97	-0.52	-0.56	-1.23	-1.05	-1.22	-1.250(14)
$\Lambda\Sigma^0$	1.38	1.68	1.86	1.58	1.88	1.65	$\pm 1.61(8)$
b_6^D	2.40	4.71	5.88	3.92	5.76	4.30	
b_6^F	0.77	2.48	2.49	1.28	1.03	1.03	
$\bar{\chi}^2$	0.46	1.01	2.58	0.18	1.06	0.22	

In the covariant formulation with consistent couplings, the decuplet contributions are small and added to the octet contributions provide an overall description of the same quality as that obtained with only octet-baryons within EOMS. In this case, we can study the convergence properties of the chiral series factorizing the tree-level at $\mathcal{O}(p^2)$ from the whole result up to $\mathcal{O}(p^3)$. We also separate the loop fraction into the octet (second number) and the decuplet (third number) parts in the parentheses

$$\begin{aligned}
 \mu_p &= 3.46(1 - 0.28 + 0.035) , & \mu_n &= -2.86(1 - 0.16 - 0.06) , \\
 \mu_\Lambda &= -1.43(1 - 0.46 - 0.12) , & \mu_{\Sigma^-} &= -0.60(1 + 0.25 + 0.70) , \\
 \mu_{\Sigma^+} &= 3.46(1 - 0.34 + 0.025) , & \mu_{\Sigma^0} &= 1.41(1 - 0.47 - 0.11) , \\
 \mu_{\Xi^-} &= -0.60(1 - 0.07 + 0.61) , & \mu_{\Xi^0} &= -2.86(1 - 0.48 - 0.09) , \\
 \mu_{\Lambda\Sigma^0} &= 2.48(1 - 0.28 - 0.06) .
 \end{aligned}$$

Except for the Σ^- , the contributions of the octet and the decuplet and the total $\mathcal{O}(p^3)$ corrections, are consistent with a maximal correction of about $m_\eta/\Lambda_{\chi SB}$.

We can also investigate the set of sum-rules obtained by Caldi and Pagels [102] that hold in the HB expansion. One finds that two of them survive up to the leading breaking corrections provided by any of the covariant χ PT approaches considered. Namely, we found that our results verify

$$\mu_{\Sigma^+} + \mu_{\Sigma^-} = -2\mu_\Lambda, \quad \mu_{\Lambda\Sigma^0} = \frac{1}{\sqrt{3}}(\mu_\Lambda - \mu_{\Xi^0} - \mu_n). \quad (2.17)$$

The first relation in combination with the assumed isospin symmetry is the cause of $\mu_\Lambda = -\mu_{\Sigma^0}$ in the results of Table 2.2. Experimentally, the two relations in Eq. (2.17) are satisfied rather accurately, $1.298(27)=1.226(8)$ for the first relation and $1.61(8)=1.472(8)$ for the second. A combination of them produces the Okubo sum-rule [110]. The third sum-rule derived in [102], although fulfilled in the HB expansions of our results (see Ref. [103]), is broken when the relativistic corrections to the loops are included.

The comparison between the results of the three approaches to implement the decuplet resonances presented in this work deserves some comments. The covariant framework provides a much better description of the resonances effects than the HB one. For the results obtained in the latter, one is unavoidably led to wonder about the contributions of higher-mass resonances. In the covariant formulation, relativistic corrections in form of higher-order terms in the expansion on $m/\Lambda_{\chi SB}$ and $\delta/\Lambda_{\chi SB}$, are resummed in a way that preserves analyticity. However, in the covariant approach one faces the problem of the spurious degrees of freedom and their unphysical contributions. We identified above the term that produces the difference between the two covariant calculations, Eqs. (2.15) and (2.16). Moreover, we interpreted this difference in the context of the spin-3/2 gauge symmetry as a contribution of the spin-1/2 modes that are decoupled after applying a suitable field redefinition. In conclusion, the differences exhibited in Table 2.2 highlight the importance of settling a proper framework to implement the spin-3/2 resonances into an EFT.

In Fig. 2.3 we collect the uncertainties of the numerical results due to the values of the parameters used in this work. The graphs represent the dependence of $\tilde{\chi}^2$ on the regularization scale μ (*left*), the baryon mass M_{B0} (*center*) and the decuplet-octet mass splitting δ (*right*) in HB (dotted line) and in the covariant formulation using conventional (dashed line) and consistent (thick solid line) couplings. We also show the $\tilde{\chi}^2$ of the results without decuplet resonances in grey (solid and dotted for covariant and HB respectively) and of the $SU(3)_F$ -symmetric description (horizontal thin solid line). The three graphs show that the results given in Table 2.2 are representative of those obtained

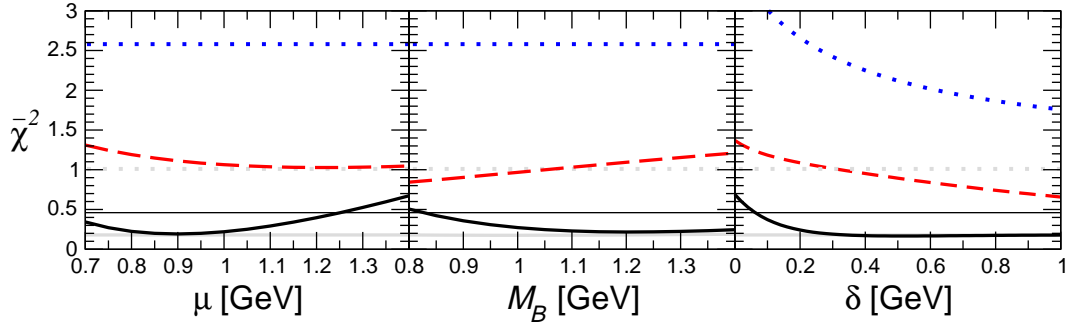


Figure 2.3: Uncertainties of the numerical results of Table 2.2 due to the values of the regularization scale μ (*left panel*), the average baryon mass M_{B0} (*center panel*) and the decuplet-octet mass splitting δ (*right panel*). The lines represent the $\bar{\chi}^2$ for the results obtained in HB (dotted line) and in covariant approach using conventional (dashed line) and consistent (thick solid line) couplings. The grey lines represent the $\bar{\chi}^2$ for the case without explicit decuplet resonances in HB (dotted) and in covariant formulation (solid). For reference we also include the $SU(3)$ -symmetric description (thin solid line).

for any other values of the parameters μ , M_{B0} and δ chosen within reasonable intervals. In particular, the first graph shows that the covariant calculation with consistent couplings improves the $SU(3)_F$ -symmetric description for $0.7 \text{ GeV} \leq \mu \leq 1.3 \text{ GeV}$, being the best description for $\mu \sim M_N \simeq 0.94 \text{ GeV}$. From the second graph we conclude that the results are solid with respect to a variation of the average baryon mass and keeping $\delta = 0.231 \text{ GeV}$. We have observed numerically that the size of the decuplet contributions in the covariant case with consistent couplings decreases as δ increases and practically reaches the decoupling for $\delta \sim 0.3 \text{ GeV}$. A manifestation of this can be seen in the *right panel*.

2.1.3 Summary

In this section, we have analyzed the description of the baryon-octet magnetic moments in different approaches to $SU(3)_F$ -B χ PT. On one hand, we have found that an improvement of the CG model is possible within the EOMS scheme, solving a problem known since the first chiral calculations in the mid-seventies. The comparison of our results with those obtained in the HB or IR formalisms highlights the importance of including the relativistic corrections in consistency with analyticity. On the other hand, we have also shown that the effects of the decuplet resonances are reasonably small whenever the spu-

rious degrees of freedom contained in the spin-3/2 fields are removed. The comparison within the HB (SSE) expansion of the covariant results shows that relativistic corrections are even more important for the decuplet contributions.

2.2 Electromagnetic structure of the decuplet

The analysis of the magnetic moments of the baryon octet can be extended to the investigation of the electromagnetic structure of the decuplet resonances. This is more complex because of the structure of the spin-3/2 fields and includes a magnetic dipole moment (MDM), which is equivalent to the conventional magnetic moment of spin-1/2 particles, a electric quadrupole moment (EQM) and an octupole magnetic moment (MOM). The fact that most of these particles decay strongly, $\tau \sim 10^{-23}s$ makes it extremely difficult to probe their properties in laboratories. Nevertheless, the MDMs of the Δ^{++} and of the Δ^+ have been the subject of various experimental projects and have been measured. In the former case, the radiative pion-nucleon scattering ($\pi^+p \rightarrow \pi^+p\gamma$) is analyzed although the results of the different experiments [111, 112] obtained in a model dependent way [113, 114] are not completely consistent. This is the reason behind the large uncertainties of the estimation quoted in the current Particle Data Group (PDG) review, $\mu_{\Delta^{++}} = 3.7 \sim 7.5 \mu_N$ [108]. On the other hand, the magnetic dipole moment of Δ^+ has been recently extracted from the radiative photo-production of neutral pions ($\gamma p \rightarrow \pi^0 p \gamma'$) first proposed in Ref. [115], $\mu_{\Delta^+} = 2.7_{-1.3}^{+1.0}(\text{stat}) \pm 1.5(\text{syst}) \pm 3(\text{theor}) \mu_N$ [116]. A new experiment with the Crystal Ball detector at MAMI is expected to give soon new results with improved statistics [117, 118] and using theoretical extraction methods based either on a dynamical model [119] or on chiral effective field theory [77]. Concerning the $SU(3)_F$ -multiplet partners of the $\Delta(1232)$ resonances only the magnetic dipole moment of the Ω^- (that decays weakly) has been measured, $\mu_{\Omega^-} = -2.02 \pm 0.05 \mu_N$ [108].

The electromagnetic properties of the decuplet resonances have been studied theoretically during the last two decades, and information not only on MDMs but also on other moments like the EQM, the MOM, or on the charge radius (CR) and the q^2 dependence of the form factors, have arisen from many different frameworks. Indeed, the electromagnetic structure of the decuplet baryons has been studied within the non relativistic quark model (NRQM) [120, 121], the relativistic quark model (RQM) [122], the chiral quark model (χ QM) [123, 124], the chiral quark soliton model (χ QSM) [125, 126], the spectator quark model (SpQM) [127, 128, 129], the general parametrization method (GP) [130, 131], QCD sum rules (QCD-SR) [132, 133, 134, 135], large N_c [136, 137, 138], chiral perturbation theory (χ PT) [72, 77, 139, 140, 141, 75, 142] and in LQCD [143, 144, 145, 146, 147, 148, 149, 150]. Lately, the LQCD calculations have experienced a remarkable progress that allows a quantitative description of these properties from first principles.

In the present section, we will use the covariant χ PT formalism to describe the leading $SU(3)_F$ -breaking of the electromagnetic static properties of the

decuplet baryons, and more particularly, of the $\Delta(1232)$ resonance. We present the predictions for the MDMs, the EQMs, the MOMs and the CRs that are compared with the results obtained in some of the approaches listed above. We will use the well measured MDM of the Ω^- and its EQM and CR calculated in LQCD to fix the various LECs appearing in χ PT up to $\mathcal{O}(p^3)$.

2.2.1 Formalism

The structure of the spin-3/2 particles, as probed by photons, is encoded into four electromagnetic form factors [143]

$$\begin{aligned} \langle T(p') | J^\mu | T(p) \rangle &= -\bar{u}_\alpha(p') \left\{ \left[F_1^*(\tau) \gamma^\mu + \frac{i\sigma^{\mu\nu} q_\nu}{2M_T} F_2^*(\tau) \right] g^{\alpha\beta} \right. \\ &\quad \left. + \left[F_3^*(\tau) \gamma^\mu + \frac{i\sigma^{\mu\nu} q_\nu}{2M_{T0}} F_4^*(\tau) \right] \frac{q^\alpha q^\beta}{4M_T^2} \right\} u_\beta(p), \end{aligned} \quad (2.18)$$

where u_α are the Rarita-Schwinger spinors, M_T is their mass and $\tau = -q^2/(4M_T^2)$. We can define the electric monopole and quadrupole and the magnetic dipole and octupole form factors in terms of the F_i^* 's:

$$G_{E0}(\tau) = (F_1^*(\tau) - \tau F_2^*(\tau)) + \frac{2}{3}\tau G_{E2}(\tau), \quad (2.19)$$

$$G_{E2}(\tau) = (F_1^*(\tau) - \tau F_2^*(\tau)) - \frac{1}{2}(1 + \tau)(F_3^*(\tau) - \tau F_4^*(\tau)), \quad (2.20)$$

$$G_{M1}(\tau) = (F_1^*(\tau) + F_2^*(\tau)) + \frac{4}{5}\tau G_{M3}(\tau), \quad (2.21)$$

$$G_{M3}(\tau) = (F_1^*(\tau) + F_2^*(\tau)) - \frac{1}{2}(1 + \tau)(F_3^*(\tau) + F_4^*(\tau)). \quad (2.22)$$

At $q^2 = 0$, the multipole form factors define the static electromagnetic moments, namely, the charge Q , the magnetic dipole moment μ , the electric quadrupole moment \mathcal{Q} and the magnetic octupole moment O

$$Q = G_{E0}(0) = F_1^*(0), \quad (2.23)$$

$$\mu = \frac{e}{2M_T} G_{M1}(0) = \frac{e}{2M_T} (Q + F_2^*(0)), \quad (2.24)$$

$$\mathcal{Q} = \frac{e}{M_T^2} G_{E2}(0) = \frac{e}{M_T^2} (Q - \frac{1}{2} F_3^*(0)), \quad (2.25)$$

$$O = \frac{e}{2M_T^3} G_{M3}(0) = \frac{e}{2M_T^3} \left(G_{M1}(0) - \frac{1}{2} (F_3^*(0) + F_4^*(0)) \right). \quad (2.26)$$

The electromagnetic multipole moments of the spin-3/2 resonances are connected with their spatial electromagnetic distributions and, therefore, with

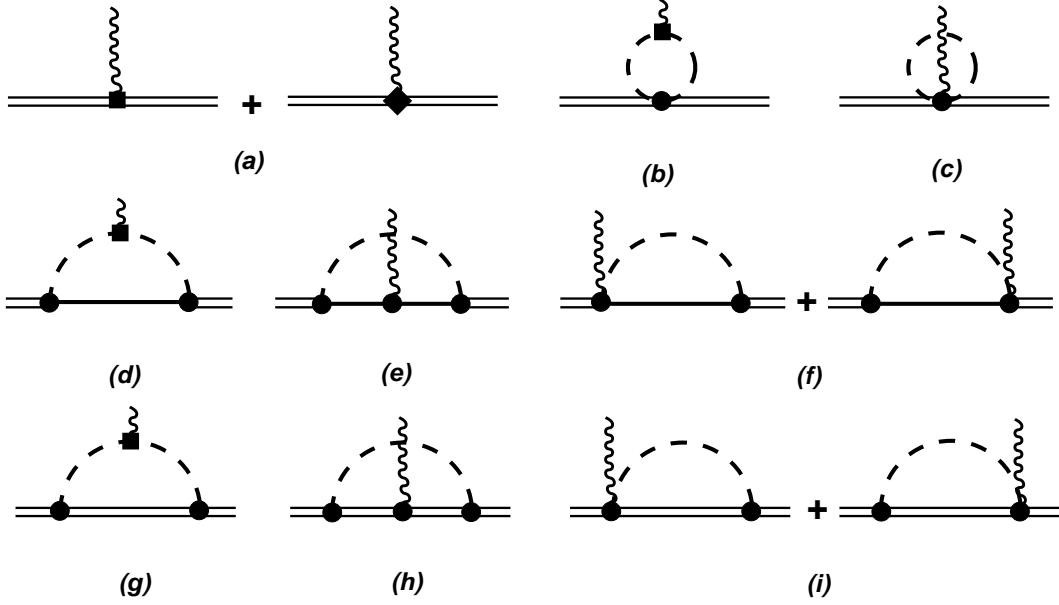


Figure 2.4: Feynman graphs that contribute up to $\mathcal{O}(p^3)$ to the decuplet electromagnetic form factors. The external double solid lines correspond to decuplet baryons, whereas the internal single (double) solid lines correspond to octet (decuplet) baryons. The dashed lines represent mesons. Black circles, black squares and black diamonds represent first-, second- and third-order couplings respectively.

their internal structure. Particularly, the EQM and MOM measure the departure from a spherical shape of the charge and from a dipole magnetic distribution respectively.

Besides the static electromagnetic moments, the slope of the form factors at $q^2 = 0$ is also of phenomenological interest. In particular the one corresponding to G_{E0} is the so-called squared CR:

$$\langle r_{E0}^2 \rangle = 6 \frac{dG_{E0}(q^2)}{dq^2} \Big|_{q^2=0} = 6 \frac{dF_1^*(q^2)}{dq^2} \Big|_{q^2=0} + \frac{3}{2M_T^2} F_2^*(0) - \frac{1}{M_T^2} G_{E2}(0). \quad (2.27)$$

The Feynman graphs that give contribution to the decuplet electromagnetic form factors are shown in Fig. 2.4. Up to third order, there are three terms in the chiral Lagrangian providing the tree-level contribution **(a)** to the

observables we are studying

$$\mathcal{L}_{\gamma DD}^{(2)} = -\frac{g_d}{8M_{T0}} \bar{T}_\mu^{abc} \sigma^{\rho\sigma} g^{\mu\nu} (F_{+\rho\sigma}, T_\nu)^{abc}, \quad (2.28)$$

$$\begin{aligned} \mathcal{L}_{\gamma DD}^{(3)} = & -\frac{g_q}{16M_{T0}^2} \bar{T}_\mu^{abc} \gamma^{\mu\rho\sigma} ((\partial^\nu F_{+\rho\sigma}), T_\nu)^{abc}, \\ & -\frac{g_{cr}}{12} \bar{T}_\mu^{abc} \gamma^{\mu\nu\sigma} ((\partial^\rho F_{+\rho\sigma}), T_\nu)^{abc}, \end{aligned} \quad (2.29)$$

where $(X, T_\mu)^{abc} \equiv (X)_d^a T_\mu^{dbc} + (X)_d^b T_\mu^{adc} + (X)_d^c T_\mu^{abd}$. The LEC g_d gives at $\mathcal{O}(p^2)$ the $SU(3)_F$ -symmetric description of the anomalous part of the MDMs of the decuplet baryons, while the LECs g_q and g_{cr} appear at $\mathcal{O}(p^3)$ and describe a $SU(3)_F$ -symmetric part of the EQMs and CRs respectively. Up to $\mathcal{O}(p^3)$ there is not any unknown LEC contributing exclusively to the MOM and, therefore it comes as a prediction from the chiral loops. Finally, it is worth to observe that working out the flavor-index summations in Eqs. (2.28) and (2.29), we find that the $SU(3)_F$ -symmetric contribution to the observables is proportional to the charge of the particular decuplet-baryon (see, e.g., Ref. [139]).

The loop contributions **(b)**-**(i)** in Fig. 2.4 to any of the four form factors for a particular decuplet-baryon T , $\delta F_{j,T}^*(\tau)$ with $j = 1, \dots, 4$ can be expressed as

$$\delta F_{j,T}^*(\tau) = \frac{1}{(4\pi F_\phi)^2} \sum_{\substack{\phi=\pi,K,\eta \\ \alpha=b,\dots,i}} \xi_{T\phi}^{(\alpha)} H_j^{(\alpha)}(\tau, m_\phi), \quad (2.30)$$

where $H_j^{(\alpha)}(\tau, m_\phi)$ are the loop-functions and $\xi_{T\phi}^{(\alpha)}$ the Clebsch-Gordan coefficients. The latter can be found in Table C.2 of Appendix C.2. The additional character that appears in (α) in the diagrams **(f)** and **(i)** indicates whether the seagull-diagram comes from the minimal substitution performed on the derivative of the meson fields (*I*) or of the decuplet fields (*II*). The loop-functions for $j = 2, \dots, 4$ at $q^2 = 0$, and the first derivative with respect to q^2 of the one for $j = 1$ at $q^2 = 0$ are given in Appendix C.2. All this information, together with Eq. (4.11), is what is required for obtaining, through the Eqs. (2.20)-(2.27), the loop results of the observables discussed in this section. The contact interactions, diagrams **(a)** in Fig. 2.4, provide the $SU(3)_F$ -symmetric contribution and ensure the regularization of the divergences coming from the loops up to $\mathcal{O}(p^3)$. They also allow to recover the power-counting by applying the EOMS renormalization scheme. The values for the couplings and parameters necessary for the computation of the loop graphs can be found in Appendix B.

We have done some checks on the calculation of the loops of Fig. 2.4. The first one concerns the electromagnetic gauge invariance as well as the completeness of the Lorentz decomposition of Eq. (2.18). Besides the structures

collected there, one also obtains contributions to $g^{\alpha\mu}q^\beta$ and $g^{\beta\mu}q^\alpha$ and to the electromagnetic-gauge violating ones, $g^{\alpha\beta}q^\mu$ and $q^\alpha q^\beta q^\mu$. In order to fit the results of the loops into the representation (2.18) we have used that [143]

$$g^{\beta\mu}q^\alpha = g^{\alpha\mu}q^\beta + 2M_{T0}(1 + \tau)g^{\alpha\beta}\gamma^\mu - g^{\alpha\beta}P^\mu + \frac{1}{M_{T0}}\gamma^\mu q^\alpha q^\beta, \quad (2.31)$$

where $P^\mu = p^\mu + p'^\mu$ and obtained that the resulting coefficients of $g^{\alpha\mu}q^\beta$, $g^{\alpha\beta}q^\mu$ and $q^\alpha q^\beta q^\mu$ are identically zero. On top of that, we have tested the electromagnetic-gauge invariance by checking that the loop contributions to the electric charge vanish after including the wave-function renormalization Σ'_T . Indeed, for each decuplet-baryon T of electric charge Q_T , we get $\delta F_{1,T}^*(0) + Q_T \Sigma'_T = 0$.

2.2.2 Results

In this section we present the results on the MDMs, the EQMs, MOMs and CRs obtained in covariant χ PT up to $\mathcal{O}(p^3)$ within the EOMS prescription. It is worth to start remarking that the following relations, which are a consequence of the assumed isospin symmetry, are fulfilled for any of these observables (\mathcal{X})

$$\begin{aligned} \mathcal{X}_{\Delta^{++}} - \mathcal{X}_{\Delta^+} - \mathcal{X}_{\Delta^0} + \mathcal{X}_{\Delta^-} &= 0, \\ \mathcal{X}_{\Delta^{++}} - \mathcal{X}_{\Delta^-} - 3(\mathcal{X}_{\Delta^+} - \mathcal{X}_{\Delta^0}) &= 0, \\ 2\mathcal{X}_{\Sigma^{*0}} &= \mathcal{X}_{\Sigma^{*+}} + \mathcal{X}_{\Sigma^{*-}}. \end{aligned} \quad (2.32)$$

Furthermore, among the $SU(3)_F$ -relations discussed in Ref. [140] two,

$$\mathcal{X}_{\Delta^0} + \mathcal{X}_{\Xi^{*0}} = 0, \quad (2.33)$$

$$\mathcal{X}_{\Sigma^{*0}} = 0, \quad (2.34)$$

still hold when the higher-order relativistic corrections are incorporated. The Eqs. (2.32)-(2.34) mean that only the electromagnetic form factors of five of the ten decuplet resonances are really independent in covariant χ PT up to $\mathcal{O}(p^3)$. In the HB expansion only two of them are independent [140].

The loop diagrams **(g)**-**(i)** that include virtual decuplet fields produce higher-order divergences as it was explained in Section 1.4. The numerical results that we present in the following are obtained fixing the EOMS-renormalization scale at $\mu = 1$ GeV. We include an uncertainty estimated varying the renormalization scale and the mean baryon mass (keeping the mass splitting $M_{T0} - M_{B0} = 0.231$ GeV fixed) in the intervals $0.7 \text{ GeV} \leq \mu \leq 1.3 \text{ GeV}$ and $1 \text{ GeV} \leq M_{B0} \leq 1.3 \text{ GeV}$. In the case of the MDMs we estimate the higher-order corrections by taking 1/2 of the difference between the results obtained at LO and NLO.

Table 2.3: Values in nuclear magnetons (μ_N) of the different contributions to the MDMs of Δ^{++} , Δ^+ , Σ^{*+} , Ξ^{*-} and Ω^- after fitting the value of \hat{g}_d to obtain $\mu_{\Omega^-} = -2.02(5)$. For the MDM of each baryon we show the results either in HB or covariant χ PT separated into the $\mathcal{O}(p^2)$ tree-level (TL) contribution, the $\mathcal{O}(p^3)$ chiral loop contributions coming from internal octet-baryons (B), the $\mathcal{O}(p^3)$ chiral loop contributions coming from internal decuplet-baryons (T) and the total final values. We also list the fitted value of \hat{g}_d .

	HB $\mathcal{O}(p^3)$				Covariant $\mathcal{O}(p^3)$			
\tilde{g}_d	7.64				4.71			
Cont.	TL	B	T	Total	TL	B	T	Total
Δ^{++}	11.75	-2.85	-0.96	7.94	7.76	-1.09	-0.63	6.04
Δ^+	5.87	-1.98	-0.57	3.32	3.88	-0.70	-0.34	2.84
Σ^{*+}	5.87	-0.86	-0.39	4.62	3.88	-0.46	-0.35	3.07
Ξ^{*-}	-5.87	+1.98	+0.57	-3.32	-3.88	+0.89	+0.44	-2.55
Ω^-	-5.87	+3.11	+0.75	-2.02	-3.88	+1.34	+0.52	-2.02

Magnetic dipole moments

The MDMs are the only observable among those discussed in this chapter for which there exist experimental data. More precisely, the MDM of the Δ^{++} , the Δ^+ and the Ω^- have been measured. In order to obtain the MDMs of the different members of the decuplet in χ PT, we calculate the contributions to $F_2^*(0)$ of the diagrams listed in Figure 2.4 and use Eq. (2.24). We apply the EOMS prescription performing a redefinition of the LEC g_d as explained in Appendix C.2. From the renormalized loop functions $\tilde{H}^{(\alpha)}$ we can then obtain the HB limit applying that $M_{T0} = M_{B0} + \delta$ (SSE) and $M_{B0} \sim \Lambda_{\chi SM}$. The HB formulas are displayed in the Appendix C.2 and they agree with the ones that have been obtained previously by other groups [140].

Since the only precise experimental value on the decuplet MDMs is used to determine the unknown LEC \tilde{g}_d , it is not really possible to directly compare the quality of the HB and covariant χ PT results confronted to experimental data. Nonetheless, we can compare the convergence properties of both schemes. In Table 2.3, we show the values in nuclear magnetons (μ_N) of the different contributions to the MDMs of Δ^{++} , Δ^+ , Σ^{*+} , Ξ^{*-} and Ω^- after fitting the value of \tilde{g}_d to obtain $\mu_{\Omega^-} = -2.02(5)$. The equivalent information for the rest of the decuplet resonances can be obtained using Eqs. (2.32), (2.33) and (2.34). For the MDM of each baryon we show the results either in HB or covariant χ PT

Table 2.4: Values in nuclear magnetons (μ_N) of the decuplet magnetic dipole moments in Lorentz covariant chiral perturbation theory up to $\mathcal{O}(p^3)$ calculated in this work. The theoretical error bars quoted for these results are estimated taking 1/2 of the NLO contributions. We compare our results with the $SU(3)_F$ -symmetric description and with those obtained in the large N_c [136] and in (extrapolated) LQCD [144]. The experimental values are also included for reference [108].

	$SU(3)_F$	HB	Cov.	Large N_c [136]	LQCD [144]	Expt. [108]
Δ^{++}	4.04	7.94	6.0(1.0)	5.9(4)	6.09(88)	5.6 ± 1.9
Δ^+	2.02	3.32	2.84(50)	2.9(2)	3.05(44)	$2.7_{-1.3}^{+1.0} \pm 1.5 \pm 3$
Δ^0	0	-1.3	-0.36(18)	—	0	
Δ^-	-2.02	-5.92	-3.6(5)	-2.9(2)	-3.05(44)	
Σ^{*+}	2.02	4.62	3.07(40)	3.3(2)	3.16(40)	
Σ^{*0}	0	0	0	0.3(1)	0.329(67)	
Σ^{*-}	-2.02	-4.62	-3.07(40)	-2.8(3)	-2.50(29)	
Ξ^{*0}	0	1.30	0.36(18)	0.65(20)	0.58(10)	
Ξ^{*-}	-2.02	-3.32	-2.6(7)	-2.30(15)	-2.08(24)	
Ω^-	-2.02*	-2.02*	-2.02*	-1.94*	-1.73(22)	

separated into the $\mathcal{O}(p^2)$ tree-level (TL) contribution, the $\mathcal{O}(p^3)$ chiral loop contributions coming from internal octet-baryons (B) and the $\mathcal{O}(p^3)$ chiral loop contributions coming from internal decuplet-baryons (T).

For any of the five baryons displayed in Table 2.3, we observe that the HB loop contributions are larger than the covariant ones. The main difference arises from the loops with internal octet-baryons for which HB gives more than two times the covariant approach for most of the channels. The chiral corrections with internal decuplet-baryons in the two schemes are rather more similar, with the HB ones about 50% larger than those obtained in the covariant calculation. Particularly for the Δ^{++} , we find that the heavy-baryon prediction $\mu_{\Delta^{++}} = 7.94 \mu_N$ is bigger than the upper bound provided by the PDG, $\mu_{\Delta^{++}} \leq 7.5 \mu_N$ [108]. These comparisons suggest that the heavy-baryon expansion probably overestimates the size of the chiral corrections to the MDMs of the decuplet resonances as it occurred for the case of the baryon-octet magnetic moments.

In Table 2.4 we compare the results on the MDMs obtained in the HB

Table 2.5: Values of the loop contributions to the electric quadrupole moments of the decuplet resonances in Lorentz covariant chiral perturbation theory up to $\mathcal{O}(p^3)$ (in units of 10^{-2} fm^2) in a renormalization prescription in which $\tilde{g}_q = \mathcal{Q}_{\Omega^-}$.

Δ^{++}	Δ^+	Δ^0	Δ^-	Σ^{*+}
-0.9(3.3)	-1.6(1.5)	-2.20(24)	-2.8(2.0)	+1.9(1.3)
Σ^{*0}	Σ^{*-}	Ξ^{*0}	Ξ^{*-}	Ω^-
0	-1.9(1.3)	2.20(24)	-1.0(0.6)	0

and covariant χ PT approaches with those in the $SU(3)_F$ -symmetric limit or $\mathcal{O}(p^2)$, in large N_c [136] and in (extrapolated) LQCD [144]. A more exhaustive comparison with the values predicted in many other theoretical frameworks can be found in [4]. We also list the experimental values as averaged by the PDG [108]. In general, our results are consistent with the central value of the experimental numbers for $\mu_{\Delta^{++}}$ and μ_{Δ^+} . Moreover, for the former our results agree very satisfactorily with the latest experimental analysis, $\mu_{\Delta^{++}} = 6.14 \pm 0.51$ [114].

The covariant χ PT results are also consistent with those obtained in the other approaches, although some caution should be exercised with the LQCD results [144] since the chiral extrapolation has been performed without taking into account the non-trivial analytical structure across the point $m_\phi = M_{T0} - M_{B0}$ [72] and the artifacts introduced by the quenched approximation at such values of m_ϕ . The present work is also to be compared with studies focused on the MDM of the $\Delta(1232)$ resonance. We find that the values predicted in covariant χ PT are larger than those found in LQCD ($\mu_{\Delta^+} = 2.32(16)\mu_N$ [147], $\mu_{\Delta^+} = 2.49(27)\mu_N$ [145]), in the SpQM ($\mu_{\Delta^+} = 2.51\mu_N$ [127]) and with light cone QCD-SRs ($\mu_{\Delta^+} = 2.2(4)\mu_N$ [133]).

Electric quadrupole moments

Although so far there is not experimental information on the EQMs of the decuplet, they have motivated several theoretical studies in the past. Their interest lie in that they provide information on the deviation from a spherical shape of the charge distribution and, consequently, on the internal structure of the spin-3/2 resonances. To obtain the covariant χ PT results for the EQMs it is required to determine the unknown LEC g_q and use Eq. (2.20) after evaluating the loop contributions given by the diagrams of Fig. 2.4. The LEC g_q could be fixed with an eventual experimental value of the EQM of one of the members of

Table 2.6: Values of the electric quadrupole moments in units of 10^{-2} fm^2 in different theoretical approaches. We compare the results obtained using the latest quenched LQCD result [150] in combination with the relativistic chiral corrections (Table 2.5) with those obtained in the NRQM [121], in χ QM [124], in GP [130] and in light cone QCD-SR [134, 135].

	Cov.+LQCD	NRQM [121]	χ QM [124]	GP [130]	QCD-SR [134, 135]
Δ^{++}	-2.7(3.3)	-9.3	-25.2	-22.6	-2.8(8)
Δ^+	-2.4(1.5)	-4.6	-12.6	-11.3	-1.4(4)
Δ^0	-2.20(24)	0	0	0	0
Δ^-	-2.0(2.0)	4.6	12.6	11.3	1.4(4)
Σ^{*+}	1.1(1.3)	-5.4	-12.3	-1.7	-2.5(8)
Σ^{*0}	0	-0.7	-2.1	-1.7	0.1(3)
Σ^{*-}	-1.1(1.3)	4.0	8.2	7.4	3(1)
Ξ^{*0}	2.20(24)	-1.3	-3.0	-2.3	0.23(7)
Ξ^{*-}	-0.1(6)	3.4	4.8	4.4	4(1)
Ω^-	0.86*	2.8	2.6	2.4	10(3)

the decuplet-baryons, most likely the one of the Ω^- (for proposed experimental methods to measure it we refer to Ref. [130] and references therein). An alternative source of information could come from LQCD since the properties of the Ω^- can be obtained at the physical point and, consequently, a full-dynamical LQCD (unquenched) calculation of its electromagnetic properties could be reached in the near future. Once this value is used to determine g_q , χ PT provides a prediction on the EQMs of the rest of the decuplet-baryons and, in particular of the $\Delta(1232)$. Therefore, it is particularly interesting to express the χ PT results of the EQMs for the decuplet in terms of the EQM of the Ω^- . This is done just redefining g_q

$$\tilde{g}_q = g_q + \delta Q_{\Omega^-}, \quad (2.35)$$

where δQ_{Ω^-} is the loop contribution to the EQM of the Ω^- , and \tilde{g}_q would then mean the physical Q_{Ω^-} . In Table 2.5 we list the results obtained for the loop contributions to the EQMs of the decuplet in covariant χ PT up to $\mathcal{O}(p^3)$ in the renormalization prescription of Eq. (2.35). The full results are obtained adding the contribution of the LEC \tilde{g}_q that is proportional to the charge of the corresponding baryon. If in a first approximation we use the

Table 2.7: Values in units of $e/(2M_N^3)$ of the magnetic octupole moments of the members of the decuplet resonances in covariant chiral perturbation theory up to $\mathcal{O}(p^3)$ where $\tilde{\mathcal{Q}} = (\mathcal{Q}_{\Omega^-}/M_{T0}) [e/(2M_N^3)]$ (see text).

Δ^{++}	Δ^+	Δ^0	Δ^-	Σ^{*+}
$-2\tilde{\mathcal{Q}} - 1.6(4.2)$	$-\tilde{\mathcal{Q}} - 0.8(2.1)$	$0.026(16)$	$\tilde{\mathcal{Q}} + 0.8(2.1)$	$-\tilde{\mathcal{Q}} - 0.5(2.0)$
Σ^{*0}	Σ^{*-}	Ξ^{*0}	Ξ^{*-}	Ω^-
0	$\tilde{\mathcal{Q}} + 0.5(2.0)$	$-0.026(16)$	$\tilde{\mathcal{Q}} + 0.3(1.9)$	$\tilde{\mathcal{Q}} + 0(1.7)$

quenched LQCD result $\mathcal{Q}_{\Omega^-} = 0.86(12)10^{-2} \text{ fm}^2$ [150] to fix g_q , we obtain the results displayed in Table 2.6 compared with those obtained in NRQM [121], χ QM [124] and in QCD-SR [134, 135]. We observe that with this value of \mathcal{Q}_{Ω^-} , the loop contributions are quite large and the EQMs of the decuplet-baryons are dominated by the chiral $SU(3)_F$ -breaking corrections¹.

We can also compare with calculations focused on the $\Delta(1232)$ isospin multiplet. The result on the Δ^+ given in Table 2.6, $\mathcal{Q}_{\Delta^+} = -2.5(1.5)10^{-2} \text{ fm}^2$, marginally agrees with recent theoretical determinations within the χ QSM ($\mathcal{Q}_{\Delta^+} = -5.09 \cdot 10^{-2} \text{ fm}^2$ [126]) and the SpQM ($\mathcal{Q}_{\Delta^+} = -4.2 \cdot 10^{-2} \text{ fm}^2$ [128]).

Magnetic Octupole Moments

The MOMs of the decuplet baryons are experimentally unknown and only few theoretical predictions are available. Their interest also lie in that they contain information on the internal structure of the spin-3/2 baryons, more precisely on the current and spin distribution beyond the dipole form one given by the MDMs. From the χ PT perspective, there are no LECs contributing exclusively to the MOMs up to $\mathcal{O}(p^3)$, although they depend on the ones that contribute to the MDMs, g_d , and to the EQMs, g_q (see Eq. (2.26)). Once these LECs are fixed, the MOMs come as a true prediction from the chiral loops in the covariant formalism. In the HB scheme, the loop contributions to the MOMs are at least of order $\mathcal{O}(p^4)$ so that the relativistic results could be considered from that perspective as pure recoil corrections. In Table 2.7, we show the results for the MOMs once \tilde{g}_d is fixed with the Ω^- MDM and the g_q dependence is introduced in terms of the Ω^- EQM (in the proper units $\tilde{\mathcal{Q}} = (\mathcal{Q}_{\Omega^-}/M_{T0}) [e/(2M_N^3)]$).

¹These results are consistent with those that one obtains using the recent unquenched LQCD calculation of Ref [151]. For instance, the value obtained in this calculation $\mathcal{Q}_{\Omega^-} = 0.898(60) e/M_{\Omega^-}^2$, leads to $\mathcal{Q}_{\Delta^+} = -2.8(1.5) \cdot 10^{-2} \text{ fm}^2$

Table 2.8: Values in units of $e/(2M_N^3)$ of the magnetic octupole moments of the members of the decuplet resonances in different theoretical approaches.

	Cov.+LQCD	GP [131]	QCD-SR [134, 135]
Δ^{++}	-1.8(4.2)	-5.2	-1.3(4)
Δ^+	-0.9(2.1)	-2.6	-0.65(21)
Δ^0	0.026(16)	0	0
Δ^-	1.0(2.1)	2.6	0.65(21)
Σ^{*+}	-0.7(2.0)	-0.87	-2.6(9)
Σ^{*0}	0	0.43	-0.11(2)
Σ^{*-}	0.7(2.0)	1.7	2.6(9)
Ξ^{*0}	-0.026(16)	0.43	-0.28(11)
Ξ^{*-}	0.4(1.9)	1.1	2.2(9)
Ω^-	0.2(1.8)	0.7	3.3(1.1)

If we use again the value obtained in quenched LQCD [150] for the Ω^- EQM, $\tilde{Q} = 0.113 e/(2M_N^3)$, we obtain the results displayed in the last row of Table 2.8. Moreover, in the same table we also collect the ones obtained previously in the general parameterization method [131] and in light-cone QCD sum-rules [134, 135]. Our results favor a negative value for the MOM of the Δ^+ , in agreement with those obtained in the two latter approaches. Remarkably, our prediction for O_{Ω^-} agrees with the recent determination from the same quenched LQCD calculation² used to fix \tilde{Q} , $O_{\Omega^-} = 0.2(1.2)e/(2M_N)^3$ [150].

Charge radii

In Table 2.9, we show the loop results for the leading $SU(3)_F$ -breaking corrections to the quadratic CR of the decuplet baryons within a renormalization prescription in which the LEC g_{cr} is equivalent to the one performed for the EQMs, Eq. (2.35). This LEC could be determined either from experiment or, in a model independent way, from LQCD. A remarkable feature of the chiral corrections to the squared CR is that they are quite small. Taking the value from quenched LQCD for the Ω^- , $r_{\Omega^-}^2 = -0.307(15)$ [150], we observe that the calculated chiral loops represent less than a 10% correction to the $SU(3)_F$ -symmetric prediction. Therefore, we may anticipate that the description of

²The presented results also agree with those obtained the unquenched LQCD result for Q_{Ω^-} reported in Ref. [151].

Table 2.9: Values in units of fm^2 of loop contributions to the squared CR of the members of the decuplet resonances in Lorentz covariant χPT up to $\mathcal{O}(p^3)$ in a renormalization prescription in which $g_{cr} = r_{\Omega^-}^2$.

Δ^{++}	Δ^+	Δ^0	Δ^-	Σ^{*+}
+0.035(13)	+0.021(6)	0.006(1)	-0.009(8)	+0.008(6)
Σ^{*0}	Σ^{*-}	Ξ^{*0}	Ξ^{*-}	Ω^-
0	-0.008(6)	-0.006(1)	-0.005(3)	0

the CR is dominated by short-range physics. Moreover, using the value from the lattice we can predict the CR of the rest of the decuplet baryons and, in particular, of the $\Delta(1232)$ isospin multiplet. Indeed, we obtain for the Δ^+ a quadratic radii $r_{E0}^2 = 0.328(16) \text{ fm}^2$ that we can compare with recent results obtained in the χQM ($r_{E0}^2 = 0.781 \text{ fm}^2$ [123]), the χQSM ($r_{E0}^2 = 0.794 \text{ fm}^2$ [126]), the SpQM ($r_{E0}^2 = 0.325 \text{ fm}^2$ [127]) and in LQCD ($r_{E0}^2 = 0.477(8) \text{ fm}^2$ [147]).

2.2.3 Summary

In summary, we have studied the electromagnetic static properties of the lowest-lying decuplet of baryons in covariant χPT , with special attention given to the $\Delta(1232)$ isospin multiplet. The MDMs are of most relevance since they are the only diagonal electromagnetic observables for which there exist some experimental information. By fixing the only LEC appearing up to $\mathcal{O}(p^3)$ with the MDM of the Ω^- the covariant χPT prediction is that $\mu_{\Delta}^{++} = 6.0(1.0) \mu_N$ and $\mu_{\Delta}^+ = 2.84(20) \mu_N$, which are very close to the central values of the current PDG [108]. Moreover, our agreement with the latest experimental value for the $\Delta^{++} = \mu_{\Delta}^{++} = 6.14 \pm 0.51$ [114] is excellent. Nevertheless, the PDG averages are still afflicted with large uncertainties and the results coming from any of the theoretical approaches collected in Table 2.4 are consistent with the current experimental information. Therefore the new and high precision data for the MDM of the Δ^+ that is expected to come soon [117] will be extremely valuable to assess the quality of the different theoretical predictions.

We have also studied the higher-order electromagnetic multipoles, the EQMs and the MOMs, and the CR. These properties that give insight into the spin-3/2 internal structure have been receiving increasing attention lately. Although experimental data is not available yet and it is doubtful it will be in a near future, the rapid development of LQCD could lead soon to model-independent

results on these observables. In covariant χ PT, the EQMs, the MOMs and the CRs depend on two unknown LECs that we have related with the CR and the EQM of the Ω^- , which is the decuplet baryon for which reliable information is expected to come sooner. With the current results obtained in quenched LQCD, we predict for the $\Delta(1232)$ values of these observables that are consistent with other approaches. In particular we predict negative values for the EQM and MOM of the Δ^+ , and a squared CR that is almost half that of the proton. Concerning the future of LQCD in the evaluation of the observables discussed in this work, we want to stress the non-trivial analytical structure across the point $m_\phi = M_{T0} - M_{B0}$ unveiled by different χ PT studies. In this regard we want to highlight that the present calculation provides for the first time the covariant χ PT $\mathcal{O}(p^3)$ results including the contributions of octet- and decuplet-baryons and may be helpful to extrapolate the LQCD results.

Hyperon semileptonic decays

The Cabibbo-Kobayashi-Maskawa (CKM) matrix [152, 153] plays an essential role in our understanding of flavor physics. In particular, its first row allows for a precise test of the SM through the CKM unitarity relation,

$$|V_{ud}|^2 + |V_{us}|^2 + |V_{ub}|^2 = 1, \quad (3.1)$$

where one needs values for V_{ud} , V_{us} , and V_{ub} . Among them, V_{ub} is quite small and can be neglected at the present accuracy [108]. The element V_{ud} can be obtained from super-allowed nuclear β -decays [154], from the neutron decay lifetime and the axial charge g_A (see the Review in Ref. [108]) or from π decays [155]. The first among the previous methods provides a well established determination

$$V_{ud} = 0.97425(22), \quad (3.2)$$

that leads to the following value for V_{us} consistent with the CKM-matrix unitarity condition of Eq. (3.1)

$$V_{us}^U = 0.2254(10). \quad (3.3)$$

The CKM matrix element V_{us} can be extracted from kaonic decays [156], kaonic and pionic decay ratios with LQCD determinations of f_K/f_π [157, 158], hadronic τ decays [159] or semileptonic hyperon decays [160, 3]. The latest determinations from $K_{\ell 3}$ decays and the f_K/f_π ratio give the values $V_{us} = 0.2254(13)$ [156] and $V_{us} = 0.2256(18)$ [158] respectively, which are completely consistent with the unitarity one of Eq. (3.3). A smaller value has been obtained from the τ decays, $V_{us} = 0.2208(34)$, although a recent analysis of the BaBar collaboration finds a result in agreement with Eq. (3.3), $V_{us} = 0.2255(24)$ [161].

In the case of the hyperon semileptonic decays, an accurate determination of V_{us} can be achieved only if certain baryonic matrix elements are well known. In particular, a precise knowledge of the value of the hyperon vector coupling $f_1(0)$ is required [160, 162]. As a consequence of the conservation of the vector current, the Ademollo-Gatto theorem [163] states that $f_1(0)$ does not receive leading $SU(3)_F$ -breaking corrections. Taking a $SU(3)_F$ -symmetric model and ignoring other subleading contributions one again obtains a value in agreement with Eq. (3.3), $V_{us} = 0.2250(27)$ [160, 162]. However, the error band does not include theoretical uncertainties and the subleading contributions have a sizable impact on the value of the extracted V_{us} [164, 165, 3].

The calculation presented here [3] updates previous studies in χ PT [166, 167, 168, 169] focusing on the effects of the $SU(3)_F$ -breaking of $f_1(0)$ which are expected to provide the dominant corrections [164]. In this chapter we present the calculation of these corrections up to $\mathcal{O}(p^4)$ or NNLO in the chiral expansion and show the effect they have in the determination of V_{us} from hyperon semileptonic decay data.

3.1 Formalism

3.1.1 Hyperon semileptonic decays

We consider the hyperon semileptonic decay

$$B_1 \rightarrow B_2 + \ell + \bar{\nu}_\ell, \quad (3.4)$$

where B_1 and B_2 are octet baryons, ℓ is the charged lepton ($\ell = e, \nu$), and $\bar{\nu}_\ell$ is the accompanying antineutrino or neutrino. We find five different strangeness changing hyperon decays (that we denote as $B_1 B_2$) that have been measured, Λp , $\Sigma^- n$, $\Xi^- \Lambda$, $\Xi^- \Sigma^0$ and $\Xi^0 \Sigma^+$. These decays can be studied using the low-energy weak interaction Hamiltonian for semileptonic processes

$$H_W = \frac{G_F}{\sqrt{2}} J_\alpha L^\alpha + \text{H.c.}, \quad (3.5)$$

where G_F is the Fermi weak coupling and L_α and J_α denote the leptonic and hadronic currents, respectively. The former is given by

$$L^\alpha = \bar{\psi}_e \gamma^\alpha (1 - \gamma_5) \psi_{\nu_e} + \bar{\psi}_\mu \gamma^\alpha (1 - \gamma_5) \psi_{\nu_\mu}, \quad (3.6)$$

while J^α have a $V - A$ structure, being V and A the vector and axial currents respectively

$$V^\alpha = V_{us} \bar{u} \gamma^\alpha s, \quad (3.7)$$

$$A^\alpha = V_{us} \bar{u} \gamma^\alpha \gamma_5 s. \quad (3.8)$$

The baryonic matrix elements of J^α can be expressed in terms of six form factors

$$\begin{aligned} \langle B_2 | V^\alpha | B_1 \rangle = \\ V_{us} \bar{u}_2(p_2) \left[f_1(q^2) \gamma^\alpha + \frac{2f_2(q^2)}{M_1 + M_2} \sigma^{\alpha\beta} q_\beta + \frac{2f_3(q^2)}{M_1 + M_2} q^\alpha \right] u_1(p_1), \end{aligned} \quad (3.9)$$

$$\begin{aligned} \langle B_2 | A^\alpha | B_1 \rangle = \\ V_{us} \bar{u}_2(p_2) \left[g_1(q^2) \gamma^\alpha + \frac{2g_2(q^2)}{M_1 + M_2} \sigma^{\alpha\beta} q_\beta + \frac{2g_3(q^2)}{M_1 + M_2} q^\alpha \right] \gamma_5 u_1(p_1), \end{aligned} \quad (3.10)$$

where p_i and M_i are the four-momentum and mass of the initial ($i = 1$) or final ($i = 2$) baryon in Eq. (3.4), $q \equiv p_1 - p_2$ is the four-momentum transfer and u_1 and \bar{u}_2 are the Dirac spinors of the corresponding hyperons. The functions $f_1(q^2)$ and $g_1(q^2)$ are called the vector and axial form factors, $f_2(q^2)$ and $g_2(q^2)$ the weak magnetic and electric form factors, and $f_3(q^2)$ and $g_3(q^2)$ the induced scalar and pseudoscalar form factors, respectively. The contributions of $f_3(q^2)$ and $g_3(q^2)$ for electron emission give negligible contributions to the decay rate due to the smallness of the factor (m_ℓ/M_1) appearing in the contraction with the leptonic vector L^α . Therefore, to a high degree of accuracy, the e -modes of the hyperon semileptonic decays studied here are described in terms of four, rather than six, form factors.

The decay rate of the semileptonic decay will then be determined by these form factors, the Fermi constant G_F , and the CKM element V_{us} . Indeed, if we define as a relevant $SU(3)_F$ -breaking parameter $\beta = \frac{M_1 - M_2}{M_1}$, we can perform a power expansion of the uncorrected decay rate R^0 about the $SU(3)_F$ -symmetric limit

$$\begin{aligned} R^0 = G_F^2 V_{us}^2 \frac{(M_1 - M_2)^5}{60\pi^3} \left(\left(1 - \frac{3}{2}\beta + \frac{6}{7}\beta^2\right) f_1^2 + \frac{4}{7}\beta^2 f_2^2 + \left(3 - \frac{9}{2}\beta + \frac{12}{7}\beta^2\right) g_1^2 \right. \\ \left. + \frac{12}{7}g_2^2 + \frac{6}{7}\beta^2 f_1 f_2 + (-4\beta + 6\beta^2) g_1 g_2 + \mathcal{O}(\beta^3) \right), \end{aligned} \quad (3.11)$$

where the form factors are evaluated at $q^2 = 0$, although a linear q^2 dependence in f_1 and g_1 must also be considered at this order [165]. To extract V_{us} accurately from semileptonic hyperon decay data, one requires to understand the $SU(3)_F$ -breaking pattern of the form factors in the Eq. (3.11). Moreover, it is also necessary to consider the radiative corrections. These can be implemented using $R = R^0 \cdot [1 + (\alpha/\pi)\Phi]$ with Φ a function describing a model-independent part [165]. A model-dependent part of the radiative corrections

can be absorbed into the G_F measured in μ decays, $G_F = 1.166371(6) \cdot 10^{-5} \text{ GeV}^{-2}$ [170].

Among the contributions of the different form factors to the corrected rate R , the $SU(3)_F$ -symmetric limit for f_2 can be used. The g_2 vanishes in the symmetric limit and we will assume thereafter that $g_2 = 0$. The axial charge g_1 , which is described in the symmetric limit by the LECs D and F , receives $\mathcal{O}(\beta)$ breaking corrections. Nevertheless, as it has been proposed in Ref. [162], we can use the measured g_1/f_1 ratios as the basic experimental data to equate g_1 in terms of f_1 in Eq. (3.11). Therefore, at first instance, all the knowledge on the baryonic structure we need to accurately extract V_{us} from semileptonic hyperon decay data reduces to the value of $f_1(0)$ that receives $SU(3)_F$ -breaking correction starting at $\mathcal{O}(\beta^2)$ as stated by the Ademollo-Gatto Theorem. One recovers the Cabibbo model of Ref. [162] upon the same assumptions as above and taking the symmetric value for $f_1(0)$.

3.1.2 χ PT calculation of $f_1(0)$

The Ademollo-Gatto theorem is a consequence of the underlying $SU(3)_F$ symmetry of QCD, which has also important consequences when addressing a calculation of $f_1(0)$ in χ PT. Namely, one finds no unknown LECs contributing to this vector charge up to $\mathcal{O}(p^5)$. Therefore, a loop calculation up to and including NNLO only depends on known masses and couplings and is a genuine prediction of χ PT (we use again the values listed in Appendix B). Moreover, there are not ultraviolet divergences or power counting breaking terms up to this order and none of the counting restoration procedures introduced in Sec. 1.3.2 are necessary in this case.

The Feynman graphs contributing to the hyperon vector coupling $f_1(0)$ up to $\mathcal{O}(p^4)$ or NNLO in χ PT are drawn in Fig. 3.1. The coupling with the external weak strangeness-changing current is obtained using the external field method (Sec. 1.2.3)

$$r^\mu = 0, \quad l^\mu = -V_{us} \frac{g}{\sqrt{2}} (T_+ W_\mu^+ + \text{h.c.}), \quad (3.12)$$

where W_μ^\pm are the massive weak charged bosons, g the weak coupling and $T_+ = (\lambda_4 + i\lambda_5)/2$, with λ_4 y λ_5 Gell-Mann matrices that can be found in Appendix A. The weak coupling is related to the Fermi constant and the mass of the W_μ^\pm boson M_W through

$$G_F = \sqrt{2} \frac{g^2}{8M_W^2}. \quad (3.13)$$

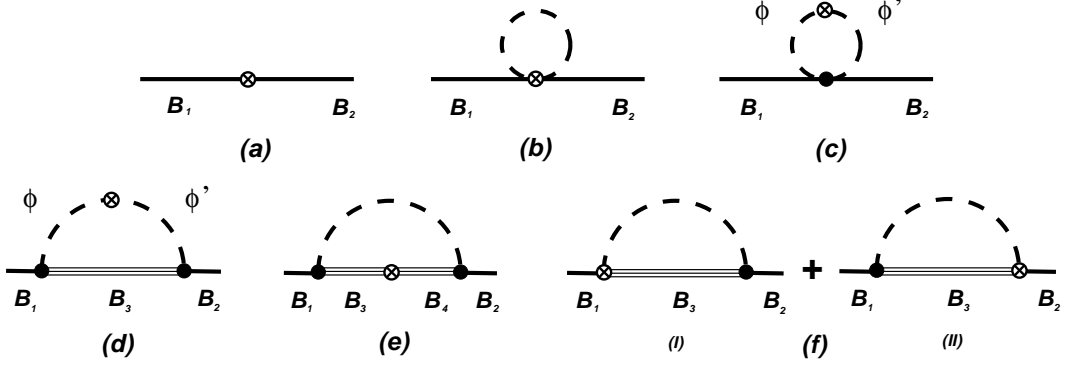


Figure 3.1: Feynman diagrams contributing to the hyperon vector charge $f_1(0)$ up to $\mathcal{O}(p^4)$ in χ PT. The solid external lines correspond to the initial and final baryons, the triple lines to either octet or decuplet-baryons and dashed lines to mesons. The black dots indicate meson-baryon 1^{st} -order couplings and the crossed dots represent the coupling of the external weak-vector current which also is of 1^{st} -order. The fourth-order contributions is accounted for by the inclusion of the leading $SU(3)_F$ -breaking corrections to the mass of any of the baryons in the diagrams.

At leading order we find

$$f_1(0) = g_V, \quad (3.14)$$

where the values of g_V are $-\sqrt{\frac{3}{2}}$, $-\frac{1}{\sqrt{2}}$, -1 , $\sqrt{\frac{3}{2}}$, $\frac{1}{\sqrt{2}}$, 1 for $\Lambda \rightarrow p$, $\Sigma^0 \rightarrow p$, $\Sigma^- \rightarrow n$, $\Xi^- \rightarrow \Lambda$, $\Xi^- \rightarrow \Sigma^0$, and $\Xi^0 \rightarrow \Sigma^+$, respectively. In the isospin-symmetric limit only four of these channels, which we take as $\Lambda \rightarrow N$, $\Sigma \rightarrow N$, $\Xi \rightarrow \Lambda$, and $\Xi \rightarrow \Sigma$, provide independent information. We will parameterize the $SU(3)_F$ -breaking corrections order-by-order in the relativistic chiral expansion as follows

$$f_1(0) = g_V (1 + \delta^{(2)} + \delta^{(3)} + \dots), \quad (3.15)$$

where $\delta^{(2)}$ and $\delta^{(3)}$ are $SU(3)_F$ -breaking corrections corresponding to $\mathcal{O}(p^3)$ (NLO) and $\mathcal{O}(p^4)$ (NNLO) in the chiral expansion.

The loop graphs in Fig. 3.1 give the $\mathcal{O}(p^3)$ contribution to $f_1(0)$ when the octet- and decuplet-baryons have the masses M_{B_0} and M_{T_0} respectively. At $\mathcal{O}(p^4)$, there are many new diagrams that may contribute to $f_1(0)$ like the tadpoles diagrams (b) and (c) but with $\mathcal{O}(p^2)$ $\phi\phi BB$ vertices. However, one can see that the only new contributions are those arising from the loop diagrams (d)-(f) when the splittings at $\mathcal{O}(p^2)$ in the chiral expansion of the baryon masses are considered. Namely, we implement them as given by Eqs. (4.8)

and (4.9) that describe the leading $SU(3)_F$ -breaking corrections to the masses (see Chap. 4 for details). Moreover, we do not expand the resulting expressions in powers of the baryon mass-shifts, procedure that would give exactly the $\mathcal{O}(p^4)$ contribution in the covariant approach. We instead include their corrections to all orders coming from both the on-mass shell condition in the external baryons ($p_1^2 = M_1^2$, $p_2^2 = M_2^2$) and the dressed propagator of the internal baryons. This procedure introduces divergences of order larger than $\mathcal{O}(p^4)$ that we regularize using the higher-order chiral Lagrangian in the \overline{MS} -scheme. We do not introduce the corresponding LECs explicitly but study the effect of the renormalization scale dependence in the range $0.7 \text{ GeV} \leq \mu \leq 1.2 \text{ GeV}$ (as in the case of the decuplet contributions discussed in Sec. 1.4). This allows us to estimate an uncertainty to our $\mathcal{O}(p^4)$ results coming from unknown higher order contributions.

The expression for the $\mathcal{O}(p^3)$ and $\mathcal{O}(p^4)$ loop corrections is rather involved. Among the seagull diagrams (**fI**) and (**fII**) there are two kind of contributions in the case of the loops with internal decuplet baryons. The conventional ones coming from the minimal coupling on the derivative of the pseudoscalar mesons are denoted as (**fIa**) and (**fIIa**). The other ones arise from the covariant derivative upon the decuplet fields which is characteristic of the consistent couplings and will be denoted as (**fIb**) and (**fIIb**). A similar issue has been discussed in the calculation of the baryon octet magnetic moments and of the decuplet electromagnetic structure. Finally, the effect of the wave-function renormalization of the external baryons

$$\Sigma'_B = -\frac{1}{2(4\pi F_\phi)^2} \left(\sum_{\substack{\phi=\pi,K,\eta \\ B'=N,\dots,\Xi}} \xi_{\phi,BB'} \Sigma'_{BB'}(m_\phi) + \sum_{\substack{\phi=\pi,K,\eta \\ T'=\Delta,\dots,\Omega}} \xi_{\phi,BT'} \Sigma'_{BT'}(m_\phi) \right), \quad (3.16)$$

has to be accounted for up to the present accuracy in the tree-level diagram (**a**). With these observations, the final result up to $\mathcal{O}(p^4)$ can be expressed as

$$\begin{aligned} [\delta^{(2)} + \delta^{(3)}]_{B_1 B_2} &= \frac{1}{2} (\Sigma'_{B_1} + \Sigma'_{B_2}) \\ &+ \frac{1}{(4\pi F_\phi)^2} \left[\sum_{\phi=\pi,K,\eta} \xi_\phi^{(b)} H^{(b)}(m_\phi) + \sum_{\phi\phi'=\pi K,\eta K} \xi_{\phi\phi'}^{(c)} H^{(c)}(m_\phi, m_{\phi'}) \right] \\ &+ \sum_{\substack{\phi\phi'=\pi K,\eta K,K\pi,K\eta \\ B_3=N,\dots,\Xi}} \xi_{\phi\phi',B_3}^{(d,B)} H_{B_1 B_2}^{(d,B)}(m_\phi, m_{\phi'}, M_3) \end{aligned}$$

$$\begin{aligned}
 & + \sum_{\substack{\phi\phi'=\pi K, \eta K, K\pi, K\eta \\ B_3=\Delta, \dots, \Omega}} \xi_{\phi\phi', B_3}^{(d,T)} H_{B_1 B_2}^{(d,T)}(m_\phi, m_{\phi'}, M_3) \\
 & + \sum_{\substack{\phi=\pi, K, \eta \\ B_3 B_4=\Lambda N, \Sigma N, \Xi\Lambda, \Xi\Sigma}} \xi_{\phi, B_1 B_2, B_3 B_4}^{(e,B)} H_{B_1 B_2}^{(e,B)}(m_\phi, M_3, M_4) \\
 & + \sum_{\substack{\phi=\pi, K, \eta \\ B_3 B_4=\Sigma^* \Delta, \Xi^* \Sigma^*, \Omega \Xi^*}} \xi_{\phi, B_1 B_2, B_3 B_4}^{(e,T)} H_{B_1 B_2}^{(e,T)}(m_\phi, M_3, M_4) \\
 & + \sum_{\substack{\phi=\pi, K, \eta \\ B_3=N, \dots, \Xi}} \left(\xi_{\phi B_3}^{(f,I)} H_{B_3}^{(f,B)}(m_\phi, M_2, M_1) + \xi_{\phi B_3}^{(f,II)} H_{B_3}^{(f,B)}(m_\phi, M_1, M_2) \right) \\
 & + \sum_{\substack{\phi=\pi, K, \eta \\ B_3=\Delta, \dots, \Omega}} \left(\xi_{\phi B_3}^{(f, Ia)} H_{B_3}^{(f, Ta)}(m_\phi, M_2, M_1) + \xi_{\phi B_3}^{(f, IIa)} H_{B_3}^{(f, Ta)}(m_\phi, M_1, M_2) \right) \\
 & + \sum_{\substack{\phi=\pi, K, \eta \\ B_3=\Delta, \dots, \Omega}} \left(\xi_{\phi B_3}^{(f, Ib)} H_{B_3}^{(f, Tb)}(m_\phi, M_2, M_1) + \xi_{\phi B_3}^{(f, IIb)} H_{B_3}^{(f, Tb)}(m_\phi, M_1, M_2) \right) \Big],
 \end{aligned} \tag{3.17}$$

where the Clebsch-Gordan coefficients $\xi_x^{(\alpha)}$ and loop functions $H_x^{(\alpha)}$ can be found in the Appendix C.3. The notation $\phi\phi'$ in the Clebsch-Gordan coefficients of the diagrams **(c)** and **(d)** indicates that the external strangeness changing current couples to the meson cloud transforming the \bar{K} in π or η and, inversely, the π and the η in K .

The result up to $\mathcal{O}(p^3)$ can be recovered from Eqs. (3.16) and (3.17) imposing the $SU(3)_F$ -limit in the baryon masses appearing in the contributions of diagrams **(d)** to **(f)**. One can see that at $\mathcal{O}(p^3)$ the contributions of diagrams **(d)** become symmetric respect with commuting the masses of the mesons ϕ and ϕ' in the loop. It is interesting to note that although separately these loop functions contain divergences up to $\mathcal{O}(p^4)$ and power-counting breaking terms, they all cancel when the different contributions are summed together, in agreement with the Ademollo-Gatto theorem. Finally, we have checked that our results up to $\mathcal{O}(p^3)$ are the same as those obtained in Ref. [66], while in the $M_B \sim \Lambda_{\chi SB}$ limit our results recover the HB ones [168] at $\mathcal{O}(p^3)$. We discuss below the details of the matching of our results to the HB formulas at $\mathcal{O}(p^4)$.

Table 3.1: Octet contributions to the $SU(3)_F$ -breaking corrections to $f_1(0)$ (in percentage). The central values of the Lorentz covariant results at $\mathcal{O}(p^4)$ are calculated with $\mu = 1$ GeV and the uncertainties are obtained by varying μ from 0.7 to 1.3 GeV.

	Covariant			HB [168]			IR [169]		
	$\delta^{(2)}$	$\delta^{(3)}$	$\delta^{(2)} + \delta^{(3)}$	$\delta^{(2)}$	$\delta^{(3)}$	$\delta^{(2)} + \delta^{(3)}$	$\delta^{(2)}$	$\delta^{(3)}$	$\delta^{(2)} + \delta^{(3)}$
$\Lambda \rightarrow N$	-3.8	$0.2^{+1.2}_{-0.9}$	$-3.6^{+1.2}_{-0.9}$	-9.5	12.3	2.7	-9.7	4.0	-5.7 ± 2.1
$\Sigma \rightarrow N$	-0.8	$4.7^{+3.8}_{-2.8}$	$3.9^{+3.8}_{-2.8}$	0.7	3.3	4.1	0.8	2.0	2.8 ± 0.2
$\Xi \rightarrow \Lambda$	-2.9	$1.7^{+2.4}_{-1.8}$	$-1.2^{+2.4}_{-1.8}$	-6.2	10.5	4.3	-6.3	5.2	-1.1 ± 1.7
$\Xi \rightarrow \Sigma$	-3.7	$-1.3^{+0.3}_{-0.2}$	$-5.0^{+0.3}_{-0.2}$	-9.2	10.1	0.9	-9.4	3.8	-5.6 ± 1.6

3.2 Results

3.2.1 Octet-baryon contributions

In Table 3.1, we show the $SU(3)_F$ -breaking corrections in the notation of Eq. (3.15) when the octet-baryon contributions in the Feynman graphs (**d**) to (**f**) of Fig. 3.1 are included. For comparison, we also list the numbers obtained in HB [168] and IR [169]. We have checked that we match the HB results at $\mathcal{O}(p^4)$ [168] in the $M_{B0} \sim \Lambda_{\chi SB}$ limit when the $1/M_{B0}$ recoil corrections are considered. First, in the covariant approach we note that in three of the four channels, the $\delta^{(3)}$ numbers are smaller than the $\delta^{(2)}$ ones. The situation is similar in IR but quite different in HB. In the HB calculation, the $\delta^{(3)}$ contribution is larger than the $\delta^{(2)}$ one for the four cases.¹ This tells that recoil corrections (in the HB language) or relativistic effects are important. On the other hand, the total covariant results and those obtained in IR are consistent despite they disagree at each order. They both are very different from the HB predictions, even for the signs in three of the four cases. Obviously, as stressed in Ref. [169], one should trust more the relativistic than the non-relativistic results, which have to be treated with caution whenever $1/M_{B0}$ recoil corrections become large. In any case, it is clear from Table 3.1 that the convergence is slow even when the relativistic corrections are considered.

¹What we denote by $\delta^{(3)}$ is the sum of those labeled by $\alpha^{(3)}$ and $\alpha^{(1/M)}$ in Ref. [168].

Table 3.2: Decuplet contributions to the $SU(3)_F$ -breaking corrections to $f_1(0)$ (in percentage). The central values of the Lorentz covariant results at $\mathcal{O}(p^4)$ are calculated with $\mu = 1$ GeV and the uncertainties are obtained by varying μ from 0.7 GeV to 1.3 GeV.

	Covariant			HB		
	$\delta^{(2)}$	$\delta^{(3)}$	$\delta^{(2)} + \delta^{(3)}$	$\delta^{(2)}$	$\delta^{(3)}$	$\delta^{(2)} + \delta^{(3)}$
$\Lambda \rightarrow N$	0.7	$3.0^{+0.1}_{-0.1}$	$3.7^{+0.1}_{-0.1}$	1.8	1.3	3.1
$\Sigma \rightarrow N$	-1.4	$6.2^{+0.4}_{-0.3}$	$4.8^{+0.4}_{-0.3}$	-3.6	8.8	5.2
$\Xi \rightarrow \Lambda$	-0.02	$5.2^{+0.4}_{-0.3}$	$5.2^{+0.4}_{-0.3}$	-0.05	4.2	4.1
$\Xi \rightarrow \Sigma$	0.7	$6.0^{+1.9}_{-1.4}$	$6.7^{+1.9}_{-1.4}$	1.9	-0.2	1.7

3.2.2 Decuplet-baryon contributions

We now investigate the contributions of the decuplet resonances to $f_1(0)$ when they are included as virtual states in the Feynman graphs **(d)** to **(f)** of Fig. 3.1. The numerical results are summarized in Table 3.2. It can be seen that at $\mathcal{O}(p^3)$, the decuplet contributions are relatively small compared to the octet ones at the same order. On the other hand, the $\mathcal{O}(p^4)$ contributions are sizable and all of them have positive signs. It is worth noticing that, besides the $\Xi\Sigma$ channel, the results in the covariant and HB approaches are quite consistent with each other. This is in complete contrast with the problems reported in Ref. [168], where it is obtained that $\delta^{(3)} = +6.8, +36.3, +17.8$ and -1.5 for the $\Lambda N, \Sigma N, \Xi\Lambda$ and $\Xi\Sigma$ decays respectively within the HB approach. Some of these contributions at NNLO are tremendously large, pointing to a lack of convergence of the chiral series in this observable.

To obtain the HB results at $\mathcal{O}(p^3)$ we have applied the SSE scheme and have performed an expansion in terms of the decuplet-octet mass splitting, δ . To obtain the results at $\mathcal{O}(p^4)$, we have used physical masses for both the octet and the decuplet baryons and have performed an additional expansion in the octet- and the decuplet-baryon mass splittings. This procedure is the same as that of Ref. [168]. We find that the discrepancy comes from the octet mass-splitting corrections to the diagram **(d)** of Fig. 3.1. If we had mistakenly exchanged the masses of the mesons in the loop, we would have obtained the same results as those of Ref. [168]. Thus, the correct HB contributions of the decuplet to $f_1(0)$ are the ones shown in Table 3.2.

As it was discussed in Sec. 2.1, one expects that the decuplet contribu-

tions decrease and eventually vanish as the splitting goes to infinity. This is indeed the case, as can be clearly seen from Fig. 3.2, where the $\mathcal{O}(p^3)$ decuplet contributions are plotted as a function of the decuplet-octet mass splitting.

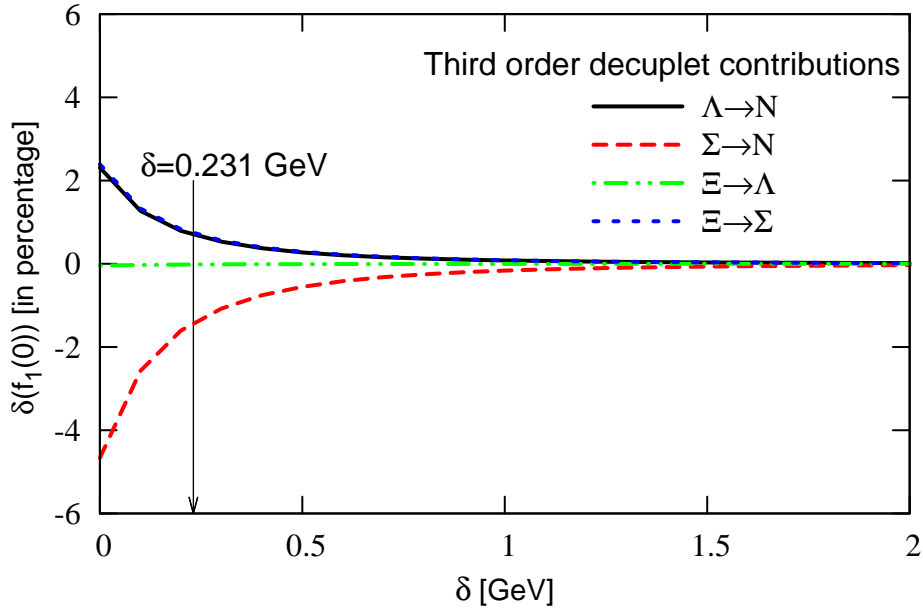


Figure 3.2: Decuplet $\mathcal{O}(p^3)$ contributions to the $SU(3)_F$ -breaking corrections to the hyperon vector coupling $f_1(0)$ as a function of the decuplet-octet mass splitting δ .

3.2.3 Full results and comparison with other approaches

Summing the octet and the decuplet contributions, we obtain the numbers shown in Table 3.3. In Table 3.4, we compare the results obtained in the covariant formalism with those obtained from other approaches, including HB, large N_c fits [165], quark models [171, 172], and two quenched LQCD calculations [173, 174]. The corrected HB results are now consistent with those given when the relativistic corrections are considered within the covariant approach. The results quoted from Ref. [171] are quite general in quark model calculations and reflect the naive expectation that $SU(3)_F$ -breaking corrections, at least for the ΣN channel, should be negative. It is interesting to note that in the quark model of Ref. [172] the valence quark effects give negative contributions, as in the other quark models, while the chiral effects provide positive

Table 3.3: Total $SU(3)_F$ -breaking corrections to $f_1(0)$ up to $\mathcal{O}(p^4)$.

	$\delta^{(2)}$	$\delta^{(3)}$	$\delta^{(2)} + \delta^{(3)}$
$\Lambda \rightarrow N$	-3.1	$3.2_{-1.0}^{+1.3}$	$0.1_{-1.0}^{+1.3}$
$\Sigma \rightarrow N$	-2.2	$10.9_{-3.1}^{+4.2}$	$8.7_{-3.1}^{+4.2}$
$\Xi \rightarrow \Lambda$	-2.9	$6.9_{-2.1}^{+2.8}$	$4.0_{-2.1}^{+2.8}$
$\Xi \rightarrow \Sigma$	-3.0	$4.7_{-1.6}^{+2.2}$	$1.7_{-1.6}^{+2.2}$

Table 3.4: $SU(3)_F$ -breaking corrections (in percentage) to $f_1(0)$ obtained in different approaches. The star in the HB results means that they are those obtained in the present work.

	Covariant	HB*	Large N_c Ref. [165]	Quark model Ref. [171]	Ref. [172]	quenched LQCD
$\Lambda \rightarrow N$	$0.1_{-1.0}^{+1.3}$	+5.8	2 ± 2	-1.3	0.1	
$\Sigma \rightarrow N$	$8.7_{-3.1}^{+4.2}$	+9.3	4 ± 3	-1.3	0.9	$-1.2 \pm 2.9 \pm 4.0$ [173]
$\Xi \rightarrow \Lambda$	$4.0_{-2.1}^{+2.8}$	+8.4	4 ± 4	-1.3	2.2	
$\Xi \rightarrow \Sigma$	$1.7_{-1.6}^{+2.2}$	+2.6	8 ± 5	-1.3	4.2	-1.3 ± 1.9 [174]

contributions, resulting in net positive corrections. Therefore, the different chiral approaches agree in the sign and the approximate size of these corrections, what may indicate the non-triviality of the multi-quark effects induced by the chiral dynamics. This result contrasts with the rather similar case of the kaon decays where the negative sign of the $SU(3)_F$ -breaking corrections for the vector form factor $f_+(0)$ expected from quark-models have been confirmed by χ PT (see e.g. Ref. [175]).

It is also remarkable the agreement of our results with those obtained in a different systematic approach to non-perturbative QCD as the Large N_c . The results of LQCD are marginally compatible with ours although they favor negative corrections to $f_1(0)$. It must be pointed out that these simulations, besides being quenched, are still performed with rather high pion masses, namely ~ 400 MeV for $\Xi^0 \rightarrow \Sigma^+$ [174] and ~ 700 MeV for $\Sigma^- \rightarrow n$ [173]. In this sense, our results may be helpful for the chiral extrapolation of future LQCD simulations focused on $f_1(0)$. And the other way around, the LQCD could provide information about the higher-order local contributions and could reduce the theoretical uncertainty of the $B\chi$ PT calculation [173]. In any case, a dynamical

	$\Lambda \rightarrow p$	$\Sigma^- \rightarrow n$	$\Xi^- \rightarrow \Lambda$	$\Xi^0 \rightarrow \Sigma^+$
$ \tilde{f}_1 V_{us} $	0.2221 (33)	0.2274 (49)	0.2367 (97)	0.216 (33)
V_{us}	0.2217 (42)	0.209 (8)	0.228 (11)	0.2124 (50)

Table 3.5: Results for $|\tilde{f}_1 V_{us}|$ and V_{us} obtained from the measured rates and g_1/f_1 ratios and using the covariant results for $f_1(0)$. We use here the notation $\tilde{f}_1 = f_1/g_V$ [165].

lattice simulation close to the physical point will be very helpful and eventually conclusive about the nature of the $SU(3)_F$ -breaking corrections to $f_1(0)$.

3.2.4 Determination of V_{us}

With the elements developed above we can obtain a determination of the CKM element V_{us} . Using the assumptions made in Sec. 3.1, i.e. f_2 equal to the $SU(3)_F$ -symmetric value, $g_2 = 0$ and g_1 taken from the measured ratios g_1/f_1 , we can express the decays rates in terms of the values for $|\tilde{f}_1 V_{us}|$, where $\tilde{f}_1 = f_1/g_V$. In Table 3.5, we display the values of $|\tilde{f}_1 V_{us}|$ for any of the channels studied in this thesis and their corresponding extracted values for V_{us} . Combining them such that both the statistical and theoretical error bars are included one obtains [3]

$$V_{us} = 0.2176 \pm 0.0029 \pm \Delta_V, \quad (3.18)$$

where Δ_V accounts for other systematic uncertainties. At the order we work in Eq. (3.11), this uncertainty is due to the $SU(3)_F$ -breaking correction to g_2 that has not been considered. This contribution is $\sim \mathcal{O}(\beta^2)$ and potentially as important for the extraction of V_{us} as the $SU(3)_F$ -breaking correction to f_1 .

We first compare our result with other determinations obtained from the decay rates and g_1/f_1 in the hyperon semileptonic data; namely, $V_{us} = 0.2199 \pm 0.0026$ in Large N_c [165] and $V_{us} = 0.2250(27)$ in the $SU(3)_F$ -symmetric model [162]. The comparison with the latter indicates the sensitivity to a breaking correction to $f_1(0)$ of $\sim \mathcal{O}(\beta^2)$ and suggests that the $SU(3)_F$ -symmetric assumption is not reliable enough for the accuracy required by the determination of V_{us} . The agreement between the B χ PT and the Large N_c is a consequence of the consistency shown in Table 3.4 and of the fact that in both approaches the $SU(3)_F$ -breaking correction to g_2 have been ignored.

On the other hand, our result is somewhat smaller than the ones obtained from kaon and tau decays or from the f_K/f_π ratio shown in the introduction. It

is not compatible either with the unitarity condition of Eq. (3.3). Nonetheless, the result shown in Eq. (3.18) is not complete and has to be improved with the model-independent description of the $SU(3)_F$ -breaking corrections to g_2 . As argued in Ref. [162], the trends shown by $\Sigma^- \rightarrow n$ and $\Lambda \rightarrow p$ data indicate that the incorporation of the $SU(3)_F$ -breaking corrections to g_2 will raise the value of V_{us} in these two channels. Unfortunately, the data for hyperon decays is not yet precise enough to address a quantitative study of this form factor. From the theoretical side, a determination of these corrections in LQCD and an analysis in B χ PT would be useful to ascertain the effects that g_2 may have on the determination of V_{us} .

3.3 Summary

We have performed a study of the $SU(3)_F$ -breaking corrections to the hyperon vector coupling $f_1(0)$ in covariant baryon chiral perturbation theory including both the octet and the decuplet contributions. We confirm earlier findings in HB and IR χ PT that the convergence of the chiral series is slow in the case with only dynamical octet baryons. Our study of the decuplet contributions shows that at $\mathcal{O}(p^3)$ they are in general smaller than those of their octet counterparts, while at $\mathcal{O}(p^4)$ they are sizable. Combining both octet and decuplet contributions, we found positive $SU(3)_F$ -breaking corrections to all the four independent $f_1(0)$'s, which compare favorably with the large N_c fits and those of the quark model taking into account chiral effects.

The fact that the $\mathcal{O}(p^4)$ chiral contributions are comparable to the $\mathcal{O}(p^3)$ ones suggests that the $\mathcal{O}(p^5)$ chiral effects may not be negligible. We have estimated their size by varying μ from 0.7 to 1.3 GeV. Taking into account these higher-order uncertainties, our results still favor positive $SU(3)_F$ -breaking corrections to the four $f_1(0)$'s. Despite that these corrections are tiny, they sensibly affect the value obtained for V_{us} . Nevertheless, we argued that an extraction of this CKM matrix element from hyperon semileptonic decay data should not be trusted until the effects of other form factors, mainly g_2 , have been included.

Masses of the baryons

In the last decades there has been a sustained interest in the description of the lowest-lying baryon mass spectrum by means of $SU(3)_{F-B}\chi$ PT [176, 177, 178, 179, 180, 181, 182, 183, 184, 185, 186, 187]. The chiral corrections to the Gell-Mann-Okubo baryon octet mass relation and Gell-Mann’s decuplet equal spacing rules (that we denote generically as GMO) [52, 53]

$$3M_{\Lambda} + M_{\Sigma} - 2M_N - 2M_{\Xi} = 0, \tag{4.1}$$

$$M_{\Sigma^*} - M_{\Lambda} = M_{\Xi^*} - M_{\Sigma^*} = M_{\Omega^-} - M_{\Xi^-}, \tag{4.2}$$

have received special attention. More specifically, the GMO relations are known to work with an accuracy of ~ 7 MeV and a puzzling and not yet well understood feature of the leading chiral corrections is that they preserve the GMO equations within ~ 10 MeV whereas the corrections to any of the individual baryon masses are of order ~ 100 - 1000 MeV [177, 188, 189, 190]. Another interesting aspect is that the analysis of the baryon masses provides hints on their scalar structure, i.e. the sigma terms [36, 178]. These magnitudes, besides providing a measure of the explicit symmetry breaking and of the meson-cloud contribution to the baryon masses [36], are relevant for other areas of phenomenology¹.

On the other hand, LQCD calculations have experienced an impressive development in the last few years and reliable calculations on the low-lying baryon spectroscopy and structure are starting to appear. The celebrated studies of the lowest-lying baryon mass spectrum that have been undertaken by different LQCD collaborations using dynamical actions with light quark masses close to the physical point [192, 193, 194, 195, 196, 197, 198] are a

¹The importance that a model-independent and accurate determination of these quantities have for supersymmetric dark matter searches has been recently pointed out [191].

remarkable example of the progress in this field. It is still an open question whether the quark-mass dependence of the LQCD results on the baryonic sector can be understood within χ PT. For instance, big difficulties have been found to describe the LQCD simulations of the octet- and decuplet-baryon masses within HB χ PT [192, 199]. This problem is usually referred to as an example of the lack of convergence of $SU(3)_F$ -HB χ PT and of the difficulties of this approach to interpret LQCD results. Different alternative proposals, like the $SU(2)_F$ -flavor hyperon B χ PT [200] which is motivated by previous work done on the nucleon and $\Delta(1232)$ masses [201, 202, 203, 78, 200, 204], or the use of different variants of cut-off renormalization [205, 206], have then arisen.

In this chapter we want to explore the potential of the covariant formulation of $SU(3)_F$ -B χ PT within the EOMS scheme to conciliate the description of baryon phenomenology and the description of the quark mass dependence of 2 + 1-flavor LQCD results. In particular, we will study those of the PACS-CS [193] and LHP [192] collaborations on the baryon-octet and -decuplet masses.

4.1 Formalism

We define the self-energy $\Sigma_B(\not{p})$ of a spin-1/2 baryon B through the non-reducible contributions to its propagator [28, 29]

$$\tilde{S}_B(\not{p}) = \frac{i}{\not{p} - M_{B0} - \Sigma_B(\not{p})}, \quad (4.3)$$

where \tilde{S}_B is the dressed propagator. The physical mass of the particle B , M_B , is then defined as the real part of the position of the pole of the last equation

$$[\not{p} - M_{B0} - \Sigma_B(\not{p})]_{\not{p}=M_B} = 0. \quad (4.4)$$

For a spin-3/2 particle T , the self-energy $\Sigma_T(\not{p})_{\mu\nu}$ is a tensor that can be decomposed, in general, in terms of 10 independent structures [207, 208]. As in the case of the bare propagator (see Eq. (1.52) in Sec. 1.4), in consistent theories one only needs to consider the spin-3/2 sector of the self-energy operator [26]

$$(\Sigma_T)_{\mu\nu}(\not{p}) = \Sigma_T(\not{p})(P^{\frac{3}{2}})_{\mu\nu}, \quad (4.5)$$

such that its non-reducible pieces contribute to the dressed propagator, $(\tilde{S}_T)_{\mu\nu}$, analogously to the spin-1/2 particles,

$$(\tilde{S}_T)_{\mu\nu}(\not{p}) = -\frac{i}{\not{p} - M_{T0} - \Sigma_T(\not{p})}(P^{\frac{3}{2}})_{\mu\nu}, \quad (4.6)$$

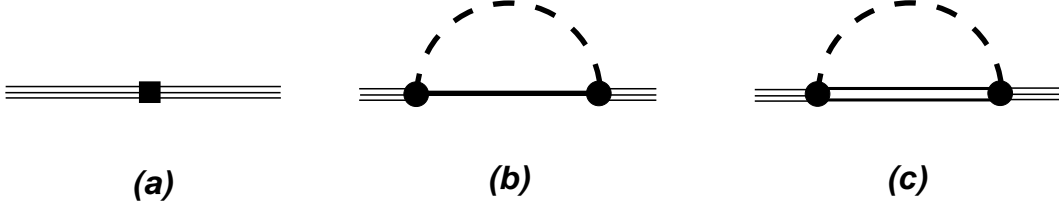


Figure 4.1: Feynman diagrams contributing to the octet- and decuplet-baryons (B and T respectively) up to $\mathcal{O}(p^3)$ in χ PT. The solid lines correspond to octet-baryons, double lines to decuplet-baryons and dashed lines to mesons. The black dots indicate 1^{st} -order couplings while boxes, 2^{nd} -order couplings.

with the consequent definition of the physical mass M_T as the solution of

$$[\not{p} - M_{T0} - \Sigma_T(\not{p})]_{\not{p}=M_T} = 0. \quad (4.7)$$

In order to find the physical masses solving the Eqs. (4.4) and (4.7) we follow the conventional methods in quantum field theory [28, 29].

In the Figure 4.1 we show the Feynman diagrams that contribute to the self-energy of the lowest-lying baryons in χ PT up to $\mathcal{O}(p^3)$. At $\mathcal{O}(p^2)$ the following terms in the chiral Lagrangian

$$\mathcal{L}_B^{(2)} = b_0 \langle \chi_+ \rangle \langle \bar{B} B \rangle + b_{D/F} \langle \bar{B} [\chi_+, B]_{\pm} \rangle, \quad (4.8)$$

and

$$\mathcal{L}_T^{(2)} = \frac{t_0}{6} \bar{T}_\mu^{abc} g^{\mu\nu} T_\nu^{abc} \langle \chi_+ \rangle + \frac{t_D}{2} \bar{T}_\mu^{abc} g^{\mu\nu} (\chi_+, T_\nu)^{abc}, \quad (4.9)$$

give the tree-level contribution, diagram (a) of Fig. 4.1, to the baryon-octet and decuplet-resonance self-energies respectively. In these equations, $(X, T_\mu)^{abc} \equiv (X)_d^a T_\mu^{dbc} + (X)_d^b T_\mu^{adc} + (X)_d^c T_\mu^{abd}$, and the coefficients b_0 , b_D , b_F , and t_0 , t_D are unknown LECs. These give contributions that are linear in the quark masses or, according to the Gell-Mann-Oakes-Renner relation, Eq. (1.13), quadratic in the pseudoscalar meson masses. They provide the leading $SU(3)_F$ -breaking corrections to the chiral limit masses appearing in the free Lagrangians

$$M_B^{(2)} = M_0 - \sum_{\phi=\pi, K} \xi_{B,\phi}^{(a)} m_\phi^2, \quad (4.10)$$

where the Gell-Mann-Okubo mass formula for the pseudoscalar mesons, Eq. (1.14), is implicitly used and $\mathcal{B} = N, \Lambda, \Sigma, \Xi$ or $\Delta, \Sigma^*, \Xi^*, \Omega^-$, with $M_0 = M_{B0}$ or M_{T0} respectively. In Eq. (4.10), the coefficients $\xi_{B,M}^{(a)}$ are $SU(3)_F$ Clebsch-Gordan

coefficients that can be found in the Table C.15 of Appendix C.4. Equating the LECs M_{B0} , b_0 , b_D , b_F , and M_{T0} , t_0 , t_D , in terms of the masses $M_B^{(2)}$ one recovers the GMO baryon mass relations of Eqs. (4.1) and (4.2).

At $\mathcal{O}(p^3)$ the diagrams **(b)** and **(c)** give the leading loop corrections to the baryon masses

$$M_B^{(3)} = M_B^{(2)} + \frac{1}{(4\pi F_\phi)^2} \sum_{\phi=\pi,K,\eta} \left(\xi_{B,\phi}^{(b)} H_X^{(b)}(m_\phi) + \xi_{B,\phi}^{(c)} H_X^{(c)}(m_\phi) \right). \quad (4.11)$$

The coefficients $\xi_{B,M}^{(\alpha)}$ are again Clebsch-Gordan coefficients and $H_X^{(\alpha)}(m)$ are loop functions which are different for octet ($X = B$) or decuplet ($X = T$) external baryon lines. The values of the coefficients for each diagram, $\alpha = b$ or c can be found in the Table C.15 of the Appendix C.4 and the corresponding loop-functions are displayed in the same Appendix. The values of the couplings and pseudoscalar meson masses used in the loop functions are those shown in Appendix B.

As in all the previous cases, we recover the power-counting in the loop graphs applying the EOMS scheme that we have introduced in Sec. 1.3.2. In the Appendix C.4 we present a detailed description of the redefinition of the bare LECs necessary to cancel the $d - 4$ divergencies in the \overline{MS} scheme and the additional redefinition to be done afterwards in order to absorb the power-counting breaking terms in the EOMS scheme. The regularized loop-functions then lead to the HB results (i.e. those reported in Refs. [179]) when one considers $M_{T0} = M_{B0} + \delta$ and applies the SSE expansion in the limit $M_{B0} \rightarrow \infty$. For completeness, the loop results in HB have also been displayed in Appendix C.4.

4.2 Results

We analyze in χ PT up to NLO first the experimental numbers of the baryon masses and then the quark-mass dependence of the LQCD results of two different collaborations.

4.2.1 Experimental data

The singlet term associated to b_0 in Eq. (4.8) cannot be disentangled from M_{B0} when comparing with the experimental data. Therefore, we define $M_{B0}^{eff} = M_{B0} - b_0(4m_K^2 + 2m_\pi^2)$ and perform the fits using M_{B0}^{eff} , b_D and b_F as free parameters. Equivalently, for the decuplet-baryons we use $M_{T0}^{eff} = M_{T0} - t_0(2m_K^2 + m_\pi^2)$ and t_D as the fitting parameters. The loop-functions now depend

Table 4.1: Results of the fits to the physical values of the baryon-octet masses (in MeV) in B χ PT up to $\mathcal{O}(p^3)$ or NLO.

	GMO	HB	Covariant	Expt.
M_N	942(2)	939(2)	941(2)	940(2)
M_Λ	1115(1)	1116(1)	1116(1)	1116(1)
M_Σ	1188(4)	1195(4)	1190(4)	1193(5)
M_Ξ	1325(3)	1315(3)	1322(3)	1318(4)
$M_{B_0}^{eff}$ [MeV]	1192(5)	2422(5)	1840(5)	
b_D [GeV $^{-1}$]	0.060(4)	0.412(4)	0.199(4)	
b_F [GeV $^{-1}$]	-0.213(2)	-0.781(2)	-0.530(2)	

Table 4.2: Results of the fits to the physical values of the baryon-decuplet masses (in MeV) in B χ PT up to $\mathcal{O}(p^3)$ or NLO.

	GMO	HB	Covariant	Expt.
M_Δ	1233(2)	1235(2)	1234(2)	1232(2)
M_{Σ^*}	1380(1)	1372(1)	1376(1)	1385(4)
M_{Ξ^*}	1526(1)	1518(1)	1523(1)	1533(4)
M_{Ω^-}	1672(1)	1673(1)	1673(1)	1672(1)
$M_{T_0}^{eff}$ [MeV]	1215(2)	1763(2)	1519(2)	
t_D [GeV $^{-1}$]	-0.326(2)	-0.960(2)	-0.694(2)	

on M_{B_0} and M_{T_0} which are different to the effective ones. In studying the experimental values, we fix the chiral limit masses used in the loop-functions using those obtained at $\mathcal{O}(p^0)$, namely, the averaged octet and decuplet masses, $M_{B_0}^{(0)} = 1151$ MeV and $M_{T_0}^{(0)} = 1382$ MeV.

In Tables 4.1 and 4.2, we display the results of the fits to the baryon-octet and -decuplet experimental values respectively. The error bar of the experimental numbers accounts for the mass splitting within any isospin multiplet with a minimum error of 1 MeV for the isospin singlets. The first row in these tables reflects the quality of the GMO description which is just few MeV off from the experimental values. At $\mathcal{O}(p^3)$, the leading chiral loops preserve the GMO equations within ~ 10 MeV although the corrections given to any of the

masses ($\delta M_{B/T}^{(3)}$) are of order ~ 100 - 1000 MeV

$$\begin{aligned}\delta M_N^{(3)} &= -228 \text{ MeV}, & \delta M_\Lambda^{(3)} &= -470 \text{ MeV}, \\ \delta M_\Sigma^{(3)} &= -634 \text{ MeV}, & \delta M_\Xi^{(3)} &= -799 \text{ MeV}.\end{aligned}\tag{4.12}$$

in the covariant approach (in HB the corrections are almost double). In the case of the decuplet resonances at NLO, the description in the covariant approach is reasonably good and the chiral corrections to the masses are again large

$$\begin{aligned}\delta M_\Delta^{(3)} &= -324 \text{ MeV}, & \delta M_{\Sigma^*}^{(3)} &= -494 \text{ MeV}, \\ \delta M_{\Xi^*}^{(3)} &= -659 \text{ MeV}, & \delta M_{\Omega^-}^{(3)} &= -821 \text{ MeV}.\end{aligned}\tag{4.13}$$

It is worth mentioning that the inclusion of the decuplet contributions is essential to produce some improvement over GMO in the octet masses and not to spoil those on the decuplet masses. The reason why the GMO relations are well preserved by the chiral loops despite the large corrections they provide to the individual masses has not been well understood yet. However, some hints have been obtained in the Large- N_c approach to QCD where the part of the NLO chiral corrections contributing to the GMO equations are found to be subleading in the $1/N_c$ expansion [188, 190].

4.2.2 Analysis of lattice results

Method

As we have shown above, the physical masses of the lowest-lying baryons are successfully described in the different approaches of χ PT even at relatively low orders. For the study of the LQCD results, the convergence of the chiral series is more critical because of the larger quark mass involved in the simulations. In the following, we extend our analysis to the $N_f = 2 + 1$ LQCD results, in particular, to those reported by the PACS-CS collaboration in Ref. [193] and by the LHP collaboration in Ref. [192]. The PACS-CS collaboration employs the non-perturbatively $\mathcal{O}(a)$ -improved Wilson quark action and the Iwasaki gauge action. The numerical simulations are carried at one lattice spacing, $a = 0.0907(13)$, in grids with a spatial length of $L \simeq 2.9$ fm. The LHP collaboration uses a mixed-action consisting of domain wall fermions (with an approximate lattice realization of chiral symmetry) and staggered sea-quarks. The simulations are done at the lattice spacing $a = 0.1241(25)$ and in a box $L \simeq 2.5$ fm long. For an introduction to LQCD and the different discretization techniques we refer the reader to Refs. [209, 210, 211].

We include in the study the lattice ensembles for which both the pion and kaon masses are approximately below 600 MeV, which is a limit of the meson mass we deem acceptable for the convergence of covariant $SU(3)_F$ -B χ PT up to NLO. The mass of the η -meson we determine using the Gell-Mann-Okubo relation for the pseudoscalar meson masses, Eq.(1.14), which remains valid up to the considered accuracy. The LQCD results on the masses used in this thesis are transformed from lattice to physical units using the respective lattice spacing a . These, in physical units, are collected in Table D.1 of Appendix D.

The analysis of the LQCD simulations disentangles the singlet parts b_0 and t_0 from the respective chiral limit masses. Therefore we perform fits of the 7 parameters, M_{B0} , b_0 , b_D , b_F , M_{T0} , t_0 and t_D , to the chosen lattice points that we assume to have independent statistical errors (σ_i) but fully-correlated errors propagated from the lattice spacing a (Δa_i). The resulting uncertainties σ_i and Δa_i are shown in the first and second parenthesis for each LQCD point in Table D.1. Our χ^2 incorporates the inverse of the resulting correlation matrix $C_{ij} = \sigma_i \sigma_j \delta_{ij} + \Delta a_i \Delta a_j$. Besides that, the fits to the octet and decuplet masses are connected through the diagrams with baryons of both multiplets.

We have also computed the finite volume corrections in the covariant framework. The relevant formulae have been included in Appendix C, while the numerical results of these corrections to any of the LQCD points are shown in box brackets in the Table D.1. As it is expected, the lightest ensembles obtain the largest finite volume corrections although one should be aware that $m_\pi L < 4$ in this region, which is below the limit deemed acceptable to obtain perturbatively the finite volume corrections in the so-called p -regime [204]. Nevertheless, the lightest points are also afflicted by large statistical uncertainties such that the inclusion of the corrections does not affect the quality of the fits.

Finally, we estimate two types of uncertainties in any of the extrapolated results on the baryon masses. The error bar quoted in the GMO and HB columns and the first one assigned to the covariant results are the uncertainties propagated from the fitted parameters. The second error bar in the covariant results is a theoretical uncertainty coming from the truncation of the chiral expansion which is estimated by taking 1/2 of the difference between the results obtained at LO and NLO.

Extrapolation results

Among the PACS-CS results, we take the lightest three lattice points for each baryon, what includes an ensemble with a strange quark with mass lighter than the physical one. We select the two lighter ensembles of the LHP collaboration for each baryon. This amounts to a total of either 24 PACS-CS points or 16

LHP points, that are used to fit the 7 LECs appearing up to NLO. Notice that while the lightest PACS-CS configurations are almost at the physical point ($m_\pi \simeq 156$ MeV), those of LHP are still quite far away from it ($m_\pi \simeq 293$ MeV).

The results of the extrapolations, the fitted values of the LECs and the quality of the fits in the different approaches considered in this thesis are displayed in Table 4.3. At LO (GMO), the fits to the quark-mass dependence of the results of the two lattice collaborations have $\chi_{\text{d.o.f.}}^2$'s that are smaller than 1. The values of the masses extrapolated to the physical point are rather good using the PACS-CS ensembles, although those using LHP results present sizable disagreements with the experimental data for some of the baryons like the nucleon or the Δ .

The extrapolation is expected to improve with the addition of the leading non-analytic chiral terms at NLO. However, in the HB approach the description of the quark-mass dependence is much worse and the extrapolated values are ~ 100 MeV off the experimental ones (for both the PACS-CS and LHP results). This is in agreement with the problems reported in Refs. [192, 199] where reasonable fits using $SU(3)_F$ -HB χ PT are only obtained with unreasonably small values (even compatible with zero) of the ϕB and ϕBT couplings.

In the covariant formulation of $SU(3)_F$ -B χ PT, a good description of the LQCD results can be achieved using the phenomenological values for these couplings. Moreover, the extrapolation is better at NLO in the covariant framework than at LO (GMO), what suggests the importance of the non-analytic chiral structure nearby the physical point. This can be more quantitatively assessed including the experimental data into the fits. Their quality is shown in Table 4.3 through the corresponding estimator that we denote by $\bar{\chi}_{\text{d.o.f.}}^2$. We indeed see that the covariant approach accommodates the LQCD results and the experimental data manifestly better than the GMO based model. This improvement, obtained at NLO in covariant $SU(3)_F$ -B χ PT, highlights the effect of the leading chiral non-analytical terms in the extrapolation even from light quark masses as small as those used by PACS-CS. [193] ($m_\pi \simeq 156$ MeV). On the other hand, the comparison between the covariant and HB results illustrates the importance of the relativistic corrections in the understanding of the dependence shown by the lattice simulations on the baryon masses at relatively heavy quark-masses. This is specially true for the extrapolation of the LHP results, that are quite far away from the physical point of quark masses ($m_\pi \gtrsim 293$ MeV). Finally, the large $\bar{\chi}^2$ obtained in the analysis of the LHP results deserves a comment. Indeed, one can notice that the extrapolation in the octet sector is better than the one of the PACS-CS collaboration. The large contributions to this estimator in the case of the LHP actually come from the

Table 4.3: Extrapolation in MeV and values of the LECs from the fits to the PACS-CS [193] and LHP [192] results on the baryon masses using B χ PT up to NLO. The χ^2 is the estimator for the fits to the LQCD results whereas $\bar{\chi}^2$ include also experimental data. See the text for details.

	PACS-CS			LHP			Expt.
	GMO	HB	Covariant	GMO	HB	Covariant	
M_N	971(22)	764(21)	893(19)(39)	1044(42)	770(24)	924(22)(60)	940(2)
M_Λ	1115(21)	1042(20)	1088(20)(14)	1158(55)	1031(26)	1100(25)(29)	1116(1)
M_Σ	1165(23)	1210(22)	1178(24)(7)	1231(32)	1240(27)	1223(29)(4)	1193(5)
M_Ξ	1283(22)	1392(21)	1322(24)(20)	1309(41)	1384(28)	1332(30)(12)	1318(4)
M_Δ	1319(28)	1264(22)	1222(24)(49)	1409(36)	1333(29)	1301(30)(50)	1232(2)
M_{Σ^*}	1433(27)	1466(22)	1376(24)(29)	1478(38)	1496(30)	1414(31)(32)	1385(4)
M_{Ξ^*}	1547(27)	1622(23)	1531(25)(8)	1548(42)	1613(31)	1527(35)(10)	1533(4)
M_{Ω^-}	1661(27)	1733(25)	1686(28)(13)	1617(46)	1685(33)	1641(38)(12)	1672(1)
M_{B_0} [MeV]	900(39)	508(32)	756(32)	1023(39)	463(36)	780(31)	
b_0 [GeV $^{-1}$]	-0.264(24)	-1.656(19)	-0.978(38)	-0.210(21)	-1.735(18)	-1.044(45)	
b_D [GeV $^{-1}$]	0.042(9)	0.368(9)	0.190(24)	0.061(4)	0.404(5)	0.236(24)	
b_F [GeV $^{-1}$]	-0.174(7)	-0.824(6)	-0.519(19)	-0.147(4)	-0.817(4)	-0.523(21)	
M_{T_0} [MeV]	1245(48)	1117(32)	954(37)	1260(59)	1068(36)	944(42)	
t_0 [GeV $^{-1}$]	-0.12(5)	-0.709(37)	-1.05(8)	-0.28(6)	-0.953(39)	-1.28(8)	
t_D [GeV $^{-1}$]	-0.254(10)	-0.739(10)	-0.682(20)	-0.154(7)	-0.651(8)	-0.609(14)	
$\chi^2_{\text{d.o.f.}}$	0.63	9.2	2.1	0.33	10.46	1.95	
$\bar{\chi}^2_{\text{d.o.f.}}$	4.2	36.6	2.8	55.8	127.	13.4	

decuplet sector where one finds that the agreement of the extrapolation with the experimental data is rather poor. Similar problems on these LQCD results for the decuplet masses were already noticed by the LHP collaboration [192].

In Fig. 4.2, we give a graphical representation of the extrapolation of the PACS-CS results. We plot the quark-mass dependence of the baryon masses in covariant $SU(3)_F$ -B χ PT compared to the PACS-CS points, which are represented by their corresponding error bars (only describe the statistical uncertainties). The lattice points in $m_\pi^2 \simeq 0.15 \text{ GeV}^2$ involve a lighter strange quark mass. The diamonds denote our results (the experimental values are not fitted) and they are connected by a dotted line added to guide the eye. As we can see in the figure, the light and strange quark mass dependence of the PACS-CS results on the masses are very well described in covariant $SU(3)_F$ -B χ PT. The boxes are from a lattice ensemble with kaons quite heavier than 600 MeV and is not included in the fit. The comparison of the latter with our results indicates that the agreement between the PACS-CS calculation and the $SU(3)_F$ -B χ PT NLO amplitude is still quite good at these relatively heavy quark masses. Finally, the filled diamonds are the values extrapolated to the physical point which exhibit the consistency with the experimental data (crosses) shown in Table 4.3 and discussed above.

4.2.3 Phenomenological applications

As we have seen in Chap. 1, the LECs are the parameters of χ PT that may enclose relations among seemingly unrelated observables in the low-energy (non-perturbative) regime of QCD. These are not constrained by the global symmetries of QCD and their values are, in practice, obtained using experimental data. Another source of model-independent information to fix the LECs is provided by the quark-mass dependence of different hadronic properties in LQCD simulations. A reliable combination of LQCD and χ PT becomes a powerful framework to understand hadron phenomenology from first principles and may have sound applications.

We first study the reliability of the covariant approach for using the PACS-CS and LHP results on the baryon masses to fix the corresponding set of LECs up to NLO. Afterwards, we will use this information to provide accurate predictions on the baryonic sigma terms.

Determination of the LECs

In Tables 4.4 and 4.5, we compare the values of the LECs determined studying the experimental values of the baryon masses with those obtained when fitting the corresponding quark-mass dependence of the PACS-CS or the LHP

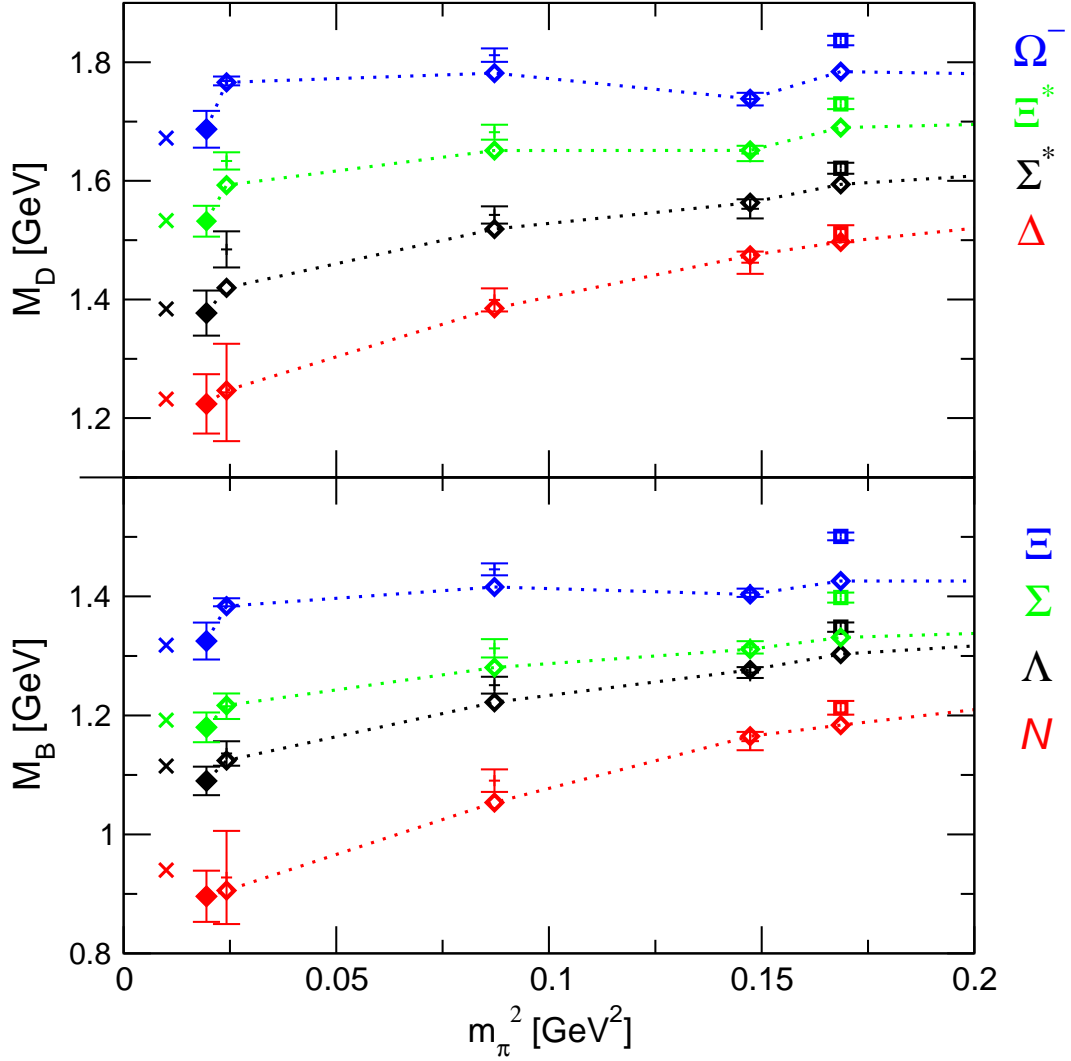


Figure 4.2: Extrapolation of the PACS-CS results [193] on the lowest-lying baryon masses within the Lorentz covariant formulation of $SU(3)_F$ -B χ PT up to NLO. The LQCD points used in the fit are represented with the corresponding error bars which do not include the correlated uncertainties. The lattice points in $m_\pi^2 \simeq 0.15 \text{ GeV}^2$ involve a lighter strange quark mass. The diamonds denote our results after the fit and they are connected by a dotted line added to guide the eye. The boxes are lattice points not included in the fit (heavier kaon mass) and the filled diamonds are the extrapolated values which are to be compared with experimental data (crosses). The latter are slightly shifted for a better comparison with the extrapolation results.

Table 4.4: Values of the LECs in the baryon-octet sector from the fits to the experimental, the PACS-CS [193] and the LHP [192] results on the baryon masses using Lorentz covariant B χ PT up to NLO.

	M_{B_0} [GeV]	b_0 [GeV $^{-1}$]	$M_{B_0}^{eff}$ [GeV]	b_D [GeV $^{-1}$]	b_F [GeV $^{-1}$]
Expt.	-	-	1.840(5)	0.199(4)	-0.530(2)
PACS-CS	0.756(32)	-0.978(38)	1.76(7)	0.190(24)	-0.519(19)
LHP	0.780(31)	-1.044(45)	1.85(8)	0.236(24)	-0.523(21)

Table 4.5: Values of the LECs in the baryon-decuplet sector from the fits to the experimental, the PACS-CS [193] and the LHP [192] results on the baryon masses using Lorentz covariant B χ PT up to NLO.

	M_{T_0} [GeV]	t_0 [GeV $^{-1}$]	$M_{T_0}^{eff}$ [GeV]	t_D [GeV $^{-1}$]
Expt.	-	-	1.519(2)	-0.694(2)
PACS-CS	954(37)	-1.05(8)	1.49(8)	-0.682(20)
LHP	944(42)	-1.28(8)	1.60(8)	-0.609(14)

results². In the case of the baryon-octet masses, the values of the LECs determined using either of the two LQCD sets of results agree with each other. Moreover, these values also agree, within error bars, with those resulting from the experimental determination. This suggests a non-trivial consistency in the baryon-octet sector between the lattice actions employed by the two collaborations (at different lattice spacings) and the experimental information on the masses through covariant B χ PT up to NLO of accuracy. This is reflected in the quality of the extrapolations shown in Table 4.3. Notice that such self-consistency between LQCD, χ PT and experiment is not achieved neither at LO (GMO) nor at NLO within the HB approach.

For the masses of the decuplet-baryons there is not a general agreement among the values of the LECs obtained from the different sources. While the values obtained using the PACS-CS results agree with those determined with the experimental data, the fit to the LHP results presents a value of t_D that is not consistent with the experimental one. Besides that, the analysis of the two LQCD sets of results lead to different values on t_0 , although consistent on

²Since the experimental data do not disentangle M_{B_0} (M_{T_0}) from b_0 (t_0) for the baryon-octet (-decuplet), in the comparison with the experimental determinations we must consider the effective masses $M_{B_0}^{eff}$ ($M_{T_0}^{eff}$) instead of these LECs.

M_{T0} and M_{T0}^{eff} . These problems in the decuplet sector of the LHP results also appeared in the extrapolation to the physical point as it is shown in Table 4.3 and was discussed in the previous section.

Pionic and strange σ -terms

The σ terms are defined as the matrix elements of the commutators

$$\sigma^{ab}(x) = [Q^a(x'), [Q^b(x'), \mathcal{H}_{sb}(x)]] , \quad (4.14)$$

with $Q^{a,b}$ any of the eight axial charges, and $\mathcal{H}_{sb}(x) = \bar{q}\mathcal{M}q = m(\bar{u}u + \bar{d}d) + m_s\bar{s}s$ the part of the Hamiltonian explicitly breaking chiral symmetry. We will focus on the matrix elements of the pion and strangeness sigma commutators defined respectively as

$$\sigma_{\pi\mathcal{B}} = m\langle\mathcal{B}|\bar{u}u + \bar{d}d|\mathcal{B}\rangle, \quad (4.15)$$

$$\sigma_{s\mathcal{B}} = m_s\langle\mathcal{B}|\bar{s}s|\mathcal{B}\rangle, \quad (4.16)$$

$$(4.17)$$

where \mathcal{B} may denote an octet or decuplet baryon. The sigma terms can be obtained from the chiral corrections to the baryon masses through the Hellman-Feynman theorem [212, 213]

$$\sigma_{\pi\mathcal{B}} = m \frac{\partial M_{\mathcal{B}}}{\partial m}, \quad (4.18)$$

$$\sigma_{s\mathcal{B}} = m_s \frac{\partial M_{\mathcal{B}}}{\partial m_s}. \quad (4.19)$$

Up to the order considered in this work, we can express these sigma elements as

$$\sigma_{\pi\mathcal{B}} = \frac{m_\pi^2}{2} \left(\frac{1}{m_\pi} \frac{\partial M_{\mathcal{B}}}{\partial m_\pi} + \frac{1}{2m_K} \frac{\partial M_{\mathcal{B}}}{\partial m_K} + \frac{1}{3m_\eta} \frac{\partial M_{\mathcal{B}}}{\partial m_\eta} \right), \quad (4.20)$$

$$\sigma_{s\mathcal{B}} = \left(m_K^2 - \frac{m_\pi^2}{2} \right) \left(\frac{1}{2m_K} \frac{\partial M_{\mathcal{B}}}{\partial m_K} + \frac{2}{3m_\eta} \frac{\partial M_{\mathcal{B}}}{\partial m_\eta} \right). \quad (4.21)$$

The LECs determined with the LQCD results can be used to predict the pionic and strangeness sigma terms of the low-lying baryons. This is the most relevant consequence of fixing the LECs within a reliable combination of LQCD and χ PT, i.e. it leads to solid predictions. The results are shown in Table 4.6 and 4.7 for the baryon-octet and -decuplet respectively. If we consider only baryon loops we get central values for the $\sigma_{\pi N}$ term close to the classical value of 45 MeV [214], e.g. $\sigma_{\pi N} = 44$ MeV using the PACS-CS data set. The addition

Table 4.6: Predictions on the σ_π and σ_s terms (in MeV) of the baryon-octet in covariant $SU(3)_F$ -B χ PT after fitting the LECs to the PACS-CS [193] or LHP [192] results.

		N	Λ	Σ	Ξ
PACS-CS	σ_π	59(2)(17)	39(1)(10)	26(2)(5)	13(2)(1)
	σ_s	-7(23)(25)	123(26)(35)	157(27)(44)	264(31)(50)
LHP	σ_π	61(2)(21)	41(2)(13)	25(2)(7)	14(2)(3)
	σ_s	-4(20)(25)	103(19)(8)	164(23)(16)	234(23)(21)

Table 4.7: Predictions on the σ_π and σ_s terms (in MeV) of the baryon-decuplet in covariant $SU(3)_F$ -B χ PT after fitting the LECs to the PACS-CS [193] or LHP [192] results.

		Δ	Σ^*	Ξ^*	Ω^-
PACS-CS	σ_π	55(4)(18)	39(3)(12)	22(3)(6)	4(2)(1)
	σ_s	54(24)(1)	158(27)(7)	272(32)(15)	357(34)(26)
LHP	σ_π	60(2)(20)	45(2)(14)	28(2)(8)	12(2)(7)
	σ_s	145(30)(10)	210(30)(4)	283(31)(2)	329(32)(8)

of decuplet loops raises this value to 59 MeV. This effect of the decuplet/ Δ 's contributions in the pionic σ -term has been found in some other works and the values 54 MeV [206] MeV or 57 MeV [201] MeV have been obtained. At $\mathcal{O}(p^4)$ without the decuplet (the decuplet is partially included through the LECs) it is obtained the value $\sigma_{\pi N} \simeq 52$ MeV [182]. On the other hand, the results on σ_{sN} are consistent with 0. This result comes to be very close to the one of Ref. [206] where a chiral extrapolation to the same LQCD results have been performed using finite-range regularization. The consequences that such small values of σ_{sN} have in supersymmetric dark matter searches have been investigated in Ref. [215]. Finally, notice the large discrepancy between the results for the $\sigma_{s\Delta}$ obtained using either the PACS-CS or the LHP results. The very large value obtained from the analysis of the latter illustrate, again, the problems of the LHP data set in the decuplet sector.

4.3 Summary

In summary, we have explored the applicability of the covariant formulation of $SU(3)_F$ -B χ PT within the EOMS scheme to analyze current 2+1-flavor LQCD data, i.e. the results of the PACS-CS and LHP collaborations on the baryon masses. In contrast with the problems found in HB, the covariant approach is able to describe simultaneously the experimental data and the LQCD results. Moreover, we have found that the consistency between both is improved from the good linear extrapolation obtained at LO (GMO) with the inclusion of the leading non-analytic terms. This is achieved despite that the light quark masses from which we perform the extrapolation are close to the physical point. The success of a $SU(3)_F$ -B χ PT approach to describe current 2+1-flavor LQCD results may have important phenomenological applications, as it has been shown with the determination of the σ terms. This progress in χ PT is very timely given the various baryon observables for which LQCD simulations are entering the chiral regime. Further investigations on the recent results for the weak vector [173, 174] and axial form factors [216, 217] and on their strong pseudoscalar [218] or electromagnetic structure [219] are foreseeable.

Chapter 5

Summary and Outlook

Baryon phenomenology is a field of great interest. Strangeness production experiments are currently taking place or are scheduled in Laboratories like CERN-SPS with hadron beams (COMPASS), TJNAF in photoproduction reactions (CLAS) and parity-violating electron scattering (Q-weak), GSI in p p collisions (HADES), LNF in kaonic atoms (SIDDHARTA), MAMI in parity-violating electron scattering (A2), etc. Further experiments are planned in centers like CERN-SPS (NA-62), J-PARC, GSI (pion beam) or LNF (DAPHNE2). Moreover, the last few years have witnessed an impressive development in the LQCD description of several observables and realistic results on baryon structure are starting to appear. The $SU(3)_F$ -B χ PT, being the EFT of QCD describing the low-energy interaction of baryons with pseudoscalar mesons, is a suitable framework to analyze in a model-independent fashion the experimental data and lattice results. However, this field has been troubled for a very long time because of several conceptual problems like the power counting subtleties in presence of heavy-matter fields (baryons) or those caused by the closeness in mass of baryonic resonances.

The main subject of the present thesis has been to analyze these problems and to develop a dimensionally-renormalized $SU(3)_F$ -B χ PT framework that gives a successful description of various baryonic observables at the same time as shows a reasonable convergence of the chiral series. This approach has been worked out up to NLO and NNLO level of accuracy (one-loop) for several observables and its main ingredients can be summarized as follows

- The calculations are performed using a chiral Lagrangian that is explicitly Lorentz covariant. The power-counting rule for baryons of Eq. (1.35), that holds strictly in HB, is broken at lower orders by analytical pieces from the loops, i.e. by terms that have the same structure as the

chiral Lagrangian up to this order. On the other side, the covariant formulation provides an infinite tower of relativistic corrections (analytical and non-analytical) to the HB results.

- The power counting is recovered introducing an extension of the \overline{MS} -renormalization prescription by which the terms that break the counting from below are systematically absorbed into a finite set of LECs, i.e. the EOMS renormalization scheme.
- The effects of the lowest-lying decuplet resonances are considered introducing them as a multiplet of spin-3/2 fields described by a covariant Rarita-Schwinger Lagrangian. The problem of the spin-1/2 unphysical degrees of freedom contained in the vector-spinor representation of the spin-3/2 fields is treated, as far as possible, introducing consistent chiral interactions, i.e. those verifying Eq. (1.42)¹.
- The decuplet-octet mass difference $\delta = M_T - M_B$ is implemented non-perturbatively. Namely, we do not assign any specific order to δ as compared to the pseudoscalar meson masses m_ϕ and we apply the rule of Eq. (1.35) with the spin-3/2 propagators counting as those of the baryon octet. The new loop-graphs emerging with the decuplet also break the power-counting from below and the respective terms are absorbed again into the LECs within an extension of the conventional EOMS scheme.
- The inclusion of the decuplet resonances may produce a mismatch between the power-counting and the power of the divergence in the loop diagrams. This is due to the momentum dependence of the spin-3/2 propagator in Eq. (1.43) and it is the reason for the appearance of ultraviolet divergences of a chiral order higher than the one assigned by the power-counting formula of Eq. (1.35). We regularize these infinities into the proper higher-order chiral-invariant counter-terms. However, we do not introduce the corresponding LECs but study the residual renormalization-scale dependence that, moreover, we use to get an estimation on the potential size of the higher-order contributions.
- The HB results have been always recovered from the renormalized covariant results when the expansion in powers of $1/M_{B0}$ has been applied. In particular, in the graphs with both octet and decuplet baryons, we obtain the HB formulas in the SSE power-counting scheme ($\delta \sim m_\phi$).

¹The electromagnetic coupling to virtual spin-3/2 fields is an example of an interaction term that we do not know how to make consistent.

- We have checked that the renormalized contributions of the decuplet resonances to the observables of the baryons belonging to the octet vanish in the limit $\delta \rightarrow \infty$. This is consistent with the assumption that higher-mass degrees of freedom are irrelevant for the scales we are dealing with.

We have chosen the baryon-octet magnetic moments as a benchmark property to compare various $SU(3)_F$ -B χ PT approaches to the baryon sector and to explore the origin of their differences. Historically, B χ PT has found great difficulties to explain the experimental data of these moments and to improve in a model-independent fashion the $SU(3)_F$ -symmetric description of CG. Indeed, only within the novel covariant approach in the EOMS scheme one is able to improve the CG description at NLO. The comparison with the HB results remarks the importance of the relativistic corrections, i.e. in the $SU(3)_F$ -formulation sizable numerical cancellations occur among terms of different order in the non-relativistic expansion. These effects are found to be even more dramatic for the decuplet contributions. The comparison with the results of the IR scheme warns us on the effect that the unphysical cuts introduced in this scheme may have when dealing with pseudoscalar mesons as heavy as the K or the η . In that sense, keeping the right analytic properties of the loop contributions to the physical amplitudes can be critical to obtain a good convergence of the chiral series in $SU(3)_F$ -B χ PT.

Besides that, the inclusion of the decuplet contributions gives the chance to compare the different solutions proposed to treat the unphysical spin-1/2 degrees of freedom contained in the relativistic vector-spinor fields. In particular, we compare the approach based on demanding the lowest-order interaction couplings to be consistent in the sense of Eq. (1.42) with the one where the interaction terms depend on a off-shell parameter z that is fixed after an analysis of the constraints in the Dirac Hamiltonian formalism. These two schemes are equivalent up to the contributions of a set of chiral-invariant Lagrangian terms which embody part of those carried by unphysical spin-1/2 degrees of freedom. Despite that these contributions are formally of higher-order they are rather large. More precisely, only with the consistent couplings the $SU(3)_F$ -breaking corrections of the decuplet to the baryon-octet magnetic moments are small and the improvement over the CG is still achieved at NLO in the chiral expansion.

The analysis of the baryon-octet magnetic moments casts a surprising picture of the chiral expansion of the baryonic properties. From an EFT viewpoint it is hard to understand how different contributions that are formally of subleading order, as those provided by the relativistic corrections to the HB results ($\Lambda_{\chi SB} \sim M_{B0}$) or those carried by the unphysical degrees of freedom of the spin-3/2 fields, can have such a big impact in the description of observ-

ables. This is undoubtedly due to the fact that the chiral series with heavy pseudoscalar meson masses or in presence of the non-perturbative effects associated to the baryonic resonances are, at best, close to the limit of their radius of convergence. A prominent outcome of our analysis is that a good convergence can be achieved when the chiral series are arranged in such a way that general principles as Lorentz invariance and analyticity, or to keep the relevant physical degrees of freedom, are imposed. Given the rapid proliferation in the number of LECs at higher orders (i.e. of the order of 30 in the case of the baryon octet magnetic moments or masses at NNLO), schemes with improved convergence are essential to keep the baryonic sector of χ PT predictive.

We have extended this formalism to the study of the electromagnetic static structure of the decuplet resonances. Little is known about these properties although those of the $\Delta(1232)$ are currently the subject of an experimental effort at MAMI and of intense theoretical investigations as those carried out in LQCD. The predictive power that the $SU(3)_F$ formulation of B χ PT has been illustrated in this case. Indeed, the MDMs of the decuplet baryons, and in particular the $\Delta(1232)$, have been determined fixing the only LEC appearing up to this order with the well measured MDM of the Ω^- . Our results $\mu_{\Delta}^{++} = 6.0(1.0) \mu_N$ and $\mu_{\Delta}^+ = 2.84(50) \mu_N$ very well agree with the central values of the PDG averages or the latest experimental results, and the comparison with the HB values confirms the conclusions addressed in the previous paragraph. The EQM, MOM and CR have been predicted in terms of the latest (quenched) LQCD results on the Ω^- , baryon for which we argue that model-independent and reliable information is likely to appear either from experiment or dynamical simulation in LQCD. The EQM and MOM are dominated by the loop contributions whereas in case of the CR the tree-level (LEC) dominates by far, what may indicate the relative importance that the mesonic resonances have in this observable.

The $SU(3)_F$ -B χ PT applied to baryon phenomenology can also be used to obtain the values of some SM parameters. Equivalently as with the kaons, the CKM matrix element V_{us} is extracted from semileptonic hyperon decay data once hadronic matrix elements, and in particular the vector coupling $f_1(0)$, are determined. The subsequent value is used in addition with the V_{ud} determined from super-allowed β decays to probe beyond SM physics through the first row unitarity relation of Eq. (3.1), where V_{ub} is negligible up to the current accuracy. We have applied our covariant formalism to obtain the hadronic matrix element $f_1(0)$ up to NNLO. Differently to any of the other properties studied in this thesis, the $SU(3)_F$ -breaking corrections to $f_1(0)$ in the covariant and HB approaches are quite similar and marginally consistent. This might be due to the fact that no counter-terms contributions appear in the chiral expansion of

this observable up to NNNLO. A similar observation can be done in the comparison between the baryon-octet contributions given by the IR and EOMS schemes (Table 3.1). As a result of our calculation of $f_1(0)$, an accurate value of V_{us} is obtained using hyperon semileptonic decay data and including theoretical and experimental uncertainties. The fact that in the hyperon decays we can statistically combine the extraction of this CKM element from different channels is the key point to obtain such a high accuracy. Nevertheless, we have also argued that corrections to V_{us} potentially as large as those given by the $SU(3)_F$ -breaking to $f_1(0)$ can also be given by the corrections to $g_2(0)$.

Finally, we have analyzed the recent and celebrated LQCD results on the lowest-lying baryon masses, in particular those of the PACS-CS and LHP collaborations. In dramatic contrast with the extrapolations performed with the HB approach, we have found that a very good description of the light and strange quark-mass dependencies is obtained simultaneously for the baryon-octet and -decuplet using our covariant formulation of $B\chi$ PT. In fact, the lattice results are well described up to quark masses corresponding to π and K masses below 600 MeV and the extrapolation is improved over the one obtained at LO by the GMO model. The comparison of the covariant results with the HB ones indicates that numerical cancellations are being produced among different terms of the non-relativistic expansion when departing from the physical point. On the other hand, the comparison with the GMO results, which are linear in m_q , remarks the importance of the non-analytic chiral structures in extrapolations from masses as small as those used by the PACS-CS collaboration ($m_\pi \simeq 156$ MeV). These results with the baryon masses may anticipate the far-reaching phenomenological applications that a reliable combination of LQCD and $B\chi$ PT may have in the future. We have emphasized this particular point in the thesis with the prediction of the pionic and strange sigma terms of the baryons and, in particular, of the nucleon.

In summary, baryons are a doorway to understand non-perturbative QCD or to probe beyond SM physics. Furthermore, the knowledge of their structure or of their interactions, besides providing information on nucleon and nuclear properties, is essential to study strange matter and the physics derived thereof, i.e. hypernuclear and nuclear astrophysics. The relativistic approach to baryon χ PT we have developed in this thesis has proved to be a suitable framework to interpret and process the information on baryons that will be coming soon from both experimental facilities and lattice QCD calculations.

Appendix **A**

SU(3) algebra and Dirac matrices

An explicit representation of the Gell-Mann matrices is given by

$$\begin{aligned}
 \lambda_1 &= \begin{pmatrix} 0 & 1 & 0 \\ 1 & 0 & 0 \\ 0 & 0 & 0 \end{pmatrix}, & \lambda_2 &= \begin{pmatrix} 0 & -i & 0 \\ i & 0 & 0 \\ 0 & 0 & 0 \end{pmatrix}, & \lambda_3 &= \begin{pmatrix} 1 & 0 & 0 \\ 0 & -1 & 0 \\ 0 & 0 & 0 \end{pmatrix}, \\
 \lambda_4 &= \begin{pmatrix} 0 & 0 & 1 \\ 0 & 0 & 0 \\ 1 & 0 & 0 \end{pmatrix}, & \lambda_5 &= \begin{pmatrix} 0 & 0 & -i \\ 0 & 0 & 0 \\ i & 0 & 0 \end{pmatrix}, & \lambda_6 &= \begin{pmatrix} 0 & 0 & 0 \\ 0 & 0 & 1 \\ 0 & 1 & 0 \end{pmatrix}, \\
 \lambda_7 &= \begin{pmatrix} 0 & 0 & 0 \\ 0 & 0 & -i \\ 0 & i & 0 \end{pmatrix}, & \lambda_8 &= \sqrt{\frac{1}{3}} \begin{pmatrix} 1 & 0 & 0 \\ 0 & 1 & 0 \\ 0 & 0 & -2 \end{pmatrix}.
 \end{aligned} \tag{A.1}$$

which a basis of the Lie algebra of $SU(3)$, namely the set of Hermitian and traceless 3×3 matrices. The structure of $SU(3)$ is encoded in the commutation relations of the Gell-Mann matrices,

$$\left[\frac{\lambda_a}{2}, \frac{\lambda_b}{2} \right] = i f_{abc} \frac{\lambda_c}{2}, \tag{A.2}$$

where the structure constants f_{abc} are totally antisymmetric

$$f_{abc} = -\frac{i}{4} \text{Tr}([\lambda_a, \lambda_b] \lambda_c). \tag{A.3}$$

The anticommutation relations read

$$\{\lambda_a, \lambda_b\} = \frac{4}{3} \delta_{ab} + 2 d_{abc} \lambda_c, \tag{A.4}$$

with the totally symmetric coefficients d_{abc} given by

$$d_{abc} = \frac{1}{4} \text{Tr}(\{\lambda_a, \lambda_b\} \lambda_c). \tag{A.5}$$

Adding the ninth matrix

$$\lambda_0 = \sqrt{2/3} \text{diag}(1, 1, 1), \quad (\text{A.6})$$

to the Gell-Mann matrices we obtain the basis of the algebra of $U(3)$, i.e. the set of Hermitian 3×3 matrices.

The totally antisymmetric Gamma matrix products appearing in the consistent BT and TT Lagrangians of Sec. 1.4 are defined as

$$\gamma^{\mu\nu} = \frac{1}{2}[\gamma^\mu, \gamma^\nu], \quad (\text{A.7})$$

$$\gamma^{\mu\nu\rho} = \frac{1}{2}\{\gamma^{\mu\nu}, \gamma^\rho\} = -i\varepsilon^{\mu\nu\rho\sigma}\gamma_\sigma\gamma_5, \quad (\text{A.8})$$

$$\gamma^{\mu\nu\rho\sigma} = \frac{1}{2}[\gamma^{\mu\nu\rho}, \gamma^\sigma] = i\varepsilon^{\mu\nu\rho\sigma}\gamma_5 \quad (\text{A.9})$$

with the following conventions: $g^{\mu\nu} = \text{diag}(1, -1, -1, -1)$, $\varepsilon_{0,1,2,3} = -\varepsilon^{0,1,2,3} = 1$, $\gamma_5 = i\gamma_0\gamma_1\gamma_2\gamma_3$.

Appendix **B**

Numerical value of the coupling constants

We take the values

$$D = 0.804, \quad F = 0.463, \quad (\text{B.1})$$

for the axial and vector meson-baryon couplings appearing in $\mathcal{L}_{\phi B}^{(1)}$ which are the values obtained at the LO fit to the semileptonic-hyperon decay rates [162]. The ϕBD coupling $\mathcal{C} = \frac{h_A}{2\sqrt{2}}$ is obtained by fitting $\Delta \rightarrow N\pi$ decay width

$$\mathcal{C} = 1.0. \quad (\text{B.2})$$

This value for \mathcal{C} is different from the one often used in most of the HB calculations [103, 105, 106]. In these papers, it is applied a convention for the “vielbein” that is related to ours by a factor of 2. Consequently, the values in the HB studies, $\mathcal{C} \sim 1.5$, equal $\mathcal{C} \sim 0.75$ in our convention. The ϕTT coupling \mathcal{H} is barely known and we fix it using the large N_c relation between the nucleon and Δ axial charges, g_A and H_A respectively, $H_A = (9/5)g_A$. Given that $H_A = 2\mathcal{H}$ and $g_A = 1.26$, we use

$$\mathcal{H} = 1.13. \quad (\text{B.3})$$

Table B.1: Values of the couplings and masses used in this thesis. The masses and decay constants are in GeV.

D	F	\mathcal{C}	\mathcal{H}	f_π	F_ϕ	m_π	m_K	m_η	M_{B0}	M_{T0}
0.80	0.46	1.0	1.18	0.0924	$1.17f_\pi$	0.138	0.496	0.548	1.151	1.382

As for the meson-decay constant in the chiral limit F_0 , we choose an average between the physical values $F_\pi=92.4$ MeV, $F_K=1.22F_\pi$ and $F_\eta=1.3F_\pi$. Namely,

$$F_0 \equiv F_\phi = 1.17F_\pi. \quad (\text{B.4})$$

Finally, for the masses of the pseudoscalar mesons we take

$$m_\pi \equiv m_{\pi^\pm} = 0.140\text{GeV}, \quad m_K \equiv m_{K^\pm} = 0.494\text{GeV}, \quad (\text{B.5})$$

and, if not otherwise stated we use the experimental value for the η mass, $m_\eta = 0.548$ GeV. Finally, the loop contributions depend on the baryon-octet and decuplet masses, which are taken as the $\mathcal{O}(p^0)$ term in their chiral expansions. Namely, $M_B = M_{B0} = 1.151$ GeV and $M_T = M_{T0} = 1.382$ GeV. This is justified for most of the loop calculations presented in this thesis since the $SU(3)_F$ -breaking of the masses contributes at higher orders. An exception is in the calculation of $f_1(0)$ in Sec. 3 for which we reach $\mathcal{O}(p^4)$ and the leading breaking in the baryon masses have to be implemented.

We summarize in Table B.1 the values of the parameters used in this thesis.

Appendix C

Tables and loop functions

In the calculation of the loop diagrams, we have used the following d -dimensional integrals in Minkowski space:

$$\int d^d k \frac{k^{\alpha_1} \dots k^{\alpha_{2n}}}{(\mathcal{M}^2 - k^2)^\lambda} = i\pi^{d/2} \frac{\Gamma(\lambda - n - d/2)}{2^n \Gamma(\lambda)} \frac{(-1)^n g_s^{\alpha_1 \dots \alpha_{2n}}}{(\mathcal{M}^2)^{\lambda - n - d/2}} \quad (\text{C.1})$$

with $g_s^{\alpha_1 \dots \alpha_{2n}} = g^{\alpha_1 \alpha_2} \dots g^{\alpha_{2n-1} \alpha_{2n}} + \dots$ symmetrical with respect to the permutation of any pair of indices (with $(2n - 1)!!$ terms in the sum). We will present the divergent part of the loops as the piece $\lambda_\varepsilon = 2\mu^{2\varepsilon}/\varepsilon + \log 4\pi - \gamma_E$, where $\varepsilon = 4 - d$ and $\gamma_E \simeq 0.5772$ the Euler constant, and will express the loop functions in terms of Feynman parameter integrals. When applying the \overline{MS} prescription in dimensional regularization, we absorb the divergent piece λ_ε into suitable LECs. In the presentation of the results, we may use the dimensionless quantities $R = M_{T_0}/M_{B_0}$ and $r = 1/R = M_{B_0}/M_{T_0}$ for the baryon masses and $\bar{\mu}_B = \mu/M_{B_0}$ or $\bar{\mu}_T = \mu/M_{T_0}$ for the renormalization scale.

We fix here some typos appearing in the published works. In particular the expressions equivalent to Eq. (C.1), ε and λ_ε in Refs. [2, 4] are not completely consistent. Furthermore, we have corrected a sign error in Eqs. (A.15)-(A.16) of Ref. [2], and the divergent piece of $H_1^{(b)}$ and a factor 2 in $H_3^{(i,X)}$ of Ref. [4]. These correspond to either Eqs. (C.9), Eq. (C.12) or Eqs. (C.30)-(C.32) below. Finally, in Ref. [3], the $\mathcal{O}(p^3)$ calculation of $f_1(0)$ was presented whereas we display below the full $\mathcal{O}(p^4)$ results.

Table C.1: Coefficients of the tree-level [Eq. (2.7)] and loop contributions [Eq. (2.8)] to the magnetic moments of the octet baryons. The coefficients of the diagram (\mathbf{f}) of Fig. 2.1 can be obtained using that $\xi_{BM}^{(f,I)} = -\xi_{BM}^{(d)}$ and $\xi_{BM}^{(f,II)} = -\xi_{BM}^{(e)}$.

	p	n	Λ	Σ^-	Σ^+	Σ^0	Ξ^-	Ξ^0	$\Lambda\Sigma^0$
α_B	$\frac{1}{3}$	$-\frac{2}{3}$	$-\frac{1}{3}$	$\frac{1}{3}$	$\frac{1}{3}$	$\frac{1}{3}$	$\frac{1}{3}$	$-\frac{2}{3}$	$\frac{1}{\sqrt{3}}$
β_B	1	0	0	-1	1	0	-1	0	0
$\xi_{B\pi}^{(b)}$	$-(D+F)^2$	$(D+F)^2$	0	$\frac{2}{3}(D^2+3F^2)$	$-\frac{2}{3}(D^2+3F^2)$	0	$(D-F)^2$	$-(D-F)^2$	$-\frac{4}{\sqrt{3}}DF$
$\xi_{BK}^{(b)}$	$-\frac{2}{3}(D^2+3F^2)$	$-(D-F)^2$	$2DF$	$(D-F)^2$	$-(D+F)^2$	$-2DF$	$\frac{2}{3}(D^2+3F^2)$	$(D+F)^2$	$-\frac{2}{\sqrt{3}}DF$
$\xi_{B\pi}^{(c)}$	$-\frac{1}{2}(D+F)^2$	$-(D+F)^2$	0	$2F^2$	$-2F^2$	0	$\frac{1}{2}(D-F)^2$	$(D-F)^2$	$\frac{4}{\sqrt{3}}DF$
$\xi_{BK}^{(c)}$	$-(D-F)^2$	$(D-F)^2$	$-2DF$	$(D+F)^2$	$-(D-F)^2$	$2DF$	$(D+F)^2$	$-(D+F)^2$	$\frac{2}{\sqrt{3}}DF$
$\xi_{B\eta}^{(c)}$	$-\frac{1}{6}(D-3F)^2$	0	0	$\frac{2}{3}D^2$	$-\frac{2}{3}D^2$	0	$\frac{1}{6}(D+3F)^2$	0	0
$\xi_{B\pi}^{(d)}$	$-\frac{8}{9}\mathcal{C}^2$	$\frac{8}{9}\mathcal{C}^2$	0	$-\frac{2}{9}\mathcal{C}^2$	$\frac{2}{9}\mathcal{C}^2$	0	$-\frac{4}{9}\mathcal{C}^2$	$\frac{4}{9}\mathcal{C}^2$	$-\frac{4}{3\sqrt{3}}\mathcal{C}^2$
$\xi_{BK}^{(d)}$	$\frac{2}{9}\mathcal{C}^2$	$\frac{4}{9}\mathcal{C}^2$	$\frac{2}{3}\mathcal{C}^2$	$-\frac{4}{9}\mathcal{C}^2$	$-\frac{8}{9}\mathcal{C}^2$	$-\frac{2}{3}\mathcal{C}^2$	$-\frac{2}{9}\mathcal{C}^2$	$\frac{8}{9}\mathcal{C}^2$	$-\frac{2}{3\sqrt{3}}\mathcal{C}^2$
$\xi_{B\pi}^{(e)}$	$\frac{32}{9}\mathcal{C}^2$	$-\frac{8}{9}\mathcal{C}^2$	0	$-\frac{2}{9}\mathcal{C}^2$	$\frac{2}{9}\mathcal{C}^2$	0	$-\frac{2}{9}\mathcal{C}^2$	$-\frac{4}{9}\mathcal{C}^2$	$\frac{4}{3\sqrt{3}}\mathcal{C}^2$
$\xi_{BK}^{(e)}$	$\frac{4}{9}\mathcal{C}^2$	$-\frac{4}{9}\mathcal{C}^2$	$-\frac{2}{3}\mathcal{C}^2$	$-\frac{16}{9}\mathcal{C}^2$	$\frac{28}{9}\mathcal{C}^2$	$\frac{2}{3}\mathcal{C}^2$	$-\frac{16}{9}\mathcal{C}^2$	$-\frac{8}{9}\mathcal{C}^2$	$\frac{2}{3\sqrt{3}}\mathcal{C}^2$
$\xi_{B\eta}^{(e)}$	0	0	0	$-\frac{2}{3}\mathcal{C}^2$	$\frac{2}{3}\mathcal{C}^2$	0	$-\frac{2}{3}\mathcal{C}^2$	0	0

C.1 Baryon-octet magnetic moments

$$H^{(b)} = -\frac{M_{B0}^2}{2} \int_0^1 dx (1-x) \left(\frac{x^4}{\bar{\mathcal{M}}_B} + x(x+2) + (2x(x+1) - 1) \left(\lambda_\epsilon + \log \left(\frac{\bar{\mathcal{M}}_B}{\bar{\mu}_B^2} \right) \right) \right), \quad (\text{C.2})$$

$$H^{(c)} = M_{B0}^2 \int_0^1 dx \left(\frac{x^4}{\bar{\mathcal{M}}_B} + x^2 + x(3x-2) \left(\lambda_\epsilon + \log \left(\frac{\bar{\mathcal{M}}_B}{\bar{\mu}_B^2} \right) \right) \right), \quad (\text{C.3})$$

$$H^{(d)} = \frac{M_{B0}^2}{6R^2} \int_0^1 dx (1-x) \left(((1+R-x)(11x-2) - 14\bar{\mathcal{M}}_T + 3(-2x^2 + 2Rx + x + R + 4\bar{\mathcal{M}}_T + 1)) \left(\lambda_\epsilon + \log \left(\frac{\bar{\mathcal{M}}_T}{\bar{\mu}_B^2} \right) \right) \right), \quad (\text{C.4})$$

$$H^{(e)} = \frac{M_{B0}^2}{18R^4} \int_0^1 dx x \left((1+R-x)(42R^3 + (6x-4)R^2 + ((41-3x)x - 38)R + 8(x-1)^2) + (50(1-x) - R(48R + 15x + 4))\bar{\mathcal{M}}_T + 3((R-x+1)^2(2(x-1) + R(6R+3x-2)) - 2(R(15R-6x+13) - 4x+4)\bar{\mathcal{M}}_T) \times \left(\lambda_\epsilon + \log \left(\frac{\bar{\mathcal{M}}_T}{\bar{\mu}_B^2} \right) \right) \right), \quad (\text{C.5})$$

$$H^{(f,I)} = \frac{M_{B0}^2}{3R^2} \int_0^1 dx (1+R-x)\bar{\mathcal{M}}_T \left(6 \left(\lambda_\epsilon + \log \left(\frac{\bar{\mathcal{M}}_T}{\bar{\mu}_B^2} \right) \right) - 1 \right), \quad (\text{C.6})$$

$$H^{(f,II)} = \frac{M_{B0}^2}{3R^3} \int_0^1 dx (1+R-x)\bar{\mathcal{M}}_T \left((6R-3) \left(\lambda_\epsilon + \log \left(\frac{\bar{\mathcal{M}}_T}{\bar{\mu}_B^2} \right) \right) - R - 1 \right). \quad (\text{C.7})$$

where $\mathcal{M}_T = (1-x)m^2 + xM_{T0}^2 - x(1-x)M_{B0}^2 - i\epsilon$, $\mathcal{M}_B = (1-x)m^2 + x^2M_{B0}^2 - i\epsilon$ and $\mathcal{M}_{B/T} = \bar{\mathcal{M}}_{B/T}M_{B0}^2$.

We apply the \overline{MS} -renormalization scheme on the bare LECs b_6^D and b_6^F in order to cancel the divergencies of the loop-functions Eqs. (C.2)-(C.7). Furthermore, we redefine them in order to absorb power-counting breaking terms still remaining in the loop functions (EOMS-scheme)

$$\tilde{b}_6^D = b_6^D + \frac{M_{B0}^2}{8\pi^2 F_\phi^2} (12DF + \mathcal{C}^2 f^D(\mu)), \quad \tilde{b}_6^F = b_6^F + \frac{\mathcal{C}^2 M_{B0}^2}{8\pi^2 F_\phi^2} f^F(\mu), \quad (\text{C.8})$$

where the functions f^D and f^F used in the regularization of the loop-functions Eqs. (C.4-C.7) are

$$\begin{aligned}
f^D(\mu) &= -\frac{1}{36r^5} \left(4(r(r(r(r+4)+2) - 31) - 36) \log(\mu)r^5 \right. \\
&+ (r(r(r(2r(r(2r+5)+9) - 49) - 161) + 22) + 22) - 8)r^2 \\
&\left. - 2(r+1)^3 (r(r(r(r^2+r-4) - 23) + 44) - 23) + 4) \log(1-r^2) \right), \\
f^F(\mu) &= -\frac{5}{108r^6} \left(4(r(r+2)(r(r(r+2)+7) - 18) - 36) \log(\mu)r^5 \right. \\
&+ (r(r(r(r(r(4r(2r+5)+39) - 8) - 125) - 44) + 49) - 8) - 18)r^2 \\
&\left. - 2(r-1)^2(r+1)^4(r(r(r(r+2)+8) - 14) + 9) \log(1-r^2) \right). \quad (C.9)
\end{aligned}$$

From the EOMS-renormalized loop function one can recover the HB results applying $M_{T0} = M_{B0} + \delta$ and taking the leading order of the expansion in powers of $1/M_{B0}$. Only the diagrams **(b)** and **(f)** of Fig. 2.1 give a non-vanishing contribution in the HB limit

$$\begin{aligned}
\tilde{H}^{(b)}(m) &\simeq \pi M_{B0} m, \\
\tilde{H}^{(d)}(m) &\simeq -\delta M_{B0} \log\left(\frac{m^2}{4\delta^2}\right) + W_1(m, \delta), \quad (C.10)
\end{aligned}$$

where

$$W_1(m, \delta) = \begin{cases} 2 M_{B0} \sqrt{m^2 - \delta^2} \arccos \frac{\delta}{m} & m \geq \delta \\ M_{B0} \sqrt{\delta^2 - m^2} \log\left(\frac{\delta - \sqrt{\delta^2 - m^2}}{\delta + \sqrt{\delta^2 - m^2}}\right) & m < \delta \end{cases}. \quad (C.11)$$

C.2 Electromagnetic structure of the decuplet

$$H_1^{(b)}(m) = \frac{1}{3} \left(\lambda_\epsilon + \log \left(\frac{m^2}{\mu^2} \right) \right), \quad (\text{C.12})$$

$$H_2^{(d)} = \frac{M_{T0}^2}{2} \int_0^1 dx x(r+x)(2x-1) \left(\lambda_\epsilon + \log \left(\frac{\bar{\mathcal{M}}_B}{\bar{\mu}_T^2} \right) \right), \quad (\text{C.13})$$

$$H_3^{(d)} = \frac{M_{T0}^2}{3} \int_0^1 dx x^2 \left(\frac{2(x-1)(r+x)x}{\bar{\mathcal{M}}_B} + (3r+4x) \left(\lambda_\epsilon + \log \left(\frac{\bar{\mathcal{M}}_B}{\bar{\mu}_T^2} \right) \right) \right), \quad (\text{C.14})$$

$$H_4^{(d)} = -M_{T0}^2 \int_0^1 dx \frac{2(x-1)x^3(r+x)}{3\bar{\mathcal{M}}_B}, \quad (\text{C.15})$$

$$H_1^{(d)} = -\frac{1}{24} \int_0^1 dx x^2 \left((3r+2x) \left(\lambda_\epsilon + \log \left(\frac{\bar{\mathcal{M}}_B}{\bar{\mu}_T^2} \right) \right) - \frac{2(x-1)x(r+x)}{\bar{\mathcal{M}}_B} \right), \quad (\text{C.16})$$

$$H_2^{(e)} = -M_{T0}^2 \int_0^1 dx (x-1)^2(r+x) \left(\lambda_\epsilon + \log \left(\frac{\bar{\mathcal{M}}_B}{\bar{\mu}_T^2} \right) \right), \quad (\text{C.17})$$

$$H_3^{(e)} = -\frac{M_{T0}^2}{3} \int_0^1 dx (x-1)^2 \left(\frac{(r+x)^2(x-1)}{\bar{\mathcal{M}}_B} + \left(1-x+3(r+1) \left(\lambda_\epsilon + \log \left(\frac{\bar{\mathcal{M}}_B}{\bar{\mu}_T^2} \right) \right) \right) \right), \quad (\text{C.18})$$

$$H_4^{(e)} = M_{T0}^2 \int_0^1 dx \frac{2(x-1)^4(r+x)}{3\bar{\mathcal{M}}_B}, \quad (\text{C.19})$$

$$H_1^{(e)} = -\frac{1}{24} \int_0^1 dx (x-1)^2 \left(\frac{(r+x)^2(x-1)}{\bar{\mathcal{M}}_B} + \left(1-x-3(r+2x-1) \left(\lambda_\epsilon + \log \left(\frac{\bar{\mathcal{M}}_B}{\bar{\mu}_T^2} \right) \right) \right) \right), \quad (\text{C.20})$$

$$H_2^{(g)} = \frac{M_{T0}^2}{18} \int_0^1 dx x(x+1) \left(34x-26+3(7x-5) \left(\lambda_\epsilon + \log \left(\frac{\bar{\mathcal{M}}_T}{\bar{\mu}_T^2} \right) \right) \right), \quad (\text{C.21})$$

$$H_3^{(g)} = \frac{M_{T0}^2}{27} \int_0^1 dx x \left(4x(33-19x) - \frac{24x^2(x^2-1)}{\bar{\mathcal{M}}_T} + 27\bar{\mathcal{M}}_T + 3(36-70x^2+6x-27\bar{\mathcal{M}}_T) \left(\lambda_\epsilon + \log \left(\frac{\bar{\mathcal{M}}_T}{\bar{\mu}_T^2} \right) \right) \right), \quad (\text{C.22})$$

Table C.2: Coefficients of the loop-contribution Eq. (4.11) for any of the decuplet-baryons T . The coefficients of the diagram (i) of Fig. 2.4 can be obtained using that $\xi_{BT}^{(i,I)} = -\xi_{BT}^{(g)}$ and $\xi_{BT}^{(i,II)} = \xi_{BT}^{(h)}$.

	Δ^{++}	Δ^+	Δ^0	Δ^-	Σ^{*+}	Σ^{*0}	Σ^{*-}	Ξ^{*0}	Ξ^{*-}	Ω^-
$\xi_{\pi,T}^{(b)}$	$\frac{3}{4}$	$\frac{1}{4}$	$-\frac{1}{4}$	$-\frac{3}{4}$	$\frac{1}{2}$	0	$-\frac{1}{2}$	$\frac{1}{4}$	$-\frac{1}{4}$	0
$\xi_{K,T}^{(b)}$	$\frac{3}{4}$	$\frac{1}{2}$	$\frac{1}{4}$	0	$\frac{1}{4}$	0	$-\frac{1}{4}$	$-\frac{1}{4}$	$-\frac{1}{2}$	$-\frac{3}{4}$
$\xi_{\pi,T}^{(d)}$	$-4\mathcal{C}^2$	$-\frac{4}{3}\mathcal{C}^2$	$\frac{4}{3}\mathcal{C}^2$	$4\mathcal{C}^2$	$-\frac{8}{3}\mathcal{C}^2$	0	$\frac{8}{3}\mathcal{C}^2$	$-\frac{4}{3}\mathcal{C}^2$	$\frac{4}{3}\mathcal{C}^2$	0
$\xi_{K,T}^{(d)}$	$-4\mathcal{C}^2$	$-\frac{8}{3}\mathcal{C}^2$	$-\frac{4}{3}\mathcal{C}^2$	0	$-\frac{4}{3}\mathcal{C}^2$	0	$\frac{4}{3}\mathcal{C}^2$	$\frac{4}{3}\mathcal{C}^2$	$\frac{8}{3}\mathcal{C}^2$	$4\mathcal{C}^2$
$\xi_{\pi,T}^{(e)}$	$4\mathcal{C}^2$	$\frac{8}{3}\mathcal{C}^2$	$\frac{4}{3}\mathcal{C}^2$	0	$\frac{2}{3}\mathcal{C}^2$	0	$-\frac{2}{3}\mathcal{C}^2$	$-\frac{4}{3}\mathcal{C}^2$	$-\frac{2}{3}\mathcal{C}^2$	0
$\xi_{K,T}^{(e)}$	$4\mathcal{C}^2$	$\frac{4}{3}\mathcal{C}^2$	$-\frac{4}{3}\mathcal{C}^2$	$-4\mathcal{C}^2$	$\frac{4}{3}\mathcal{C}^2$	0	$-\frac{4}{3}\mathcal{C}^2$	$\frac{4}{3}\mathcal{C}^2$	$-\frac{4}{3}\mathcal{C}^2$	$-4\mathcal{C}^2$
$\xi_{\eta,T}^{(e)}$	0	0	0	0	$2\mathcal{C}^2$	0	$-2\mathcal{C}^2$	0	$-2\mathcal{C}^2$	0
$\xi_{\pi,T}^{(g)}$	$-\frac{4}{3}\mathcal{H}^2$	$-\frac{4}{9}\mathcal{H}^2$	$\frac{4}{9}\mathcal{H}^2$	$\frac{4}{3}\mathcal{H}^2$	$-\frac{8}{9}\mathcal{H}^2$	0	$\frac{8}{9}\mathcal{H}^2$	$-\frac{4}{9}\mathcal{H}^2$	$\frac{4}{9}\mathcal{H}^2$	0
$\xi_{K,T}^{(g)}$	$-\frac{4}{3}\mathcal{H}^2$	$-\frac{8}{9}\mathcal{H}^2$	$-\frac{4}{9}\mathcal{H}^2$	0	$-\frac{4}{9}\mathcal{H}^2$	0	$\frac{4}{9}\mathcal{H}^2$	$\frac{4}{9}\mathcal{H}^2$	$\frac{8}{9}\mathcal{H}^2$	$\frac{4}{3}\mathcal{H}^2$
$\xi_{\pi,T}^{(h)}$	$\frac{16}{3}\mathcal{H}^2$	$\frac{26}{9}\mathcal{H}^2$	$\frac{4}{9}\mathcal{H}^2$	$-2\mathcal{H}^2$	$\frac{8}{9}\mathcal{H}^2$	0	$-\frac{8}{9}\mathcal{H}^2$	$-\frac{4}{9}\mathcal{H}^2$	$-\frac{2}{9}\mathcal{H}^2$	0
$\xi_{K,T}^{(h)}$	$\frac{4}{3}\mathcal{H}^2$	$\frac{4}{9}\mathcal{H}^2$	$-\frac{4}{9}\mathcal{H}^2$	$-\frac{4}{3}\mathcal{H}^2$	$\frac{28}{9}\mathcal{H}^2$	0	$-\frac{28}{9}\mathcal{H}^2$	$\frac{4}{9}\mathcal{H}^2$	$-\frac{28}{9}\mathcal{H}^2$	$-\frac{4}{3}\mathcal{H}^2$
$\xi_{\eta,T}^{(h)}$	$\frac{4}{3}\mathcal{H}^2$	$\frac{2}{3}\mathcal{H}^2$	0	$-\frac{2}{3}\mathcal{H}^2$	0	0	0	0	$-\frac{2}{3}\mathcal{H}^2$	$-\frac{8}{3}\mathcal{H}^2$

$$\begin{aligned}
H_4^{(g)} &= \frac{4M_{T0}^2}{9} \int_0^1 dx x \left(\frac{2(x-1)(x+1)x^2}{\mathcal{M}_T} + (9(x-1) \right. \\
&\quad \left. + 9(2x^2 - 1) \left(\lambda_\varepsilon + \log \left(\frac{\bar{\mathcal{M}}_T}{\bar{\mu}_T^2} \right) \right) \right), \tag{C.23}
\end{aligned}$$

$$\begin{aligned}
H_1^{(g)} &= -\frac{1}{216} \int_0^1 dx x \left(22x(6-5x) + \frac{66x^2(1-x^2)}{\mathcal{M}_T} + 27\bar{\mathcal{M}}_T \right. \\
&\quad \left. + 3((6-77x)x - 27\bar{\mathcal{M}}_T + 36) \left(\lambda_\varepsilon + \log \left(\frac{\bar{\mathcal{M}}_T}{\bar{\mu}_T^2} \right) \right) \right), \tag{C.24}
\end{aligned}$$

$$\begin{aligned}
H_2^{(h)} &= \frac{M_{T0}^2}{108} \int_0^1 dx (1-x) (2(x+1)(x(23x+88) - 79) + \\
&\quad + (139x - 107)\bar{\mathcal{M}}_T + 3(5(x+9)x^2 + 3x - 37 \\
&\quad + (20x - 16)\bar{\mathcal{M}}_T) \left(\lambda_\varepsilon + \log \left(\frac{\bar{\mathcal{M}}_T}{\bar{\mu}_T^2} \right) \right), \tag{C.25}
\end{aligned}$$

$$\begin{aligned}
H_3^{(h)} &= \frac{M_{T0}^2}{54} \int_0^1 dx (1-x) \left(2(x(x(7x-195) + 281) + 3) - \frac{24(x^2-1)^2}{\bar{\mathcal{M}}_T} \right. \\
&\quad + (47x - 317)\bar{\mathcal{M}}_T + 3((x-93)x^2 - 25x + 21) \\
&\quad \left. + (4x + 26)\bar{\mathcal{M}}_T) \left(\lambda_\varepsilon + \log \left(\frac{\bar{\mathcal{M}}_T}{\bar{\mu}_T^2} \right) \right) \right), \tag{C.26}
\end{aligned}$$

$$\begin{aligned}
H_4^{(h)} &= \frac{2M_{T0}^2}{81} \int_0^1 dx (1-x)^2 ((43x^2 - 242x + 103) \\
&\quad + \frac{3(x^2-1)((x-10)x+1)}{\bar{\mathcal{M}}_T} \\
&\quad + 3(x(5x-118) - 79) \left(\lambda_\varepsilon + \log \left(\frac{\bar{\mathcal{M}}_T}{\bar{\mu}_T^2} \right) \right)), \tag{C.27}
\end{aligned}$$

$$\begin{aligned}
H_1^{(h)} &= -\frac{1}{432} \int_0^1 dx (2(x(x(9-x(23x+21)) + 9) + 26) + \\
&\quad + \frac{66(x-1)^3(x+1)^2}{\bar{\mathcal{M}}_T} + (1-x)(139x - 395)\bar{\mathcal{M}}_T \\
&\quad + 3(1-x)(5(x-5)x^2 - 109x + 41 + (20x+14)\bar{\mathcal{M}}_T) \times \\
&\quad \times \left(\lambda_\varepsilon + \log \left(\frac{\bar{\mathcal{M}}_T}{\bar{\mu}_T^2} \right) \right), \tag{C.28}
\end{aligned}$$

$$H_3^{(i,I)} = M_{T0}^2 \int_0^1 dx \bar{\mathcal{M}}_T \left(x + (5 - 3x) \left(\lambda_\varepsilon + \log \left(\frac{\bar{\mathcal{M}}_T}{\bar{\mu}_T^2} \right) \right) - 3 \right), \quad (\text{C.29})$$

$$H_1'^{(i,I)} = -\frac{1}{8M_{T0}^2} H_3^{(i,I)}, \quad (\text{C.30})$$

$$H_3^{(i,II)} = \frac{2M_{T0}^2}{9} \int_0^1 dx \bar{\mathcal{M}}_T \left(5x + 3(5 - 4x) \left(\lambda_\varepsilon + \log \left(\frac{\bar{\mathcal{M}}_T}{\bar{\mu}_T^2} \right) \right) - 19 \right), \quad (\text{C.31})$$

$$H_1'^{(i,II)} = -\frac{1}{8M_{T0}^2} H_3^{(i,II)}. \quad (\text{C.32})$$

where $H_1'^{(\alpha)} \equiv \partial_{q^2} H_1^{(\alpha)}|_{q^2=0}$ and $\mathcal{M}_B = xm^2 + (1-x)M_{B0}^2 - x(1-x)M_{T0}^2 - i\epsilon$, $\mathcal{M}_T = xm^2 + (1-x)^2M_{T0}^2 - i\epsilon$ and $\mathcal{M}_{B,T} = M_{T0}^2 \bar{\mathcal{M}}_{B,T}$. We apply the \overline{MS} -renormalization scheme on the bare LECs in order to cancel the divergencies of the loop-functions. Furthermore, we redefine the LEC g_d in order to absorb power-counting breaking terms still remaining in the loop functions (EOMS-scheme)

$$\tilde{g}_d = g_d + \frac{\mathcal{C}^2 M_{T0}^2}{(4\pi F_\phi)^2} f_d^1(\mu) + \frac{\mathcal{H}^2 M_{T0}^2}{(4\pi F_\phi)^2} f_d^2(\mu) \quad (\text{C.33})$$

where

$$\begin{aligned} f_d^1(\mu) &= \frac{1}{9} \left((3r(r(r(6r^2 + 8r - 7) - 11) + 3) + 34)r \right. \\ &\quad \left. - 3(r(r(2r(r(3r + 4) - 5) - 15) + 6) + 12) \log \left(\frac{r^2}{\bar{\mu}^2} \right) r^3 \right. \\ &\quad \left. + 3(r-1)(r+1)^3(r(2(r-1)r(3r+1) + 1) + 2) \log \left(\frac{1-r^2}{\bar{\mu}^2} \right) + 13 \right), \\ f_d^2(\mu) &= \frac{1}{324} (606 \log(\bar{\mu}^2) - 335). \end{aligned} \quad (\text{C.34})$$

From the EOMS-renormalized loop function one can recover the HB results applying $M_{T0} = M_{B0} + \delta$ and taking the leading order of the expansion in powers of $1/M_{B0}$. Only the diagrams **(d)** and **(g)** of Fig. 2.4 give a non-vanishing contribution in the HB limit

$$\hat{H}^{(d)}(m) \simeq \delta M_{B0} \log \left(\frac{m^2}{4\delta^2} \right) + W_2(m, \mu), \quad (\text{C.35})$$

$$\hat{H}^{(g)}(m) \simeq \frac{2M_{B0} \pi m}{3}, \quad (\text{C.36})$$

where

$$W_2(m, \mu) = \begin{cases} 2M_{B0} \sqrt{m^2 - \delta^2} \left(\frac{\pi}{2} + \arctan \left(\frac{\delta}{\sqrt{m^2 - \delta^2}} \right) \right) & m \geq \delta \\ M_{B0} \sqrt{\delta^2 - m^2} \left(-2\pi i + \log \left(\frac{\delta + \sqrt{\delta^2 - m^2}}{\delta - \sqrt{\delta^2 - m^2}} \right) \right) & m < \delta \end{cases}, \quad (\text{C.37})$$

C.3 Vector coupling $f_1(0)$

C.3.1 Tadpole diagrams

The coefficients of the $SU(3)_F$ -breaking contribution of the tadpole diagram **(b)** of Fig. 3.1, as it is expressed in Eq. (3.17) and for the various channels $B_1 B_2$, are $\xi_\pi^{(b)} = \xi_\eta^{(b)} = \frac{3}{8}$ and $\xi_K^{(b)} = \frac{3}{4}$. The coefficients of the diagram **(c)** are $\xi_{\phi\phi'}^{(b)} = -\frac{3}{8}$ for all $\phi\phi'$ and channels.

$$H^{(b)}(m) = m^2 \left(1 - \lambda_\epsilon - \log \left(\frac{m^2}{\mu^2} \right) \right), \quad (\text{C.38})$$

$$\begin{aligned} H^{(c)}(m, m') &= (m^2 + m'^2)\lambda_\epsilon + \frac{1}{8(m^2 - m'^2)} \left(2m^4 \log \left(\frac{m'^2}{m^2} \right) \right. \\ &\quad \left. - (m^4 - m'^4) \left(2 \log \left(\frac{m'^2}{\mu^2} \right) - 3 \right) \right), \end{aligned} \quad (\text{C.39})$$

where m and m' are the masses of the ϕ and ϕ' mesons respectively.

C.3.2 Wave-function renormalization diagrams

For the renormalization of the octet baryon B wave function we have contributions with virtual octet baryons

$$\begin{aligned} \Sigma'_{BB'}(m) &= \int_0^1 dx \frac{1}{\mathcal{M}_B} (2x ((M' + M(x-1)) (x-1)x^2 M^3 \\ &+ (x-1)(xM + M + M') \mathcal{M}_B M - \mathcal{M}_B^2) \\ &+ \mathcal{M}_B (\mathcal{M}_B + x(M(6xM' - 4M' + M(x-1)(9x+2)) + 3\mathcal{M}_B)) \times \\ &\times \left(\lambda_\epsilon + \log \left(\frac{\mathcal{M}_B}{\mu^2} \right) \right)), \end{aligned} \quad (\text{C.40})$$

and with decuplet baryons

$$\begin{aligned} \Sigma'_{BT'}(m) &= \int_0^1 dx \left(M ((M(x-1) (2(x-1)xM^2 + 3\mathcal{M}_B) \right. \\ &- 2M' ((x-1)xM^2 + \mathcal{M}_B)) \left(\lambda_\epsilon + \log \left(\frac{\mathcal{M}_B}{\mu^2} \right) \right) \\ &\left. - 2M^2(x-1)x(-xM + M + M') \right), \end{aligned} \quad (\text{C.41})$$

where $\mathcal{M}_B = (1-x)m^2 + x(M')^2 - x(1-x)M^2 - i\epsilon$, with m the mass of the corresponding pseudoscalar meson.

Table C.3: Coefficients $\xi_{\phi BB'}$ in Eq. (3.16) for the contributions of the baryon-octet to the renormalization of the wave-function of the baryon-octet

ϕ	B'	N	Λ	Σ	Ξ
π	N	$\frac{3}{4}(D+F)^2$	0	0	0
	Λ	0	0	$\frac{1}{3}D^2$	0
	Σ	0	D^2	$2F^2$	0
	Ξ	0	0	0	$\frac{3}{4}(D-F)^2$
K	N	0	$\frac{1}{6}(D+3F)^2$	$\frac{1}{2}(D-F)^2$	0
	Λ	$\frac{1}{12}(D+3F)^2$	0	0	$\frac{1}{12}(D-3F)^2$
	Σ	$\frac{3}{4}(D-F)^2$	0	0	$\frac{3}{4}(D+F)^2$
	Ξ	0	$\frac{1}{6}(D-3F)^2$	$\frac{1}{2}(D+F)^2$	0
η	N	$\frac{1}{12}(D-3F)^2$	0	0	0
	Λ	0	$\frac{1}{3}D^2$	0	0
	Σ	0	0	$\frac{1}{3}D^2$	0
	Ξ	0	0	0	$\frac{1}{12}(D+3F)^2$

Table C.4: Coefficients $\xi_{\phi, BT'}$ in Eq. (3.16) for the contributions of the baryon-decuplet to the renormalization of the wave-function of the baryon-octet

ϕ	T'	N	Λ	Σ	Ξ
π	Δ	$4\mathcal{C}^2$	0	0	0
	Σ^*	0	$3\mathcal{C}^2$	$\frac{2}{3}\mathcal{C}^2$	0
	Ξ^*	0	0	0	\mathcal{C}^2
	Ω^-	0	0	0	0
K	Δ	0	0	$\frac{8}{3}\mathcal{C}^2$	0
	Σ^*	\mathcal{C}^2	0	0	\mathcal{C}^2
	Ξ^*	0	$2\mathcal{C}^2$	$\frac{2}{3}\mathcal{C}^2$	0
	Ω^-	0	0	0	$2\mathcal{C}^2$
η	Δ	0	0	0	0
	Σ^*	0	0	\mathcal{C}^2	0
	Ξ^*	0	0	0	\mathcal{C}^2
	Ω^-	0	0	0	0

C.3.3 Sunset diagrams

For the diagram **(d)** of Fig. 3.1 we use $\mathcal{M}^{(d)} = (1 - x - y)m^2 + xm'^2 + yM_3^2 - y(1 - x - y)M_1^2 - xyM_2^2 - i\epsilon$. In this function, M_1 is the mass of the decaying hyperon, M_2 the one of the final baryon, M_3 the mass of the internal baryon in the loop and m and m' are the masses of the pseudoscalars, ϕ and ϕ' with $S[\phi] < S[\phi']$, where S is the *strangeness* quantum number. For the diagram **(e)** we need $\mathcal{M}^{(e)} = ym^2 + xM_4^2 + (1 - x - y)M_3^2 - y(1 - x - y)M_1^2 - xyM_2^2 - i\epsilon$, where $M_{1,2}$ are again the masses of the initial/final baryons, m is the mass of the pseudoscalar meson and M_3 and M_4 are those of the internal baryons in the diagram, where $S[3] < S[4]$. Finally, for the seagull diagrams **(f)** we define $\mathcal{M}^{(f)} = (1 - x)m^2 + xM_3^2 - x(1 - x)M^2 - i\epsilon$ where M is the mass of the initial or final baryon for either the first or the second diagram **(f)**.

Octet inside

$$\begin{aligned}
H_{B_1 B_2}^{(d,B)}(m, m', M_3) &= \frac{1}{2} \int_0^1 dx \int_0^{1-x} dy \left((M_1 + M_2) y ((y - 1)(x + y - 1)(x + y) M_1^3 \right. \\
&\quad - (x + y - 1) (-M_3 y - M_2(-yx + x + y)) M_1^2 + M_2 (M_3 y + M_2 x (-y^2 - xy \\
&\quad + y + x - 1)) M_1 + M_2^2 x (M_2(x - 1)(y - 1) - M_3 y) \left. \frac{1}{\mathcal{M}^{(d)}} \right. \\
&\quad + (M_1 + M_2) y (-xM_2 + M_2 + M_3 + M_1(x + y)) - 2\mathcal{M}^{(d)} \\
&\quad + ((y(5y - 4) + x(5y - 2) + 1)M_1^2 + y(4yM_2 + M_2 + 3M_3) M_1 + 3M_2M_3y \\
&\quad \left. + M_2^2(x(2 - 5y) + 3y - 1) + 3\mathcal{M}^{(d)}) \left(\lambda_\epsilon + \log \left(\frac{\mathcal{M}^{(d)}}{\mu^2} \right) \right) \right), \tag{C.42}
\end{aligned}$$

$$\begin{aligned}
H_{B_1 B_2}^{(e,B)}(m, M_3, M_4) &= -\frac{1}{2} \int_0^1 dx \int_0^{1-x} dy \left((y(x + y - 1)M_1^2 - M_3(y \right. \\
&\quad - 1)M_1 - M_2^2 xy) (y(x + y - 1)M_1^2 - M_2M_4(y - 1) - M_2^2 xy) \frac{1}{\mathcal{M}^{(e)}} + \\
&\quad (2y(x + y - 1)M_1^2 - (M_2 + M_4 + M_3(y - 1)) M_1 - M_3M_4 - M_2(M_3 \\
&\quad + M_4(y - 1)) - 2M_2^2 xy - \mathcal{M}^{(e)}) + (6y(x + y - 1)M_1^2 - (M_2 + M_4 \\
&\quad + M_3(3y - 2)) M_1 - M_2M_3 + 2M_2M_4 - M_3M_4 - 3M_2(M_4 + 2M_2x) y \\
&\quad \left. + 6\mathcal{M}^{(e)}) \left(\lambda_\epsilon + \log \left(\frac{\mathcal{M}^{(e)}}{\mu^2} \right) \right) \right), \tag{C.43}
\end{aligned}$$

Table C.5: Coefficients $\xi_{\phi\phi',B_3}^{(d,B)}$ in Eq. (3.17) for the contributions of the diagram **(d)** in Fig. 3.1 with octet baryons in the internal lines.

$\phi\phi'$	B_3	ΛN	ΣN	$\Xi\Lambda$	$\Xi\Sigma$
πK	N	0	0	0	0
	Λ	0	$\frac{D(D+3F)}{3}$	0	0
	Σ	$-D(D-F)$	$2F(D-F)$	0	0
	Ξ	0	0	$-\frac{(D-F)(D-3F)}{2}$	$-\frac{(D^2-F^2)}{2}$
ηK	N	0	0	0	0
	Λ	$-\frac{D(D+3F)}{3}$	0	0	0
	Σ	0	$-D(D-F)$	0	0
	Ξ	0	0	$\frac{D^2-9F^2}{6}$	$-\frac{(D+F)(D+3F)}{2}$
$K\pi$	N	$-\frac{(D+F)(D+3F)}{2}$	$-\frac{(D^2-F^2)}{2}$	0	0
	Λ	0	0	0	$\frac{D(D-3F)}{3}$
	Σ	0	0	$-D(D+F)$	$-2F(D+F)$
	Ξ	0	0	0	0
$K\eta$	N	$\frac{D^2-9F^2}{6}$	$-\frac{(D-3F)(D-F)}{2}$	0	0
	Λ	0	0	$-\frac{D(D-3F)}{3}$	0
	Σ	0	0	$-D(D+F)$	0
	Ξ	0	0	0	0

$$H_{B_3}^{(f,B)}(m_\phi, M) = \int_0^1 dx \left((M(M_3 + M(x-1))x + 2\mathcal{M}^{(f)}) \log\left(\frac{\mathcal{M}^{(f)}}{\mu^2}\right) - \mathcal{M}^{(f)} \right). \quad (\text{C.44})$$

Table C.6: Coefficients $\xi_{\phi, B_1 B_2, B_3 B_4}^{(e, B)}$ in Eq. (3.17) for the contributions of the diagram (e) in Fig. 3.1 with octet baryons in the internal lines.

ϕ	$B_3 B_4$	ΛN	ΣN	$\Xi \Lambda$	$\Xi \Sigma$
π	ΛN	0	$-D(D+F)$	0	0
	ΣN	$-D(D+F)$	$-2F(D+F)$	0	0
	$\Xi \Lambda$	0	0	0	$-D(D-F)$
	$\Xi \Sigma$	0	0	$-D(D-F)$	$-2F(F-D)$
K	ΛN	0	0	$\frac{D^2-9F^2}{6}$	$-\frac{D^2-4FD+3F^2}{2}$
	ΣN	0	0	$-\frac{D^2+4FD+3F^2}{2}$	$-\frac{D^2-F^2}{2}$
	$\Xi \Lambda$	$\frac{D^2-9F^2}{6}$	$-\frac{D^2+4FD+3F^2}{2}$	0	0
	$\Xi \Sigma$	$-\frac{D^2-4FD+3F^2}{2}$	$-\frac{D^2-F^2}{2}$	0	0
η	ΛN	$-\frac{D(D-3F)}{3}$	0	0	0
	ΣN	0	$\frac{D(D-3F)}{3}$	0	0
	$\Xi \Lambda$	0	0	$-\frac{D(D+3F)}{3}$	0
	$\Xi \Sigma$	0	0	0	$\frac{D(D+3F)}{3}$

Decuplet inside

$$\begin{aligned}
 H_{B_1 B_2}^{(d, T)}(m, M_3) = & \frac{1}{36M_3^2} \int_0^1 dx \int_0^{1-x} dy \left((-3(M_1 - M_2)^2 (M_1 + M_2)^3 \times \right. \\
 & \times xy(x+y-1)(-M_3 - M_2x + M_1(x+y-1)) - (3x-9y-1)(x+y \\
 & -1)M_1^4 - (-2xM_3 + 9yM_3 + M_3 + M_2((6-7y)y + x(4y-2) + 1))M_1^3 \\
 & + M_2M_3(2x-7y-1)M_1^2 + M_2^2(9y^2 + 6xy - 10y + 6(x-1)x + 1)M_1^2 \\
 & + M_2^2M_3(-2x-9y+1)M_1 + M_2^3(11y^2 + 4(x-3)y - 2x + 1)M_1 \\
 & - M_2^3M_3(2x+11y-1) - M_2^4x(3x+12y-2) + (-2M_1^2 + 4M_2M_1 \\
 & - 2M_2^2) \mathcal{M}^{(d)} + (-3((3x-3y-1)(x+y-1)M_1^4 + (-M_2y^2 + 3M_3y \\
 & + 4M_2xy + M_2 + M_3 - 2M_2x - 2M_3x)M_1^3 - M_2M_3(2x-y-1)M_1^2 \\
 & - M_2^2(3y^2 + 6xy - 4y + 6(x-1)x + 1)M_1^2 + M_2^2M_3(2x+3y-1)M_1 \\
 & + M_2^3(x(2-4y) + (6-5y)y-1)M_1 + M_2^3M_3(2x+5y-1) \\
 & \left. + M_2^4x(3x+6y-2)) - 3(-4M_1^2 + 2M_2M_1 - 4M_2^2), \mathcal{M}^{(d)} \right) \times \\
 & \times \left(\lambda_\epsilon + \log \left(\frac{\mathcal{M}^{(d)}}{\mu^2} \right) \right), \tag{C.45}
 \end{aligned}$$

Table C.7: Coefficients $\xi_{\phi, B_3}^{(f, I)}$ in Eq. (3.17) for the contributions of the diagram (\mathbf{f}, \mathbf{I}) in Fig. 3.1 with octet baryons in the internal lines.

ϕ	B_3	ΛN	ΣN	$\Xi \Lambda$	$\Xi \Sigma$
π	N	$\frac{D^2+4DF+3F^2}{4}$	$\frac{D^2-F^2}{4}$	0	0
	Λ	0	0	0	$-\frac{D(D-3F)}{6}$
	Σ	0	0	$\frac{D(D+F)}{2}$	$F(D+F)$
	Ξ	0	0	0	0
K	N	0	0	0	0
	Λ	$\frac{D(D+3F)}{6}$	$-\frac{D(D+3F)}{6}$	0	0
	Σ	$\frac{D(D-F)}{2}$	$\frac{D^2-3DF+2F^2}{2}$	0	0
	Ξ	0	0	$\frac{(D-3F)^2}{6}$	$\frac{(D+F)^2}{2}$
η	N	$-\frac{D^2-9F^2}{12}$	$\frac{(D^2-4DF+3F^2)}{4}$	0	0
	Λ	0	0	$\frac{D(D-3F)}{6}$	0
	Σ	0	0	0	$\frac{D(D+F)}{2}$
	Ξ	0	0	0	0

$$\begin{aligned}
H_{B_1 B_2}^{(e, T)}(m, M_3, M_4) &= \frac{1}{1728(M_3 M_4)^2} \int_0^1 dx \int_0^{1-x} dy \left(\frac{R_{-1}}{\mathcal{M}^{(e)}} \right. \\
&\quad \left. + (R_0 + R_1 \mathcal{M}^{(e)}) + (R_{L0} + R_{L1} \mathcal{M}^{(e)}) \left(\lambda_\varepsilon + \log \left(\frac{\mathcal{M}^{(e)}}{\mu^2} \right) \right) \right),
\end{aligned} \tag{C.46}$$

$$\begin{aligned}
R_{-1} &= -48 (M_1^2 - M_2^2)^2 x(x+y-1) \left(- (3M_4^2 + (M_1 + 2M_2) y M_4 \right. \\
&\quad \left. - (M_1 - M_2) y ((M_1 + M_2)(x-1) + M_1 y)) M_3^2 \right. \\
&\quad \left. - y (-y(x+y-1) M_1^3 + (M_2 y(x+y) + M_4(2x+2y-1)) M_1^2 \right. \\
&\quad \left. + 2M_4^2 M_1 + M_2 (M_4 + M_2(x-1)) y M_1 + M_2 (M_4 (-2xM_2 + M_2 \right. \\
&\quad \left. + M_4) - M_2^2 xy)) M_3 - (M_1 - M_2) M_4 y (y(x+y-1) M_1^2 - (M_2 y \right. \\
&\quad \left. + M_4(x+y)) M_1 - M_2 x (M_4 + M_2 y)) \right),
\end{aligned} \tag{C.47}$$

Table C.8: Coefficients $\xi_{B_3, \phi}^{(f, II)}$ in Eq. (3.17) for the contributions of the diagram **(f, II)** in Fig. 3.1 with octet baryons in the internal lines.

ϕ	B_3	ΛN	ΣN	$\Xi \Lambda$	$\Xi \Sigma$
π	N	0	0	0	0
	Λ	0	$-\frac{D(D+3F)}{6}$	0	0
	Σ	$\frac{D(D-F)}{2}$	$-F(D-F)$	0	0
	Ξ	0	0	$\frac{D^2-4DF+3F^2}{4}$	$\frac{D^2-F^2}{4}$
K	N	$\frac{(D+3F)^2}{6}$	$\frac{(D-F)^2}{2}$	0	0
	Λ	0	0	$\frac{D(D-3F)}{6}$	$-\frac{D(D-3F)}{6}$
	Σ	0	0	$\frac{D(D+F)}{2}$	$\frac{D^2+3DF+2F^2}{2}$
	Ξ	0	0	0	0
η	N	0	0	0	0
	Λ	0	$\frac{D(D+3F)}{6}$	0	0
	Σ	0	0	$\frac{D(D-F)}{2}$	0
	Ξ	0	0	0	$\frac{D^2+4DF+3F^2}{4}$

$$\begin{aligned}
 R_0 = & -16 (y(x+y-1)) ((M_3 - M_4) (25x - 14) + 4 (2M_3 + M_4) y) M_1^5 \\
 & + (2(x+y-1)(8x+4y-7)M_3^2 + (M_2y(-25x^2 + 11(1-3y)x + 2(5 \\
 & -4y)y) + M_4(29y^2 + 9xy - 13y - 20(x-1)x - 14)) M_3 + M_4(2M_4(x(8x \\
 & -1) + (7-8y)y) + M_2y(-4y^2 + (21x+2)y + x(25x-11)))) M_1^4 \\
 & + ((M_4(9x+25y-23) - 2M_2y(12x+4y-5)) M_3^2 - (2y(8y^2 + 31xy \\
 & -19y + x(25x-39) + 14) M_2^2 + M_4y(6x+5y-3)M_2 + M_4^2(15x+10y \\
 & -14)) M_3 + 2M_2M_4y(-4(3x+y)M_4 + 7M_4 + M_2(2y^2 + 19xy - 13y \\
 & + x(25x-39) + 14))) M_1^3 + (2y(2(4M_3 - M_4)y^2 + (31xM_3 - 5M_3 \\
 & -M_4 - 19M_4x)y + (M_3 - M_4)x(25x-11)) M_2^3 + (-2(8y^2 + 28xy \\
 & -19y + 2x(8x-15) + 14) M_3^2 + M_4(29y^2 + 40xy - 3y + 40(x-1)x \\
 & + 28) M_3 - 2M_4^2(16x^2 + (4y-2)x + (7-4y)y)) M_2^2 + M_3M_4(M_4(9x \\
 & + 34y + 14) - M_3(15x+y-1)) M_2 + 6M_3^2M_4^2) M_1^2 + M_2(y((M_3 \\
 & -M_4)(x-1)(25x-14) + (M_4(16-17x) + M_3(29x-16))y) M_2^3 \\
 & + y(2(12x+8y-5)M_3^2 + M_4(6x+y-3)M_3 + 2M_4^2(12x+8y-7)) M_2^2 \\
 & + M_3M_4(M_4(15x+14(y-1)) + M_3(-9x+25y+23)) M_2 + 42M_3^2M_4^2) M_1 \\
 & + M_2^2(xy(M_3(-25x-29y+11) + M_4(25x+17y-11)) M_2^3 + (2(-8y
 \end{aligned}$$

Table C.9: Coefficients $\xi_{\phi\phi',B_3}^{(d,T)}$ in Eq. (3.17) for the contributions of the diagram **(d)** in Fig. 3.1 with decuplet baryons in the internal lines.

$\phi\phi'$	B_3	ΛN	ΣN	$\Xi\Lambda$	$\Xi\Sigma$
πK	Δ	0	0	0	0
	Σ^*	$-2\mathcal{C}^2$	$-\frac{4}{3}\mathcal{C}^2$	0	0
	Ξ^*	0	0	$-2\mathcal{C}^2$	$-\frac{2}{3}\mathcal{C}^2$
	Ω^-	0	0	0	0
ηK	Δ	0	0	0	0
	Σ^*	0	$2\mathcal{C}^2$	0	0
	Ξ^*	0	0	$2\mathcal{C}^2$	$-2\mathcal{C}^2$
	Ω^-	0	0	0	0
$K\pi$	Δ	0	$\frac{16}{3}\mathcal{C}^2$	0	0
	Σ^*	0	0	$2\mathcal{C}^2$	$-\frac{4}{3}\mathcal{C}^2$
	Ξ^*	0	0	0	0
	Ω^-	0	0	0	0
$K\eta$	Δ	0	0	0	0
	Σ^*	0	0	0	$-2\mathcal{C}^2$
	Ξ^*	0	0	0	0
	Ω^-	0	0	0	0

$$\begin{aligned}
& +x(8x + 16y - 15) + 7)M_3^2 + M_4(x(-20x - 49y + 20) + 2(8y - 7))M_3 \\
& + 2M_4^2x(8x + 4y - 1)) M_2^2 + M_3M_4 (M_3(15x + 5y - 1) + M_4(-9x + 16y \\
& - 14)) M_2 + 6M_3^2M_4^2),
\end{aligned} \tag{C.48}$$

$$\begin{aligned}
R_1 = & -16 ((M_4(-21x - 2y + 35) + M_3(21x + 23y - 20)) M_1^3 \\
& - (M_2(-21xM_4 - 2yM_4 + M_4 + M_3(21x + 23y + 14)) - 2(M_3^2 \\
& + 22M_4M_3 - 17M_4^2)) M_1^2 - M_2(34M_3^2 + 10M_4M_3 + 34M_4^2 \\
& + M_2(M_4(-21x + 2y + 35) + M_3(21x + 19y - 20))) M_1 + M_2^2(-34M_3^2 \\
& + 44M_4M_3 + 2M_4^2 + M_2(-21xM_4 + 2yM_4 + M_4 \\
& + M_3(21x + 19y + 14))))),
\end{aligned} \tag{C.49}$$

Table C.10: Coefficients $\xi_{\phi, B_1 B_2, B_3 B_4}^{(e, T)}$ in Eq. (3.17) for the contributions of the diagram (e) in Fig. 3.1 with decuplet baryons in the internal lines.

ϕ	$B_3 B_4$	ΛN	ΣN	$\Xi \Lambda$	$\Xi \Sigma$
π	$\Sigma^* \Delta$	$8\mathcal{C}^2$	$\frac{8}{3}\mathcal{C}^2$	0	0
	$\Xi^* \Sigma^*$	0	0	$4\mathcal{C}^2$	$\frac{8}{3}\mathcal{C}^2$
	$\Omega^- \Xi^*$	0	0	0	0
K	$\Sigma^* \Delta$	0	0	0	$\frac{16}{3}\mathcal{C}^2$
	$\Xi^* \Sigma^*$	$4\mathcal{C}^2$	$\frac{4}{3}\mathcal{C}^2$	0	0
	$\Omega^- \Xi^*$	0	0	$4\mathcal{C}^2$	$4\mathcal{C}^2$
η	$\Sigma^* \Delta$	0	0	0	0
	$\Xi^* \Sigma^*$	0	0	0	$4\mathcal{C}^2$
	$\Omega^- \Xi^*$	0	0	0	0

$$\begin{aligned}
R_{L0} = & -48 (y(x+y-1) (2M_4(-4x+y+2) + M_3(8x+y-4)) M_1^5 \\
& + ((x+y-1)(5x+y-4)M_3^2 - (M_4(7(x-1)x + (2-7y)y + 4) \\
& + M_2y(8x^2 + (9y-4)x + (y-2)y)) M_3 + M_4(M_2(4x-y)y(2x+2y-1) \\
& + M_4(x(5x-1) + (4-5y)y))) M_1^4 + ((M_4(5y-4) - M_2y(6x+y-2)) M_3^2 \\
& - (y(16x^2 + (19y-24)x + 5(y-2)y + 8) M_2^2 + M_4y(6x+y-3)M_2 \\
& + M_4^2(6x-y-4)) M_3 + M_2M_4y(M_2(2y^2 + 13xy - 7y + 8x(2x-3) + 8) \\
& - M_4(6x+y-4))) M_1^3 + (y((5M_3 - 2M_4)y^2 + (19xM_3 - 2M_3 - M_4 \\
& - 13M_4x)y + 8(M_3 - M_4)x(2x-1)) M_2^3 + (- (10x^2 + 2(8y-9)x \\
& + 5(y-2)y + 8) M_3^2 + M_4(-3y + 7(y^2 + 2xy + 2(x-1)x) + 8) M_3 \\
& + M_4^2(y^2 - 4(x+1)y + 2(1-5x)x)) M_2^2 + M_3M_4(M_3(-6x+y+2) \\
& + M_4(5y+4)) M_2 + 6M_3^2M_4^2) M_1^2 + M_2(y(4(M_3 - M_4)(x(2x-3) + 1) \\
& + (M_4(5-7x) + 5M_3(2x-1))y) M_2^3 + y((6x+5y-2)M_3^2 \\
& + M_4(6x+5y-3)M_3 + M_4^2(6x+5y-4)) M_2^2 + M_3M_4(M_3(5y+4) \\
& + M_4(6x+7y-4)) M_2 + 6M_3^2M_4^2) M_1 + M_2^2(xy(M_4(8x+7y-4) \\
& - 2M_3(4x+5y-2)) M_2^3 + ((-5y+x(5x+10y-9) + 4)M_3^2 \\
& + M_4(5y-7x(x+2y-1) - 4)M_3 + M_4^2x(5x+4y-1)) M_2^2 \\
& + M_3M_4(M_4(5y-4) + M_3(6x+7y-2)) M_2 + 6M_3^2M_4^2), \tag{C.50}
\end{aligned}$$

Table C.11: Coefficients $\xi_{\phi, B_3}^{(f, I_a)}$ in Eq. (3.17) for the contributions of the diagram (f, I_a) in Fig. 3.1 with decuplet baryons in the internal lines.

ϕ	T'	ΛN	ΣN	$\Xi \Lambda$	$\Xi \Sigma$
π	Δ	0	$-\frac{8}{3}\mathcal{C}^2$	0	0
	Σ^*	0	0	$-\mathcal{C}^2$	$\frac{2}{3}\mathcal{C}^2$
	Ξ^*	0	0	0	$-\mathcal{C}^2$
	Ω^-	0	0	0	0
K	Δ	0	0	0	0
	Σ^*	\mathcal{C}^2	$-\frac{1}{3}\mathcal{C}^2$	0	0
	Ξ^*	0	0	0	$\frac{4}{3}\mathcal{C}^2$
	Ω^-	0	0	0	0
η	Δ	0	0	0	0
	Σ^*	0	0	0	\mathcal{C}^2
	Ξ^*	0	0	0	0
	Ω^-	0	0	0	0

$$\begin{aligned}
R_{L1} = & -96 \left((2M_4(-3x + 2y + 4) + M_3(6x + 2y - 5)) M_1^3 - (M_3^2 \right. \\
& - 8M_4M_3 + 10M_4^2 + M_2(-6xM_4 + 4yM_4 + M_4 + 2M_3(3x + y + 1))) M_1^2 \\
& - M_2(4(M_3^2 + M_4M_3 + M_4^2) + M_2(M_3(6x + 10y - 5) - 2M_4(3x + 2y \\
& - 4))) M_1 + M_2^2(-10M_3^2 + 8M_4M_3 - M_4^2 + M_2(-6xM_4 - 4yM_4 + M_4 \\
& \left. + 2M_3(3x + 5y + 1))) \right), \tag{C.51}
\end{aligned}$$

$$\begin{aligned}
H_{B_3}^{(f, T_a)}(m_\phi, M, M') = & \frac{1}{9M_3^2} \int_0^1 dx \left(\mathcal{M}^{(f)}((x-1)M - M_3)(-M' + M \right. \\
& \left. + 3 \left(\lambda_\epsilon + \log \left(\frac{\mathcal{M}^{(f)}}{\mu^2} \right) \right) (2M' + M) \right), \tag{C.52}
\end{aligned}$$

Table C.12: Coefficients $\xi_{\phi, B_3}^{(f, IIa)}$ in Eq. (3.17) for the contributions of the diagram **(f, IIa)** in Fig. 3.1 with decuplet baryons in the internal lines.

ϕ	T'	ΛN	ΣN	$\Xi \Lambda$	$\Xi \Sigma$
π	Δ	0	0	0	0
	Σ^*	\mathcal{C}^2	$\frac{2}{3}\mathcal{C}^2$	0	0
	Ξ^*	0	0	\mathcal{C}^2	$\frac{1}{3}\mathcal{C}^2$
	Ω^-	0	0	0	0
K	Δ	0	$-\frac{8}{3}\mathcal{C}^2$	0	0
	Σ^*	0	0	$-\mathcal{C}^2$	$\frac{5}{3}\mathcal{C}^2$
	Ξ^*	0	0	0	0
	Ω^-	0	0	0	0
η	Δ	0	0	0	0
	Σ^*	0	$-\mathcal{C}^2$	0	0
	Ξ^*	0	0	$-\mathcal{C}^2$	\mathcal{C}^2
	Ω^-	0	0	0	0

$$\begin{aligned}
 H_{B_3}^{(f, Tb)}(m_\phi, M, M') &= \frac{1}{9M_3^3} \int_0^1 dx \left(-(-xM + M + M_3) \mathcal{M}^{(f)} \times \right. \\
 &\times \left((M + M_3)(M - M') + 3 \log \left(\frac{\mathcal{M}^{(f)}}{\mu^2} \right) (M(M + M_3) \right. \\
 &\left. \left. - (M - 2M_3)M') \right) \right),
 \end{aligned} \tag{C.53}$$

where in Eqs. (C.52) and (C.53), $\mathcal{M}^{(f)}$ depends on the mass M .

Table C.13: Coefficients $\xi_{\phi, B_3}^{(f, Ib)}$ in Eq. (3.17) for the contributions of the diagram **(f, Ib)** in Fig. 3.1.

ϕ	T'	ΛN	ΣN	$\Xi \Lambda$	$\Xi \Sigma$
π	Δ	$-4\mathcal{C}^2$	$-\frac{4}{3}\mathcal{C}^2$	0	0
	Σ^*	0	0	$-2\mathcal{C}^2$	$-\frac{4}{3}\mathcal{C}^2$
	Ξ^*	0	0	0	0
	Ω^-	0	0	0	0
K	Δ	0	0	0	$-\frac{8}{3}\mathcal{C}^2$
	Σ^*	$-2\mathcal{C}^2$	$-\frac{2}{3}\mathcal{C}^2$	0	0
	Ξ^*	0	0	$-2\mathcal{C}^2$	$-2\mathcal{C}^2$
	Ω^-	0	0	0	0
η	Δ	0	0	0	0
	Σ^*	0	0	0	$-2\mathcal{C}^2$
	Ξ^*	0	0	0	0
	Ω^-	0	0	0	0

Table C.14: Coefficients $\xi_{\phi, B_3}^{(f, IIb)}$ in Eq. (3.17) for the contributions of the diagram **(f, IIb)** in Fig. 3.1.

ϕ	T'	ΛN	ΣN	$\Xi \Lambda$	$\Xi \Sigma$
π	Δ	0	0	0	0
	Σ^*	$4\mathcal{C}^2$	$\frac{4}{3}\mathcal{C}^2$	0	0
	Ξ^*	0	0	$2\mathcal{C}^2$	$\frac{4}{3}\mathcal{C}^2$
	Ω^-	0	0	0	0
K	Δ	0	0	0	0
	Σ^*	0	0	0	$\frac{8}{3}\mathcal{C}^2$
	Ξ^*	$2\mathcal{C}^2$	$\frac{2}{3}\mathcal{C}^2$	0	0
	Ω^-	0	0	$2\mathcal{C}^2$	$2\mathcal{C}^2$
η	Δ	0	0	0	0
	Σ^*	0	0	0	0
	Ξ^*	0	0	0	$2\mathcal{C}^2$
	Ω^-	0	0	0	0

C.4 Baryon masses

C.4.1 Loop functions and table of coefficients

$$H_B^{(b)} = -\frac{M_{B0}^3}{2} \int_0^1 dx \left(\left(x^3 + 3(x+1)\bar{\mathcal{M}}_B^{(b)} \right) \left(\lambda_\epsilon + \log \left(\frac{\bar{\mathcal{M}}_B^{(b)}}{\bar{\mu}_B^2} \right) \right) - (2x+1)\bar{\mathcal{M}}_B^{(b)} \right), \quad (\text{C.54})$$

$$H_B^{(c)} = -\frac{3M_{B0}^3}{4} \left(\frac{1}{R} \right)^2 \int_0^1 dx \left((1-x) + R \right) \bar{\mathcal{M}}_B^{(c)} \left(\lambda_\epsilon + \log \left(\frac{\bar{\mathcal{M}}_B^{(c)}}{\bar{\mu}_B^2} \right) \right), \quad (\text{C.55})$$

$$H_T^{(b)} = -\frac{3M_{T0}^3}{4} \int_0^1 dx \left(r + (1-x) \right) \bar{\mathcal{M}}_T^{(b)} \left(\lambda_\epsilon + \log \left(\frac{\bar{\mathcal{M}}_T^{(b)}}{\bar{\mu}_T^2} \right) - 1 \right), \quad (\text{C.56})$$

$$H_T^{(c)} = -\frac{M_{T0}^3}{20} \int_0^1 dx \left(2-x \right) \bar{\mathcal{M}}_T^{(c)} \left(15 \left(\lambda_\epsilon + \log \left(\frac{\bar{\mathcal{M}}_T^{(c)}}{\bar{\mu}_T^2} \right) \right) + 11 \right). \quad (\text{C.57})$$

In these formulas $\bar{\mathcal{M}}_{B/T}^{(\alpha)} = \mathcal{M}_{B/T}^{(\alpha)} / M_{B0/T0}$, where $\alpha = b$ or c and

$$\mathcal{M}_{B/T}^{(b)} = (1-x)m^2 + xM_{B0}^2 - x(1-x)M_{B0/T0}^2 - i\epsilon, \quad (\text{C.58})$$

$$\mathcal{M}_{B/T}^{(c)} = (1-x)m^2 + xM_{T0}^2 - x(1-x)M_{B0/T0}^2 - i\epsilon, \quad (\text{C.59})$$

with m the mass of the meson ϕ in the loop.

The loop-integrals are ultraviolet divergent and we first perform the regularization in the \overline{MS} dimensional regularization scheme. It is equivalent to

Table C.15: Coefficients of the contributions to the self-energy Eq. (4.11) for any of the octet or decuplet baryons.

	N	Λ	Σ	Ξ	Δ	Σ^*	Ξ^*	Ω^-
$\xi_{\mathcal{B},\pi}^{(a)}$	$2b_0 + 4b_F$	$\frac{2}{3}(3b_0 - 2b_D)$	$2b_0 + 4b_D$	$2b_0 - 4b_F$	$t_0 + 3t_D$	$t_0 + t_D$	$t_0 - t_D$	$t_0 - 3t_D$
$\xi_{\mathcal{B},K}^{(a)}$	$4b_0 + 4b_D - 4b_F$	$\frac{2}{3}(6b_0 + 8b_D)$	$4b_0$	$4b_0 + 4b_D + 4b_F$	$2t_0$	$2t_0 + 2t_D$	$2t_0 + 4t_D$	$2t_0 + 6t_D$
$\xi_{\mathcal{B},\pi}^{(b)}$	$\frac{3}{2}(D + F)^2$	$2D^2$	$\frac{2}{3}(D^2 + 6F^2)$	$\frac{3}{2}(D - F)^2$	$\frac{4}{3}\mathcal{C}^2$	$\frac{10}{9}\mathcal{C}^2$	$\frac{2}{3}\mathcal{C}^2$	0
$\xi_{\mathcal{B},K}^{(b)}$	$\frac{1}{3}(5D^2 - 6DF + 9F^2)$	$\frac{2}{3}(D^2 + 9F^2)$	$2(D^2 + F^2)$	$\frac{1}{3}(5D^2 + 6DF + 9F^2)$	$\frac{4}{3}\mathcal{C}^2$	$\frac{8}{9}\mathcal{C}^2$	$\frac{4}{3}\mathcal{C}^2$	$\frac{8}{3}\mathcal{C}^2$
$\xi_{\mathcal{B},\eta}^{(b)}$	$\frac{1}{6}(D - 3F)^2$	$\frac{2}{3}D^2$	$\frac{2}{3}D^2$	$\frac{1}{6}(D + 3F)^2$	0	$\frac{2}{3}\mathcal{C}^2$	$\frac{2}{3}\mathcal{C}^2$	0
$\xi_{\mathcal{B},\pi}^{(c)}$	$\frac{16}{3}\mathcal{C}^2$	$4\mathcal{C}^2$	$\frac{8}{9}\mathcal{C}^2$	$\frac{4}{3}\mathcal{C}^2$	$\frac{50}{27}\mathcal{H}^2$	$\frac{80}{81}\mathcal{H}^2$	$\frac{10}{27}\mathcal{H}^2$	0
$\xi_{\mathcal{B},K}^{(c)}$	$\frac{4}{3}\mathcal{C}^2$	$\frac{8}{3}\mathcal{C}^2$	$\frac{40}{9}\mathcal{C}^2$	$4\mathcal{C}^2$	$\frac{20}{27}\mathcal{H}^2$	$\frac{160}{81}\mathcal{H}^2$	$\frac{20}{9}\mathcal{H}^2$	$\frac{40}{27}\mathcal{H}^2$
$\xi_{\mathcal{B},\eta}^{(c)}$	0	0	$\frac{4}{3}\mathcal{C}^2$	$\frac{4}{3}\mathcal{C}^2$	$\frac{10}{27}\mathcal{H}^2$	0	$\frac{10}{27}\mathcal{H}^2$	$\frac{40}{27}\mathcal{H}^2$

the redefinition of the bare LECs of the chiral Lagrangian

$$\begin{aligned}
M_{B0}^r(\mu) &= M_{B0} + \frac{\lambda_\varepsilon M_{B0}^3}{24\pi^2 F_\phi^2} \left[5D^2 + 9F^2 + \frac{5(2R(3R^2 + R - 1) - 1)\mathcal{C}^2}{8R^2} \right], \\
b_0^r(\mu) &= b_0 + \frac{\lambda_\varepsilon M_{B0}}{288\pi^2 F_\phi^2} \left[13D^2 + 9F^2 + \frac{7(3R + 2)\mathcal{C}^2}{2R^2} \right], \\
b_D^r(\mu) &= b_D - \frac{\lambda_\varepsilon M_{B0}}{64\pi^2 F_\phi^2} \left[D^2 - 3F^2 + \frac{(3R + 2)\mathcal{C}^2}{3R^2} \right], \\
b_F^r(\mu) &= b_F + \frac{\lambda_\varepsilon M_{B0}}{96\pi^2 F_\phi^2} \left[5DF + \frac{5(3R + 2)\mathcal{C}^2}{12R^2} \right], \\
M_{T0}^r(\mu) &= M_{T0} + \frac{\lambda_\varepsilon M_{T0}^3}{96\pi^2 F_\phi^2} \left[(2r(3r^2 + r - 1) - 1)\mathcal{C}^2 + \frac{50\mathcal{H}^2}{9} \right], \\
t_0^r(\mu) &= t_0 + \frac{\lambda_\varepsilon M_{T0}}{192\pi^2 F_\phi^2} \left[(3r + 2)\mathcal{C}^2 + \frac{125\mathcal{H}^2}{27} \right], \\
t_D^r(\mu) &= t_D + \frac{\lambda_\varepsilon M_{T0}}{576\pi^2 F_\phi^2} \left[(3r + 2)\mathcal{C}^2 + \frac{25M_D\mathcal{H}^2}{3} \right]. \tag{C.60}
\end{aligned}$$

The power-counting is violated by the \overline{MS} regularized loop functions and, in order to recover it, we apply the EOMS renormalization prescription which is equivalent to redefine the renormalized couplings Eqs. (C.60) as

$$\begin{aligned}
\tilde{M}_{B0}^r(\mu) &= M_{B0}^r(\mu) + \frac{M_{B0}^3}{24\pi^2 F_\phi^2} \left[(5D^2 + 9F^2) (2 \log(\bar{\mu}_B) + 1) \right. \\
&\quad - \frac{5\mathcal{C}^2}{48R^2} (6R^6 + 12R^5 - 9R^4 - 48R^3 - 14R^2 + 20R \\
&\quad + 12(1 - 2R(3R^2 + R - 1)) \log(\bar{\mu}_B) \\
&\quad - 12(R - 1)^3(R + 1)^5 \log(R) \\
&\quad + 6(2R(3R^2 + R - 1) - 1) \log(R^2) \\
&\quad \left. + 6(R - 1)^3(R + 1)^5 \log(R^2 - 1) + 10 \right],
\end{aligned}$$

$$\begin{aligned}
\tilde{b}_0^r(\mu) &= b_0^r(\mu) + \frac{M_{B0}}{144\pi^2 F_\phi^2} \left[(13D^2 + 9F^2) (\log(\bar{\mu}_B) + 1) + \frac{7\mathcal{C}^2}{12} f(\mu) \right], \\
\tilde{b}_D^r(\mu) &= b_D^r(\mu) - \frac{M_{B0}}{32\pi^2 F_\phi^2} \left[(D^2 - 3F^2) (\log(\bar{\mu}_B) + 1) + \frac{\mathcal{C}^2}{18} f(\mu) \right], \\
\tilde{b}_F^r(\mu) &= b_F^r(\mu) + \frac{M_{B0}}{48\pi^2 F_\phi^2} \left[5DF (\log(\bar{\mu}_B) + 1) + \frac{5\mathcal{C}^2}{72} f(\mu) \right], \\
\tilde{M}_{T0}^r(\mu) &= M_{T0}^r(\mu) + \frac{M_{T0}^3}{576\pi^2 F_\phi^2} \left[\frac{10\mathcal{H}^2}{9} (60 \log(\bar{\mu}_T) + 1) \right. \\
&\quad \left. + \mathcal{C}^2 \left(-6(r-1)^3 \log\left(\frac{1}{r^2} - 1\right) (r+1)^5 \right. \right. \\
&\quad \left. \left. + r(r(3r(r(3-2r(r+2)) + 28) + 26) - 32) \right. \right. \\
&\quad \left. \left. - 12(1-2r(3r^2+r-1)) \log\left(\frac{\bar{\mu}_T}{r}\right) - 16 \right) \right], \\
\tilde{t}_0^r(\mu) &= t_0^r(\mu) + \frac{M_{T0}}{576\pi^2 F_\phi^2} \left[\frac{25\mathcal{H}^2}{27} (30 \log(\bar{\mu}_T) + 23) + \mathcal{C}^2 g(\mu) \right], \\
\tilde{t}_D^r(\mu) &= t_D^r(\mu) + \frac{M_{T0}}{1728\pi^2 F_\phi^2} \left[\frac{5\mathcal{H}^2}{3} (30 \log(\bar{\mu}_T) + 23) + \mathcal{C}^2 g(\mu) \right], \quad (\text{C.61})
\end{aligned}$$

where

$$\begin{aligned}
f(\mu) &= ((6R^4 + 9R^3 + 3R^2 + 9R + 6(3R+2) \log(\bar{\mu}_B) \\
&\quad - 6(2R^6 + 3R^5 - 3R - 2) \log(R) - 3(3R+2) \log(R^2) \\
&\quad + (6R^6 + 9R^5 - 9R - 6) \log(R^2 - 1) + 7))/R^2, \\
g(\mu) &= 3(2r+3) \log\left(\frac{1}{r^2}\right) r^5 + 3(r(r+1)(2r+1) + 6)r \\
&\quad + 6(3r+2) \log(\bar{\mu}_T) + 3(2r^6 + 3r^5 - 3r - 2) \log(1-r^2) + 13. \quad (\text{C.62})
\end{aligned}$$

The heavy-baryon expansion of the EOMS-regularized loop-graphs are

$$\begin{aligned}
H_B^{(b)} &\simeq H_T^{(c)} \simeq -\pi m^3 \\
H_B^{(c)} &\simeq -\left(\delta^2 - \frac{3}{2}m^2\right) \delta \log \frac{m^2}{4\delta^2} - \frac{m^2\delta}{2} - 2W_3(m, \delta), \\
H_T^{(b)} &\simeq \left(\delta^2 - \frac{3}{2}m^2\right) \delta \log \frac{m^2}{4\delta^2} + \frac{m^2\delta}{2} - 2W_3(m, -\delta), \quad (\text{C.63})
\end{aligned}$$

with the function $W_1(m, \delta)$ defined as

$$W_3(m, \delta) = \begin{cases} (m^2 - \delta^2)^{\frac{3}{2}} \arccos \frac{\delta}{m} & m \geq |\delta| \\ (\delta^2 - m^2)^{\frac{3}{2}} \log \left(\frac{\delta}{m} + \sqrt{\frac{\delta^2}{m^2} - 1} \right) & m < |\delta| \end{cases}. \quad (\text{C.64})$$

C.4.2 Finite volume corrections

We define the finite volume correction of a loop contribution $\delta_L H_X^{(\alpha)}(m)$ as the difference between the mass obtained evaluating the three-momentum \vec{k} loop integral in a finite box of size L (discrete spectrum of possible $|\vec{k}|$) and the usual result obtained performing the integral the infinite volume $H_X^{(\alpha)}(m)$. In case of the loop-integrals displayed above, Eqs. (C.54)-(C.57), taking the baryon rest frame $p^\mu = (M_B, \vec{0})$, we find

$$\delta_L H_X^{(\alpha)}(m) = \int_0^1 dx \left[t_{X, \frac{1}{2}}^{(\alpha)}(x) \delta_{L, \frac{1}{2}}(\mathcal{M}_X^{(\alpha)}) + t_{X, \frac{3}{2}}(\alpha)(x) \delta_{L, \frac{3}{2}}(\mathcal{M}_X^{(\alpha)}) \right], \quad (\text{C.65})$$

with $t_{X, \frac{1}{2}}^{(\alpha)}(x)$ and $t_{X, \frac{3}{2}}(\alpha)(x)$ some functions of x and physical parameters,

$$\begin{aligned} t_{B, \frac{1}{2}}^{(b)}(x) &= -\frac{1}{2} M_{B0} (2x + 1), \\ t_{B, \frac{3}{2}}^{(b)}(x) &= \frac{1}{4} M_{B0} (M_{B0}^2 x^3 + (x + 2) \mathcal{M}_B^{(b)}), \\ t_{B, \frac{1}{2}}^{(c)}(x) &= -\frac{M_{B0}^2}{6 M_{T0}^2} (M_{B0} (1 - x) + M_{T0}), \\ t_{B, \frac{3}{2}}^{(c)}(x) &= \frac{M_{B0}^2}{6 M_{T0}^2} (M_{B0} (1 - x) + M_{T0}) \mathcal{M}_B^{(c)}, \\ t_{T, \frac{1}{2}}^{(b)}(x) &= \frac{1}{4} (M_{B0} + (1 - x) M_{T0}), \\ t_{T, \frac{3}{2}}^{(b)}(x) &= 0 \\ t_{T, \frac{1}{2}}^{(c)}(x) &= -\frac{1}{12} M_{T0} (2 - x), \\ t_{T, \frac{3}{2}}^{(c)}(x) &= -\frac{1}{4} M_{T0} (2 - x) \mathcal{M}_T^{(c)}, \end{aligned} \quad (\text{C.66})$$

and

$$\delta_{L,r}(\mathcal{M}) = \frac{1}{L^3} \sum_{\vec{k}} \frac{1}{(\vec{k}^2 + \mathcal{M}^2)^r} - \int \frac{d^3 \vec{k}}{(2\pi)^3} \frac{1}{(\vec{k}^2 + \mathcal{M}^2)^r}. \quad (\text{C.67})$$

We complete the numerical evaluation of the finite volume effects using (Appendix A of Reference [204])

$$\delta_{L,r}(\mathcal{M}) = \frac{2^{-1/2-r}(\sqrt{\mathcal{M}^2})^{3-2r}}{\pi^{3/2}\Gamma(r)} \sum_{\vec{n} \neq \vec{0}} \left(L\sqrt{\mathcal{M}^2}|\vec{n}| \right)^{-3/2+r} K_{3/2-r} \left(L\sqrt{\mathcal{M}^2}|\vec{n}| \right), \quad (\text{C.68})$$

where $K_n(z)$ is a modified Bessel function of second kind.

Appendix **D**

Lattice QCD results on the baryon masses

In Table D.1 we list the LQCD results on the baryon masses of the PACS-CS collaboration [193] and the LHP collaboration [192] that are used in Chap. 4. They correspond to those points for which, both the pion and kaon masses, are below 600 MeV, that is a limit of the meson mass we deem acceptable for the convergence of covariant $SU(3)_F$ -B χ PT up to NLO. The mass of the η -meson we determine using the Gell-Mann-Okubo relation Eq.(1.14) which is also valid up to this order of accuracy. The numbers in parenthesis are first the statistical uncertainties followed by those propagated from the lattice spacing and the box brackets contain the finite volume corrections.

Table D.1: Results in MeV of the PACS-CS collaboration [193] and the LHP collaboration [192] on the masses of the pseudoscalar mesons and the lowest-lying baryons used to fit the LECs of $SU(3)_F$ -B χ PT up to $\mathcal{O}(p^3)$. The numbers in parenthesis are first the statistical uncertainties followed by those propagated from the lattice spacing and the box brackets contain the finite volume corrections.

m_π	m_K	M_N	M_Λ	M_Σ	M_Ξ	M_Δ	M_{Σ^*}	M_{Ξ^*}	M_{Ω^-}
PACS-CS									
156	553	931(78)(13)[-7]	1138(21)(16)[-5]	1217(22)(17)[-3]	1391(7)(20)[-2]	1259(82)(18)[-24]	1495(30)(21)[-16]	1640(15)(24)[-7]	1768(7)(25)[0]
295	593	1091(19)(16)[-3]	1252(14)(18)[-2]	1313(15)(19)[-1]	1445(10)(21)[-1]	1400(20)(20)[2]	1544(15)(22)[3]	1683(13)(24)[2]	1812(11)(26)[0]
383	581	1158(15)(17)[-1]	1272(9)(18)[-1]	1314(10)(19)[-1]	1406(7)(20)[0]	1462(19)(21)[-1]	1553(16)(22)[0]	1646(13)(24)[0]	1738(11)(25)[0]
LHP									
293	585	1105(11)(22)[-7]	1245(6)(25)[-5]	1329(6)(37)[-3]	1415(3)(28)[-2]	1534(21)(31)[2]	1585(14)(32)[5]	1672(8)(34)[4]	1752(5)(35)[-1]
356	602	1153(8)(23)[-5]	1277(5)(25)[-3]	1348(6)(27)[-2]	1432(3)(29)[-2]	1547(14)(31)[-2]	1629(10)(33)[0]	1704(6)(34)[1]	1774(5)(35)[-1]

Bibliography

- [1] L. S. Geng, J. Martin Camalich, L. Alvarez-Ruso, and M. J. Vicente Vacas. Leading SU(3)-breaking corrections to the baryon magnetic moments in Chiral Perturbation Theory. *Phys. Rev. Lett.*, 101:222002, 2008.
- [2] L. S. Geng, J. Martin Camalich, and M. J. Vicente Vacas. Leading-order decuplet contributions to the baryon magnetic moments in Chiral Perturbation Theory. *Phys. Lett.*, B676:63–68, 2009.
- [3] L. S. Geng, J. Martin Camalich, and M. J. Vicente Vacas. SU(3)-breaking corrections to the hyperon vector coupling $f_1(0)$ in covariant baryon chiral perturbation theory. *Phys. Rev.*, D79:094022, 2009.
- [4] L. S. Geng, J. Martin Camalich, and M. J. Vicente Vacas. Electromagnetic structure of the lowest-lying decuplet resonances in covariant chiral perturbation theory. *Phys. Rev.*, D80:034027, 2009.
- [5] J. Martin-Camalich, L. S. Geng, and M. J. Vicente Vacas. The lowest-lying baryon masses in covariant SU(3)-flavor chiral perturbation theory. *Phys. Rev.*, D, in print, 2010.
- [6] Norbert Kaiser, P. B. Siegel, and W. Weise. Chiral dynamics and the low-energy kaon - nucleon interaction. *Nucl. Phys.*, A594:325–345, 1995.
- [7] E. Oset and A. Ramos. Non perturbative chiral approach to s-wave anti- K N interactions. *Nucl. Phys.*, A635:99–120, 1998.
- [8] J. A. Oller and Ulf G. Meissner. Chiral dynamics in the presence of bound states: Kaon nucleon interactions revisited. *Phys. Lett.*, B500:263–272, 2001.

- [9] J. A. Oller, E. Oset, and A. Ramos. Chiral unitary approach to meson meson and meson baryon interactions and nuclear applications. *Prog. Part. Nucl. Phys.*, 45:157–242, 2000.
- [10] J. Nieves and E. Ruiz Arriola. The $S(11)$ $N(1535)$ and $N(1650)$ resonances in meson baryon unitarized coupled channel chiral perturbation theory. *Phys. Rev.*, D64:116008, 2001.
- [11] M. F. M. Lutz and E. E. Kolomeitsev. Relativistic chiral $SU(3)$ symmetry, large N_c sum rules and meson baryon scattering. *Nucl. Phys.*, A700:193–308, 2002.
- [12] C. Garcia-Recio, J. Nieves, E. Ruiz Arriola, and M. J. Vicente Vacas. $S = -1$ Meson-Baryon Unitarized Coupled Channel Chiral Perturbation Theory and the $S_{01} - \Lambda(1405)$ and $\Lambda(1670)$ Resonances. *Phys. Rev.*, D67:076009, 2003.
- [13] Jose A. Oller, Joaquim Prades, and Michela Verbeni. Surprises in threshold antikaon nucleon physics. *Phys. Rev. Lett.*, 95:172502, 2005.
- [14] R. Mertig, M. Bohm, and Ansgar Denner. FEYN CALC: Computer algebraic calculation of Feynman amplitudes. *Comput. Phys. Commun.*, 64:345–359, 1991.
- [15] J. A. M. Vermaseren. New features of FORM. 2000.
- [16] J. Martin Camalich and M. J. Vicente Vacas. The baryon-decuplet in the chiral dynamics of Lambda- hyperons in nuclear matter. *Phys. Rev.*, C75:035207, 2007.
- [17] L. S. Geng, J. Martin Camalich, L. Alvarez-Ruso, and M. J. Vicente Vacas. Nucleon-to-Delta axial transition form factors in relativistic baryon chiral perturbation theory. *Phys. Rev.*, D78:014011, 2008.
- [18] T. Ledwig, J. Martin-Camalich, V. Pascalutsa, and M. Vanderhaeghen. Chiral extrapolation of the nucleon and $\Delta(1232)$ electromagnetic static structure. In preparation.
- [19] J. M. Alarcón, J. Martin-Camalich, J.A. Oller, and L. Alvarez-Ruso. πN scattering in relativistic chiral perturbation theory revisited. In preparation.
- [20] L. S. Geng, N. Kaiser, J. Martin-Camalich, and W. Weise. Low-energy interactions of Nambu-Goldstone bosons with D mesons in covariant chiral perturbation theory. *Phys. Rev.*, D, in print, 2010.

- [21] G. Ecker. Chiral perturbation theory. *Prog. Part. Nucl. Phys.*, 35:1–80, 1995.
- [22] V. Bernard, Norbert Kaiser, and Ulf-G. Meissner. Chiral dynamics in nucleons and nuclei. *Int. J. Mod. Phys.*, E4:193–346, 1995.
- [23] A. Pich. Chiral perturbation theory. *Rept. Prog. Phys.*, 58:563–610, 1995.
- [24] Thomas R. Hemmert, Barry R. Holstein, and Joachim Kambor. Chiral Lagrangians and $\Delta(1232)$ interactions: Formalism. *J. Phys.*, G24:1831–1859, 1998.
- [25] Stefan Scherer. Introduction to chiral perturbation theory. *Adv. Nucl. Phys.*, 27:277, 2003.
- [26] Vladimir Pascalutsa, Marc Vanderhaeghen, and Shin Nan Yang. Electromagnetic excitation of the $\Delta(1232)$ -resonance. *Phys. Rept.*, 437:125–232, 2007.
- [27] J. F. Donoghue, E. Golowich, and Barry R. Holstein. Dynamics of the standard model. *Camb. Monogr. Part. Phys. Nucl. Phys. Cosmol.*, 2:1–540, 1992.
- [28] Michael Edward Peskin and Daniel V. Schroeder. An Introduction to quantum field theory. Reading, USA: Addison-Wesley (1995) 842 p.
- [29] Steven Weinberg. The Quantum theory of fields. Vol. 1: Foundations. Cambridge, UK: Univ. Pr. (1995) 609 p.
- [30] Steven Weinberg. The quantum theory of fields. Vol. 2: Modern applications. Cambridge, UK: Univ. Pr. (1996) 489 p.
- [31] F. J. Yndurain. The theory of quark and gluon interactions. Berlin, Germany: Springer (1999) 413 p.
- [32] D. J. Gross and Frank Wilczek. Ultraviolet behavior of non-abelian gauge theories. *Phys. Rev. Lett.*, 30:1343–1346, 1973.
- [33] Steven Weinberg. Nonabelian Gauge Theories of the Strong Interactions. *Phys. Rev. Lett.*, 31:494–497, 1973.
- [34] H. Fritzsch, Murray Gell-Mann, and H. Leutwyler. Advantages of the Color Octet Gluon Picture. *Phys. Lett.*, B47:365–368, 1973.

- [35] D. J. Gross and Frank Wilczek. Asymptotically Free Gauge Theories. 1. *Phys. Rev.*, D8:3633–3652, 1973.
- [36] Heinz Pagels. Departures from Chiral Symmetry: A Review. *Phys. Rept.*, 16:219, 1975.
- [37] Murray Gell-Mann. The Symmetry group of vector and axial vector currents. *Physics*, 1:63–75, 1964.
- [38] Dashen R.F. Adler, S.L. Current Algebras and Applications to Particle Physics. New York, USA: Benjamin (1968) 394 p.
- [39] Yoichiro Nambu. Axial vector current conservation in weak interactions. *Phys. Rev. Lett.*, 4:380–382, 1960.
- [40] Murray Gell-Mann and M Levy. The axial vector current in beta decay. *Nuovo Cim.*, 16:705, 1960.
- [41] Sidney Coleman. The Invariance of the Vacuum is the Invariance of the World. *J. Math. Phys.*, 7:787, 1966.
- [42] Murray Gell-Mann. A Schematic Model of Baryons and Mesons. *Phys. Lett.*, 8:214–215, 1964.
- [43] J. Goldstone. Field Theories with Superconductor Solutions. *Nuovo Cim.*, 19:154–164, 1961.
- [44] Steven Weinberg. Dynamical approach to current algebra. *Phys. Rev. Lett.*, 18:188–191, 1967.
- [45] Steven Weinberg. Phenomenological Lagrangians. *Physica*, A96:327, 1979.
- [46] J. Gasser and H. Leutwyler. Chiral Perturbation Theory to One Loop. *Ann. Phys.*, 158:142, 1984.
- [47] J. Gasser and H. Leutwyler. Chiral Perturbation Theory: Expansions in the Mass of the Strange Quark. *Nucl. Phys.*, B250:465, 1985.
- [48] Steven Weinberg. Nonlinear realizations of chiral symmetry. *Phys. Rev.*, 166:1568–1577, 1968.
- [49] Sidney R. Coleman, J. Wess, and Bruno Zumino. Structure of phenomenological Lagrangians. 1. *Phys. Rev.*, 177:2239–2247, 1969.

- [50] Curtis G. Callan, Jr., Sidney R. Coleman, J. Wess, and Bruno Zumino. Structure of phenomenological Lagrangians. 2. *Phys. Rev.*, 177:2247–2250, 1969.
- [51] Murray Gell-Mann, R. J. Oakes, and B. Renner. Behavior of current divergences under $SU(3) \times SU(3)$. *Phys. Rev.*, 175:2195–2199, 1968.
- [52] Susumu Okubo. Note on unitary symmetry in strong interactions. *Prog. Theor. Phys.*, 27:949–966, 1962.
- [53] Murray Gell-Mann. Symmetries of baryons and mesons. *Phys. Rev.*, 125:1067–1084, 1962.
- [54] Steven Weinberg. Pion scattering lengths. *Phys. Rev. Lett.*, 17:616–621, 1966.
- [55] H. Leutwyler. On the foundations of chiral perturbation theory. *Ann. Phys.*, 235:165–203, 1994.
- [56] J. Bijnens, G. Colangelo, and G. Ecker. Renormalization of chiral perturbation theory to order p^6 . *Annals Phys.*, 280:100–139, 2000.
- [57] J. Gasser, M. E. Sainio, and A. Svarc. Nucleons with Chiral Loops. *Nucl. Phys.*, B307:779, 1988.
- [58] Y. Tomozawa. Axial vector coupling renormalization and the meson baryon scattering lengths. *Nuovo Cim.*, 46A:707–717, 1966.
- [59] M. L. Goldberger and S. B. Treiman. Conserved Currents in the Theory of Fermi Interactions. *Phys. Rev.*, 110:1478–1479, 1958.
- [60] M. L. Goldberger and S. B. Treiman. Form-factors in Beta decay and muon capture. *Phys. Rev.*, 111:354–361, 1958.
- [61] Norman M. Kroll and Malvin A. Ruderman. A theorem on photomeson production near threshold and the suppression of pairs in pseudoscalar meson theory. *Phys. Rev.*, 93(1):233–238, Jan 1954.
- [62] Steven Weinberg. Nuclear forces from chiral Lagrangians. *Phys. Lett.*, B251:288–292, 1990.
- [63] Elizabeth Ellen Jenkins and Aneesh V. Manohar. Baryon chiral perturbation theory using a heavy fermion Lagrangian. *Phys. Lett.*, B255:558–562, 1991.

- [64] Veronique Bernard. Chiral Perturbation Theory and Baryon Properties. *Prog. Part. Nucl. Phys.*, 60:82–160, 2008.
- [65] Thomas Becher and H. Leutwyler. Baryon chiral perturbation theory in manifestly Lorentz invariant form. *Eur. Phys. J.*, C9:643–671, 1999.
- [66] A. Krause. Baryon matrix elements of the vector current in chiral perturbation theory. *Helv. Phys. Acta*, 63:3–70, 1990.
- [67] Hua-Bin Tang. A new approach to chiral perturbation theory for matter fields. 1996.
- [68] Paul J. Ellis and Hua-Bin Tang. Pion nucleon scattering in a new approach to chiral perturbation theory. *Phys. Rev.*, C57:3356–3375, 1998.
- [69] J. Gegelia and G. Japaridze. Matching heavy particle approach to relativistic theory. *Phys. Rev.*, D60:114038, 1999.
- [70] T. Fuchs, J. Gegelia, G. Japaridze, and S. Scherer. Renormalization of relativistic baryon chiral perturbation theory and power counting. *Phys. Rev.*, D68:056005, 2003.
- [71] Thomas Fuchs, Jambul Gegelia, and Stefan Scherer. Electromagnetic form factors of the nucleon in relativistic baryon chiral perturbation theory. *J. Phys.*, G30:1407–1426, 2004.
- [72] Vladimir Pascalutsa and Marc Vanderhaeghen. Magnetic moment of the $\Delta(1232)$ -resonance in chiral effective field theory. *Phys. Rev. Lett.*, 94:102003, 2005.
- [73] Vladimir Pascalutsa and Marc Vanderhaeghen. Electromagnetic nucleon to Δ transition in chiral effective field theory. *Phys. Rev. Lett.*, 95:232001, 2005.
- [74] Vladimir Pascalutsa and Marc Vanderhaeghen. Chiral effective-field theory in the $\Delta(1232)$ region. I: Pion electroproduction on the nucleon. *Phys. Rev.*, D73:034003, 2006.
- [75] C. Hacker, N. Wies, J. Gegelia, and S. Scherer. Magnetic dipole moment of the $\Delta(1232)$ in chiral perturbation theory. *Eur. Phys. J.*, A28:5–9, 2006.
- [76] M. R. Schindler, T. Fuchs, J. Gegelia, and S. Scherer. Axial, induced pseudoscalar, and pion nucleon form factors in manifestly Lorentz-invariant chiral perturbation theory. *Phys. Rev.*, C75:025202, 2007.

- [77] Vladimir Pascalutsa and Marc Vanderhaeghen. Chiral effective-field theory in the $\Delta(1232)$ region: II. radiative pion photoproduction. *Phys. Rev.*, D77:014027, 2008.
- [78] Vladimir Pascalutsa and Marc Vanderhaeghen. The nucleon and Δ -resonance masses in relativistic chiral effective-field theory. *Phys. Lett.*, B636:31–39, 2006.
- [79] Vadim Lensky and Vladimir Pascalutsa. Manifestly-covariant chiral perturbation theory calculation of nucleon Compton scattering. *Pisma Zh. Eksp. Teor. Fiz.*, 89:127–132, 2009.
- [80] Vadim Lensky and Vladimir Pascalutsa. Predictive powers of chiral perturbation theory in Compton scattering off protons. *Eur. Phys. J.*, C65:195–209, 2010.
- [81] Barry R. Holstein, Vladimir Pascalutsa, and Marc Vanderhaeghen. Sum rules for magnetic moments and polarizabilities in QED and chiral effective-field theory. *Phys. Rev.*, D72:094014, 2005.
- [82] Elizabeth Ellen Jenkins and Aneesh V. Manohar. Chiral corrections to the baryon axial currents. *Phys. Lett.*, B259:353–358, 1991.
- [83] William Rarita and Julian Schwinger. On a theory of particles with half integral spin. *Phys. Rev.*, 60:61, 1941.
- [84] V. Pascalutsa. Quantization of an interacting spin-3/2 field and the Δ isobar. *Phys. Rev.*, D58:096002, 1998.
- [85] Vladimir Pascalutsa and Rob Timmermans. Field theory of nucleon to higher-spin baryon transitions. *Phys. Rev.*, C60:042201, 1999.
- [86] Terry Pilling. Symmetry of massive Rarita-Schwinger fields. *Int. J. Mod. Phys.*, A20:2715–2742, 2005.
- [87] Kenneth Johnson and E. C. G. Sudarshan. Inconsistency of the local field theory of charged spin 3/2 particles. *Ann. Phys.*, 13:126–145, 1961.
- [88] Giorgio Velo and Daniel Zwanziger. Propagation and quantization of Rarita-Schwinger waves in an external electromagnetic potential. *Phys. Rev.*, 186:1337–1341, 1969.
- [89] C. R. Hagen. New inconsistencies in the quantization of spin 3/2 fields. *Phys. Rev.*, D4:2204–2208, 1971.

- [90] L. P. S. Singh. Non-causal propagation of classical rarita-schwinger waves. *Phys. Rev.*, D7:1256–1258, 1973.
- [91] Paul A. M. Dirac. Lectures on Quantum Mechanics. World Scientific (2001) 145 p.
- [92] V. Pascalutsa. Correspondence of consistent and inconsistent spin-3/2 couplings via the equivalence theorem. *Phys. Lett.*, B503:85–90, 2001.
- [93] Veronique Bernard, Thomas R. Hemmert, and Ulf-G. Meissner. Infrared regularization with spin-3/2 fields. *Phys. Lett.*, B565:137–145, 2003.
- [94] Hua-Bin Tang and Paul J. Ellis. Redundance of Delta isobar parameters in effective field theories. *Phys. Lett.*, B387:9–13, 1996.
- [95] N. Wies, J. Gegelia, and S. Scherer. Consistency of the pi Delta interaction in chiral perturbation theory. *Phys. Rev.*, D73:094012, 2006.
- [96] S. Kamefuchi, L. O’Raifeartaigh, and Abdus Salam. Change of variables and equivalence theorems in quantum field theories. *Nucl. Phys.*, 28:529–549, 1961.
- [97] Stanley Deser, V. Pascalutsa, and A. Waldron. Massive spin 3/2 electrodynamics. *Phys. Rev.*, D62:105031, 2000.
- [98] Massimo Porrati and Rakibur Rahman. Causal Propagation of a Charged Spin 3/2 Field in an External Electromagnetic Background. *Phys. Rev.*, D80:025009, 2009.
- [99] Vladimir Pascalutsa and Daniel R. Phillips. Effective theory of the $\Delta(1232)$ in Compton scattering off the nucleon. *Phys. Rev.*, C67:055202, 2003.
- [100] F. Piccinini, Giovanni Venturi, and R. Zucchini. Acausality and violation of S matrix unitarity for Rarita-Schwinger particles in an external electromagnetic potential. *Nuovo Cim. Lett.*, 41:536, 1984.
- [101] Sidney R. Coleman and Sheldon Lee Glashow. Electrodynamical properties of baryons in the unitary symmetry scheme. *Phys. Rev. Lett.*, 6:423, 1961.
- [102] D. G. Caldi and Heinz Pagels. Chiral Perturbation Theory and the Magnetic Moments of the Baryon Octet. *Phys. Rev.*, D10:3739, 1974.

- [103] Elizabeth Ellen Jenkins, Michael E. Luke, Aneesh V. Manohar, and Martin J. Savage. Chiral Perturbation Theory Analysis of the Baryon Magnetic Moments. *Phys. Lett.*, B302:482–490, 1993.
- [104] Ulf-G. Meissner and S. Steininger. Baryon magnetic moments in chiral perturbation theory. *Nucl. Phys.*, B499:349–367, 1997.
- [105] Loyal Durand and Phuoc Ha. Chiral perturbation theory analysis of the baryon magnetic moments revisited. *Phys. Rev.*, D58:013010, 1998.
- [106] S. J. Puglia and M. J. Ramsey-Musolf. Baryon octet magnetic moments in chiral perturbation theory: More on the importance of the decuplet. *Phys. Rev.*, D62:034010, 2000.
- [107] Bastian Kubis and Ulf G. Meissner. Baryon form factors in chiral perturbation theory. *Eur. Phys. J.*, C18:747–756, 2001.
- [108] Claude Amsler et al. Review of particle physics. *Phys. Lett.*, B667:1, 2008.
- [109] L. M. Nath, B. Etemadi, and J. D. Kimel. Uniqueness of the interaction involving spin 3/2 particles. *Phys. Rev.*, D3:2153–2161, 1971.
- [110] S. Okubo. Some consequences of unitary symmetry model. *Phys. Lett.*, 4:14–16, 1963.
- [111] B. M. K. Nefkens et al. Differential Cross-Sections for Pion-Proton Bremsstrahlung at 269-MeV, 298-MeV, and 324-MeV. *Phys. Rev.*, D18:3911, 1978.
- [112] A. Bosshard et al. Analyzing power in pion proton bremsstrahlung, and the $\Delta^{++}(1232)$ magnetic moment. *Phys. Rev.*, D44:1962–1974, 1991.
- [113] P. Pascual and R. Tarrach. Radiative $\pi^+ p$ Scattering and the Magnetic Moment of the Δ^{++} . *Nucl. Phys.*, B134:133, 1978.
- [114] G. Lopez Castro and A. Mariano. Determination of the Δ^{++} magnetic dipole moment. *Phys. Lett.*, B517:339–344, 2001.
- [115] A. I. Machavariani, A. Faessler, and A. J. Buchmann. Field-theoretical description of electromagnetic Δ resonance production and determination of the magnetic moment of the $\Delta^+(1232)$ resonance by the $ep \rightarrow e'N'\pi'\gamma'$ and $\gamma p \rightarrow N'\pi'\gamma'$ reactions. *Nucl. Phys.*, A646:231–257, 1999.

- [116] M. Kotulla et al. The reaction $\gamma p \rightarrow \pi^0 \gamma' p$ and the magnetic dipole moment of the $\Delta^+(1232)$ resonance. *Phys. Rev. Lett.*, 89:272001, 2002.
- [117] M. Kotulla. Magnetic moments of excited baryons. *Prog. Part. Nucl. Phys.*, 61:147–152, 2008.
- [118] S. Schumann et al. Radiative π^0 photoproduction on protons in the $\Delta^+(1232)$ region. 2010.
- [119] Wen-Tai Chiang, M. Vanderhaeghen, Shin Nan Yang, and D. Drechsel. Unitary model for the $\gamma p \rightarrow \gamma \pi^0 p$ reaction and the magnetic dipole moment of the $\Delta^+(1232)$. *Phys. Rev.*, C71:015204, 2005.
- [120] K. Hikasa et al. Review of particle properties. Particle Data Group. *Phys. Rev.*, D45:S1, 1992.
- [121] M. I. Krivoruchenko and M. M. Giannini. Quadrupole moments of the decuplet baryons. *Phys. Rev.*, D43:3763–3765, 1991.
- [122] Felix Schlumpf. Magnetic moments of the baryon decuplet in a relativistic quark model. *Phys. Rev.*, D48:4478–4480, 1993.
- [123] A. J. Buchmann, E. Hernandez, and Amand Faessler. Electromagnetic properties of the $\Delta(1232)$. *Phys. Rev.*, C55:448–463, 1997.
- [124] G. Wagner, A. J. Buchmann, and A. Faessler. Electromagnetic properties of decuplet hyperons in a chiral quark model with exchange currents. *J. Phys.*, G26:267–293, 2000.
- [125] Hyun-Chul Kim, Michal Praszalowicz, and Klaus Goeke. Magnetic moments of the SU(3) decuplet baryons in the chiral quark-soliton model. *Phys. Rev.*, D57:2859–2870, 1998.
- [126] Tim Ledwig, Antonio Silva, and Marc Vanderhaeghen. Electromagnetic properties of the $\Delta(1232)$ and decuplet baryons in the self-consistent SU(3) chiral quark-soliton model. *Phys. Rev.*, D79:094025, 2009.
- [127] G. Ramalho and M. T. Pena. Electromagnetic form factors of the Δ in a S-wave approach. *J. Phys.*, G36:085004, 2009.
- [128] G. Ramalho, M. T. Pena, and Franz Gross. Electric quadrupole and magnetic octupole moments of the Δ . *Phys. Lett.*, B678:355–358, 2009.
- [129] G. Ramalho, M. T. Pena, and Franz Gross. Electromagnetic form factors of the Δ with D-waves. 2010.

- [130] A. J. Buchmann and E. M. Henley. Quadrupole moments of baryons. *Phys. Rev.*, D65:073017, 2002.
- [131] A. J. Buchmann and E. M. Henley. Baryon octupole moments. *Eur. Phys. J.*, A35:267–269, 2008.
- [132] Frank X. Lee. Determination of decuplet baryon magnetic moments from QCD sum rules. *Phys. Rev.*, D57:1801–1821, 1998.
- [133] T. M. Aliev, A. Ozpineci, and M. Savci. Magnetic moments of Δ baryons in light cone QCD sum rules. *Nucl. Phys.*, A678:443–454, 2000.
- [134] K. Azizi. Magnetic Dipole, Electric Quadrupole and Magnetic Octupole Moments of the Δ Baryons in Light Cone QCD Sum Rules. *Eur. Phys. J.*, C61:311–319, 2009.
- [135] T. M. Aliev, K. Azizi, and M. Savci. Electric Quadrupole and Magnetic Octupole Moments of the Light Decuplet Baryons Within Light Cone QCD Sum Rules. *Phys. Lett.*, B681:240–246, 2009.
- [136] Markus A. Luty, John March-Russell, and Martin J. White. Baryon magnetic moments in a simultaneous expansion in $1/N_c$ and m_s . *Phys. Rev.*, D51:2332–2337, 1995.
- [137] Elizabeth Ellen Jenkins and Aneesh V. Manohar. Baryon Magnetic Moments in the $1/N_c$ Expansion. *Phys. Lett.*, B335:452–459, 1994.
- [138] Alfons J. Buchmann, Janice A. Hester, and Richard F. Lebed. Quadrupole moments of N and Δ in the $1/N_c$ expansion. *Phys. Rev.*, D66:056002, 2002.
- [139] Malcolm N. Butler, Martin J. Savage, and Roxanne P. Springer. Electromagnetic moments of the baryon decuplet. *Phys. Rev.*, D49:3459–3465, 1994.
- [140] M. K. Banerjee and J. Milana. The Decuplet revisited in chiral perturbation theory. *Phys. Rev.*, D54:5804–5811, 1996.
- [141] Daniel Arndt and Brian C Tiburzi. Electromagnetic properties of the baryon decuplet in quenched and partially quenched chiral perturbation theory. *Phys. Rev.*, D68:114503, 2003.
- [142] B. C. Tiburzi. Connected Parts of Decuplet Electromagnetic Properties. *Phys. Rev.*, D79:077501, 2009.

- [143] S. Nozawa and D. B. Leinweber. Electromagnetic form-factors of spin 3/2 baryons. *Phys. Rev.*, D42:3567–3571, 1990.
- [144] Derek B. Leinweber, Terrence Draper, and R. M. Woloshyn. Decuplet baryon structure from lattice QCD. *Phys. Rev.*, D46:3067–3085, 1992.
- [145] I. C. Cloet, Derek Bruce Leinweber, and Anthony William Thomas. Δ baryon magnetic moments from lattice QCD. *Phys. Lett.*, B563:157–164, 2003.
- [146] F. X. Lee, R. Kelly, L. Zhou, and W. Wilcox. Baryon magnetic moments in the background field method. *Phys. Lett.*, B627:71–76, 2005.
- [147] C. Alexandrou et al. Delta-baryon electromagnetic form factors in lattice QCD. *Phys. Rev.*, D79:014507, 2009.
- [148] C. Aubin, K. Orginos, V. Pascalutsa, and M. Vanderhaeghen. Magnetic Moments of Δ and Ω^- Baryons with Dynamical Clover Fermions. *Phys. Rev.*, D79:051502, 2009.
- [149] Constantia Alexandrou et al. Quark transverse charge densities in the $\Delta(1232)$ from lattice QCD. *Nucl. Phys.*, A825:115–144, 2009.
- [150] S. Boinepalli et al. Precision electromagnetic structure of decuplet baryons in the chiral regime. *Phys. Rev.*, D80:054505, 2009.
- [151] C. Alexandrou, T. Korzec, G. Koutsou, J. W. Negele, and Y. Proestos. The electromagnetic form factors of the Omega in lattice QCD. *Phys. Rev.*, D82:034504, 2010.
- [152] Nicola Cabibbo. Unitary Symmetry and Leptonic Decays. *Phys. Rev. Lett.*, 10:531–533, 1963.
- [153] Makoto Kobayashi and Toshihide Maskawa. CP Violation in the Renormalizable Theory of Weak Interaction. *Prog. Theor. Phys.*, 49:652–657, 1973.
- [154] J. C. Hardy and I. S. Towner. Superallowed 0^+ to 0^+ nuclear beta decays: A new survey with precision tests of the conserved vector current hypothesis and the standard model. *Phys. Rev.*, C79:055502, 2009.
- [155] D. Poganic et al. Precise Measurement of the $\pi^+ \rightarrow \pi^0 e^+ \nu$ Branching Ratio. *Phys. Rev. Lett.*, 93:181803, 2004.

- [156] M. Antonelli et al. An evaluation of $|V_{us}|$ and precise tests of the Standard Model from world data on leptonic and semileptonic kaon decays. 2010.
- [157] William J. Marciano. Precise determination of $|V_{us}|$ from lattice calculations of pseudoscalar decay constants. *Phys. Rev. Lett.*, 93:231803, 2004.
- [158] S. Durr et al. The ratio F_K/F_π in QCD. *Phys. Rev.*, D81:054507, 2010.
- [159] Elvira Gamiz, Matthias Jamin, Antonio Pich, Joaquim Prades, and Felix Schwab. V_{us} and m_s from hadronic tau decays. *Phys. Rev. Lett.*, 94:011803, 2005.
- [160] Nicola Cabibbo, Earl C. Swallow, and Roland Winston. Semileptonic hyperon decays and CKM unitarity. *Phys. Rev. Lett.*, 92:251803, 2004.
- [161] Bernard Aubert et al. Measurements of Charged Current Lepton Universality and $|V_{us}|$ using Tau Lepton Decays to $e^-\bar{\nu}_e\nu_\tau$, $\mu^-\bar{\nu}_\mu\nu_\tau$, $\pi^-\nu_\tau$ and $K^-\nu_\tau$. 2009.
- [162] Nicola Cabibbo, Earl C. Swallow, and Roland Winston. Semileptonic hyperon decays. *Ann. Rev. Nucl. Part. Sci.*, 53:39–75, 2003.
- [163] M. Ademollo and Raoul Gatto. Nonrenormalization Theorem for the Strangeness Violating Vector Currents. *Phys. Rev. Lett.*, 13:264–265, 1964.
- [164] V. Mateu and A. Pich. V_{us} determination from hyperon semileptonic decays. *JHEP*, 10:041, 2005.
- [165] Ruben Flores-Mendieta. V_{us} from hyperon semileptonic decays. *Phys. Rev.*, D70:114036, 2004.
- [166] Jeffrey Anderson and Markus A. Luty. Chiral corrections to hyperon vector form-factors. *Phys. Rev.*, D47:4975–4980, 1993.
- [167] Norbert Kaiser. Isospin breaking in neutron beta-decay and SU(3) violation in semi-leptonic hyperon decays. *Phys. Rev.*, C64:028201, 2001.
- [168] Giovanni Villadoro. Chiral corrections to the hyperon vector form factors. *Phys. Rev.*, D74:014018, 2006.
- [169] Andre Lacour, Bastian Kubis, and Ulf-G. Meissner. Hyperon decay form factors in chiral perturbation theory. *JHEP*, 10:083, 2007.

- [170] D. B. Chitwood et al. Improved Measurement of the Positive Muon Lifetime and Determination of the Fermi Constant. *Phys. Rev. Lett.*, 99:032001, 2007.
- [171] John F. Donoghue, Barry R. Holstein, and Stefan W. Kliment. K-m Angles and SU(3) Breaking in Hyperon beta Decay. *Phys. Rev.*, D35:934, 1987.
- [172] Amand Faessler et al. Semileptonic decays of the light J(P)=1/2(+) ground state baryon octet. *Phys. Rev.*, D78:094005, 2008.
- [173] D. Guadagnoli, V. Lubicz, M. Papinutto, and S. Simula. First lattice QCD study of the $\Sigma^- \rightarrow n$ axial and vector form factors with SU(3) breaking corrections. *Nucl. Phys.*, B761:63–91, 2007.
- [174] Shoichi Sasaki and Takeshi Yamazaki. Lattice study of flavor SU(3) breaking in hyperon beta decay. *Phys. Rev.*, D79:074508, 2009.
- [175] H. Leutwyler and M. Roos. Determination of the Elements V_{us} and V_{ud} of the Kobayashi-Maskawa Matrix. *Z. Phys.*, C25:91, 1984.
- [176] Paul Langacker and Heinz Pagels. Chiral perturbation theory. *Phys. Rev.*, D8:4595–4619, 1973.
- [177] Elizabeth Ellen Jenkins. Baryon masses in chiral perturbation theory. *Nucl. Phys.*, B368:190–203, 1992.
- [178] Veronique Bernard, Norbert Kaiser, and Ulf G. Meissner. Critical analysis of baryon masses and sigma terms in heavy baryon chiral perturbation theory. *Z. Phys.*, C60:111–120, 1993.
- [179] M. K. Banerjee and J. Milana. Baryon mass splittings in chiral perturbation theory. *Phys. Rev.*, D52:6451–6460, 1995.
- [180] B. Borasoy and Ulf-G. Meissner. Chiral expansion of baryon masses and sigma-terms. *Annals Phys.*, 254:192–232, 1997.
- [181] P. J. Ellis and K. Torikoshi. Baryon masses in chiral perturbation theory with infrared regularization. *Phys. Rev.*, C61:015205, 2000.
- [182] Matthias Frink and Ulf-G. Meissner. Chiral extrapolations of baryon masses for unquenched three-flavor lattice simulations. *JHEP*, 07:028, 2004.
- [183] Andre Walker-Loud. Octet baryon masses in partially quenched chiral perturbation theory. *Nucl. Phys.*, A747:476–507, 2005.

- [184] Brian C. Tiburzi and Andre Walker-Loud. Decuplet baryon masses in partially quenched chiral perturbation theory. *Nucl. Phys.*, A748:513–536, 2005.
- [185] B. C. Lehnhart, J. Gegelia, and S. Scherer. Baryon masses and nucleon sigma terms in manifestly Lorentz-invariant baryon chiral perturbation theory. *J. Phys.*, G31:89–104, 2005.
- [186] A. Semke and M. F. M. Lutz. Baryon self energies in the chiral loop expansion. *Nucl. Phys.*, A778:153–180, 2006.
- [187] A. Semke and M. F. M. Lutz. On the possibility of a discontinuous quark-mass dependence of baryon octet and decuplet masses. *Nucl. Phys.*, A789:251–259, 2007.
- [188] Elizabeth Ellen Jenkins. Chiral Lagrangian for Baryons in the $1/N_c$ Expansion. *Phys. Rev.*, D53:2625–2644, 1996.
- [189] Silas R. Beane, Kostas Orginos, and Martin J. Savage. The Gell-Mann - Okubo mass relation among baryons from fully-dynamical mixed-action lattice QCD. *Phys. Lett.*, B654:20–26, 2007.
- [190] Elizabeth Ellen Jenkins, Aneesh V. Manohar, John W. Negele, and Andre Walker-Loud. A Lattice Test of $1/N_c$ Baryon Mass Relations. *Phys. Rev.*, D81:014502, 2010.
- [191] John R. Ellis, Keith A. Olive, and Christopher Savage. Hadronic Uncertainties in the Elastic Scattering of Supersymmetric Dark Matter. *Phys. Rev.*, D77:065026, 2008.
- [192] A. Walker-Loud et al. Light hadron spectroscopy using domain wall valence quarks on an Asqtad sea. *Phys. Rev.*, D79:054502, 2009.
- [193] S. Aoki et al. 2+1 Flavor Lattice QCD toward the Physical Point. *Phys. Rev.*, D79:034503, 2009.
- [194] Huey-Wen Lin et al. First results from 2+1 dynamical quark flavors on an anisotropic lattice: light-hadron spectroscopy and setting the strange-quark mass. *Phys. Rev.*, D79:034502, 2009.
- [195] S. Durr et al. Ab-Initio Determination of Light Hadron Masses. *Science*, 322:1224–1227, 2008.
- [196] C. Alexandrou et al. The low-lying baryon spectrum with two dynamical twisted mass fermions. *Phys. Rev.*, D80:114503, 2009.

- [197] S. Aoki et al. Physical Point Simulation in 2+1 Flavor Lattice QCD. *Phys. Rev.*, D81:074503, 2010.
- [198] W. Bietenholz et al. Tuning the strange quark mass in lattice simulations. *Phys. Lett.*, B690:436–441, 2010.
- [199] K. I. Ishikawa et al. SU(2) and SU(3) chiral perturbation theory analyses on baryon masses in 2+1 flavor lattice QCD. *Phys. Rev.*, D80:054502, 2009.
- [200] Brian C. Tiburzi and Andre Walker-Loud. Hyperons in Two Flavor Chiral Perturbation Theory. *Phys. Lett.*, B669:246–253, 2008.
- [201] Massimiliano Procura, Thomas R. Hemmert, and Wolfram Weise. Nucleon mass, sigma term and lattice QCD. *Phys. Rev.*, D69:034505, 2004.
- [202] M. Procura, B. U. Musch, T. Wollenweber, T. R. Hemmert, and W. Weise. Nucleon mass: From lattice QCD to the chiral limit. *Phys. Rev.*, D73:114510, 2006.
- [203] Veronique Bernard, Thomas R. Hemmert, and Ulf-G. Meissner. Chiral extrapolations and the covariant small scale expansion. *Phys. Lett.*, B622:141–150, 2005.
- [204] Silas R. Beane. Nucleon masses and magnetic moments in a finite volume. *Phys. Rev.*, D70:034507, 2004.
- [205] John F. Donoghue, Barry R. Holstein, and Bugra Borasoy. SU(3) baryon chiral perturbation theory and long distance regularization. *Phys. Rev.*, D59:036002, 1999.
- [206] R. D. Young and A. W. Thomas. Octet baryon masses and sigma terms from an SU(3) chiral extrapolation. *Phys. Rev.*, D81:014503, 2010.
- [207] A. E. Kaloshin and V. P. Lomov. Propagator of the interacting Rarita-Schwinger field. *Mod. Phys. Lett.*, A19:135–142, 2004.
- [208] A. E. Kaloshin and V. P. Lomov. The Rarita-Schwinger field: Dressing procedure and spin- parity content. *Phys. Atom. Nucl.*, 69:541–551, 2006.
- [209] Rajan Gupta. Introduction to lattice QCD. 1997.
- [210] Karl Jansen. Lattice QCD: a critical status report. *PoS, LATTICE2008:010*, 2008.

- [211] Maarten Golterman. Applications of chiral perturbation theory to lattice QCD. 2009.
- [212] H Hellmann. Zur Rolle der kinetischen Elektronenenergie für die zwischenatomaren Kräfte . *Z.Phys.A*, 85:180, 1933.
- [213] R. P. Feynman. Forces in Molecules. *Phys. Rev.*, 56:340–343, 1939.
- [214] J. Gasser, H. Leutwyler, and M. E. Sainio. Sigma term update. *Phys. Lett.*, B253:252–259, 1991.
- [215] Joel Giedt, Anthony W. Thomas, and Ross D. Young. Dark matter, the CMSSM and lattice QCD. *Phys. Rev. Lett.*, 103:201802, 2009.
- [216] Huey-Wen Lin and Konstantinos Orginos. First Calculation of Hyperon Axial Couplings from Lattice QCD. *Phys. Rev.*, D79:034507, 2009.
- [217] Guray Erkol, Makoto Oka, and Toru T. Takahashi. Axial Charges of Octet Baryons in Two-flavor Lattice QCD. *Phys. Lett.*, B686:36–40, 2010.
- [218] Guray Erkol, Makoto Oka, and Toru T. Takahashi. Pseudoscalar-meson–octet-baryon coupling constants in two-flavor lattice QCD. *Phys. Rev.*, D79:074509, 2009.
- [219] Huey-Wen Lin and Kostas Orginos. Strange Baryon Electromagnetic Form Factors and SU(3) Flavor Symmetry Breaking. *Phys. Rev.*, D79:074507, 2009.

Resumen castellano

La fenomenología de bariones es un campo de gran interés. Experimentos de producción de extrañeza están recogiendo datos actualmente en el GSI, LNF y TJNAF, hay nuevos experimentos proyectados en el CERN-SPS (NA-62) y GSI (haz de piones), y nuevos laboratorios estarán pronto a disponibles en J-PARC y LNF (DAPHNE2). Además, en los últimos años se ha presenciado un impresionante progreso en la descripción de muchos observables usando cromodinámica cuántica en el retículo (LQCD)¹ y resultados realistas en estructura de bariones están comenzando a aparecer. La teoría quiral de perturbaciones (χ PT) para bariones en su versión con tres sabores, $SU(3)_F$ -B χ PT, siendo la teoría efectiva de la cromodinámica cuántica (QCD) que describe las interacciones de baja energía entre mesones pseudo-escalares y bariones, es el marco adecuado para analizar, de manera independiente de modelo, los datos experimentales así como los resultados de LQCD. Sin embargo, este campo se ha desarrollado muy poco debido a problemas conceptuales como aquellos debidos a las sutilezas del conteo quiral en presencia de campos de materia pesados (bariones) o los ocasionados por las presencia de las resonancias bariónicas.

El tema central de esta tesis doctoral ha sido analizar estos problemas y desarrollar un esquema de $SU(3)_F$ -B χ PT renormalizado dimensionalmente que dé una descripción exitosa de diversos observables bariónicos al tiempo que presente una convergencia razonable de las series quirales. Este formalismo ha sido desarrollado hasta unos niveles de precisión más allá de la contribución dominante (NLO y NNLO) y se basa en las siguientes observaciones.

- Los cálculos son realizados usando un Lagrangiano quiral que es explícitamente covariante Lorentz. La regla de conteo descrita en la Eq. (1.35), que es válida para el esquema denominado barión pesado (HB), está rota a órdenes inferiores por términos que son analíticos, esto es, por términos que tienen la misma estructura que el Lagrangiano quiral hasta el orden

¹A lo largo de este resumen usamos los acrónimos ingleses que son los utilizados a lo largo de la presente tesis doctoral.

considerado. Por otro lado, la formulación covariante provee el resultado HB de una torre de correcciones relativistas (analíticas y no analíticas).

- Recuperamos el contaje definiendo una extensión del esquema de renormalización dimensional \overline{MS} por el cual los términos que lo rompen *por debajo* son sistemáticamente absorbidos en un conjunto finito de constantes de baja energía (LECs); esto es, por medio del esquema de renormalización denominado esquema en la capa másica extendido (EOMS).
- El efecto de las resonancias bariónicas del decuplete son incorporadas explícitamente como el correspondiente multiplete de sabor compuesto por campos de espín 3/2 descritos por un Lagrangiano covariante de Rarita-Schwinger. El problema de los grados de libertad no físicos de espín 1/2 contenidos en la representación vectorial-espinorial de los campos 3/2 es tratada al límite de los posible por medio de interacciones consistentes, esto es, aquellas verificando la Eq. (1.42). El vértice electromagnético que acopla un fotón a un campo 3/2 virtual es un ejemplo de interacción que todavía no se sabe hacer consistente al tiempo que invariante gauge local.
- La diferencia de masa entre el decuplete y el octete $\delta = M_T - M_B$ es incorporado de manera no perturbativa. Es decir, no asignamos ningún orden en el contaje para δ en comparación con la masa de los mesones pseudo-escalares m_ϕ y aplicamos la fórmula de la Eq. (1.35) donde el propagador del campo 3/2 cuenta como aquellos del octete bariónico. Los nuevos diagramas de lazo que aparecen con la inclusión del decuplete también rompen el contaje por debajo y los términos correspondientes son de nuevo absorbidos en las LECs en una extensión sobre el EOMS convencional.
- La inclusión de las resonancias del decuplete puede producir una falta de correlación entre la potencia de divergencia y el contaje en los diagramas de lazo. Esto es, debido a la dependencia en momentos del propagador del campo de espín 3/2 en la Eq. (1.43) aparecen divergencias ultravioletas de orden quiral superior al asignado por la fórmula de la Eq. (1.35). Regularizamos esos infinitos en los contra-términos adecuados. Sin embargo, no promocionamos los correspondientes LECs sino que estudiamos la dependencia en escala de renormalización residual que, por otro lado, nos proporciona una estimación de las incertidumbres ocasionadas por el truncamiento de la expansión quiral.
- En todos los casos estudiados en esta tesis, hemos recuperado los resultados HB desde los covariantes cuando la expansión en potencias de $1/M_{B0}$

ha sido empleada. En particular, en los diagramas de lazo con bariones del octete y del decuplete, obtenemos las fórmulas en el llamado SSE o expansión en la pequeña escala ($\delta \sim m_\phi$).

- Hemos comprobado que las contribuciones renormalizadas del decuplete a las propiedades de los bariones del octete desaparecen en el límite en el que $\delta \rightarrow \infty$. Esto es consistente con la expectativa de que las contribuciones originadas por los estados de masa mayor deben ser irrelevantes para las escalas en las que estamos trabajando.

Hemos escogido los momentos magnéticos del octete bariónico como propiedad básica en la que comparar los distintos esquemas $SU(3)_F$ -B χ PT al sector bariónico y para explorar sus diferencias. Históricamente, $SU(3)_F$ -B χ PT ha encontrado grandes dificultades para mejorar de manera independiente de modelo la descripción $SU(3)_F$ simétrica de Coleman y Glashow (CG). De hecho, solo en el novedoso marco covariante en el que se usa el esquema EOMS somos capaces de mejorar CG a NLO. La comparación con los resultados HB resalta la importancia de las correcciones relativistas, esto es, en la formulación covariante importantes cancelaciones tienen lugar entre distintos términos de la expansión no relativista. Estas cancelaciones son incluso más dramáticas en el caso de las contribuciones del decuplete. La comparación con el llamado esquema de renormalización infrarrojo (IR) nos previene de los efectos que los cortes no físicos pueden tener en cuanto se trabaja con mesones tan pesados como el kaón o la eta. En este sentido, mantener las propiedades analíticas correctas de las contribuciones de lazo puede ser crítico para obtener una buena convergencia de las series quirales en $SU(3)_F$ -B χ PT.

Aparte de esto, la inclusión de las contribuciones del decuplete nos da la oportunidad de comparar las diferentes soluciones propuestas para resolver el problema de los grados de libertad no físicos contenidos en la representación relativista de los campos $3/2$. En particular, comparamos el método de exigir a los vértices de interacción que sean consistentes en el sentido de la Eq. (1.42) con aquel basado en el parámetro fuera de capa másica z que es fijado por medio del análisis de las ligaduras usando el formalismo Hamiltoniano de Dirac. Estos dos esquemas son equivalentes salvo por las contribuciones de un conjunto de Lagrangianos quirales que representan aquellas dadas por los grados de libertad no físicos de espín $1/2$. A pesar de que esas contribuciones son formalmente de orden superior, son numéricamente importantes. En otras palabras, solo con las interacciones consistentes las correcciones de rotura $SU(3)_F$ proporcionadas por el decuplete bariónico son pequeñas y conducen a una mejora de los momentos magnéticos del octete bariónico a NLO.

El análisis de los momentos magnéticos del octete bariónico proyecta una imagen bastante sorprendente de la expansión quiral de las propiedades de los

bariones. Desde la filosofía propia de las teorías efectivas es difícil entender como contribuciones que son formalmente de orden superior, como aquellas proporcionadas por las correcciones relativistas a las fórmulas HB ($\Lambda_{\chi SB} \sim M_{B0}$) o esas otras dadas por los grados de libertad no físicos de los campos $3/2$, puede tener un impacto tan grande en la descripción de observables. Que esto sea así indudablemente se debe al hecho de que las series quirales con mesones pseudo-escalares pesados o en presencia de los efectos no perturbativos encarnados por las resonancias bariónicas se encuentran, en el mejor de los casos, en el límite del radio de convergencia. El descubrimiento más prominente de nuestro análisis es que una buena convergencia puede obtenerse reordenando las series quirales de manera que principios generales como invarianza Lorentz y analiticidad, o conservar los grados de libertad físicos, sean verificados. Dado el incremento vertiginoso en el número de LECs a órdenes superiores (del orden de 30 para el caso de los momentos magnéticos y masas del octete bariónicos a NNLO), esquemas con una convergencia mejorada son esenciales para preservar la capacidad predictiva de $SU(3)_F$ - $B\chi$ PT.

Hemos extendido este formalismo para estudiar la estructura electromagnética estática del decuplete bariónico. Muy poco es sabido acerca de las mismas, aunque aquellas de la $\Delta(1232)$ son el objeto de un esfuerzo experimental en MAMI al tiempo que de un intensa campaña de investigación teórica como la llevada a cabo en el retículo. La potencia predictiva de la formulación con tres sabores de $B\chi$ PT ha sido ilustrada en este caso. Así, los momentos dipolar magnéticos (MDM) del decuplete, y en particular de la $\Delta(1232)$, han sido determinados fijando la única LEC que aparece hasta este orden con el MDM de la Ω^- que ha sido medido con precisión. Nuestros resultados, $\mu_{\Delta}^{++} = 6.0(1.0) \mu_N$ and $\mu_{\Delta}^+ = 2.84(20) \mu_N$ están perfectamente de acuerdo con los valores centrales del PDG al tiempo que con las mediciones realizadas en los experimentos más recientes. Más aún, la comparación entre los esquemas covariante y HB confirma las conclusiones del párrafo anterior. Los momentos cuadrupolar eléctrico (EQM), octupolar magnético (MOM) y el radio de carga (CR) han sido predichos a partir del más reciente resultado en el retículo para la Ω^- , que es el barión para el que creemos que es más probable obtener información independiente de modelo bien sea en un experimento o en una simulación completamente dinámica en el retículo. Los EQM y MOM están dominados por las contribuciones de lazo mientras que en el caso de los radios de carga los diagramas de árbol dominan por mucho, lo que puede indicar la importancia de las resonancias mesónicas para este último caso.

La $SU(3)_F$ - $B\chi$ PT aplicada a la fenomenología bariónica puede ser empleada para obtener los valores de los parámetros del modelo estándar (SM). De manera equivalente al caso de kaones, el elemento de la matriz de Cabibbo-

Kobayashi-Maskawa (CKM) V_{us} es extraído de los datos de desintegraciones semilépticas de hiperones una vez que los elementos de matriz hadrónicos, y en particular el acoplamiento vectorial $f_1(0)$, son determinados. El valor obtenido puede ser entonces empleado conjuntamente al valor de V_{ud} obtenido por medio de desintegraciones nucleares β super-permitidas para probar el SM a través de la relación de unitariedad de la primera fila de la CKM, Eq. (3.1), donde el elemento V_{ub} es despreciable con la presente precisión. Nosotros aquí hemos presentado un cálculo del elemento de matriz $f_1(0)$ hasta una precisión NNLO. En contraste con cualquiera de las otras propiedades estudiadas en la tesis, las correcciones finales de rotura de $SU(3)_F$ al $f_1(0)$ en el formalismo covariante y aquellas en HB son bastante similares y marginalmente consistentes. Esto puede deberse al hecho de que contribuciones de contra-términos no aparecen en la expansión quirál de $f_1(0)$ hasta NNNLO. Una observación similar sigue de la comparación entre las contribuciones del octete en el esquema IR y EOMS (Tabla 3.1). Como resultado del cálculo, un valor preciso de V_{us} puede ser obtenido desde los datos de desintegración semileptónicas que incluyen incertidumbres tanto experimentales como teóricas. El hecho de que en las desintegraciones de hiperones podamos combinar la determinación en diversos canales es el origen de esa precisión tan alta en nuestra determinación. En cualquier caso, también hemos prevenido de que las contribuciones a V_{us} tan importantes como las proporcionadas por la rotura $SU(3)_F$ a $f_1(0)$ pueden ser originadas también por las correspondientes correcciones a $g_2(0)$.

Para terminar, hemos analizado los recientes y célebres resultados en el retículo del espectro bariónico, en particular los de las colaboraciones PACS-CS y LHP. En dramático contraste con las extrapolaciones realizadas con HB, hemos encontrado que una descripción muy buena de la dependencia tanto en la masa ligera como extraña de los quarks puede ser obtenida de manera simultánea para el octete y el decuplete usando la formulación covariante de B χ PT. Más concretamente, los resultados en el retículo son muy bien descritos para masas de quark correspondiendo a piones y kaones ambos por debajo de los 600 MeV y la extrapolación es mejorada respecto a la obtenida a orden dominante por el modelo de Gell-Mann-Okubo (GMO). La comparación entre los resultados covariantes y aquellos de HB indica que importantes cancelaciones numéricas se producen entre distintos términos de la expansión no relativista en cuanto se parte del punto físico. Por otro lado, la comparación con los resultados GMO, que son lineales en la masa de los quarks, resalta la importancia de los términos no analíticos quirales para la extrapolación desde masas tan bajas como la empleadas por la colaboración PACS-CS ($m_\pi \simeq 156$ MeV la más ligera). Estos resultados en las masas bariónicas pueden ser el anticipo de las importantes aplicaciones que una combinación sólida de LQCD

y $B\chi$ PT pueden tener en el futuro. En la tesis hemos enfatizado esto con la predicción de los llamados términos sigma de los bariones y, en particular, del nucleón. En efecto, una determinación independiente de modelo de estas magnitudes, que proveen información acerca de la estructura de los bariones, se han convertido en una pieza de información esencial para las búsquedas de materia oscura supersimétrica.

En resumen, los bariones son una ventana a QCD no perturbativa o a física más allá del SM. Más aún, el conocimiento de su estructura o de sus interacciones, además de proveernos información acerca de los nucleones o propiedades nucleares, son esenciales para estudiar materia extraña y sus aplicaciones en física de hipernúcleos o astronuclear. El esquema de $B\chi$ PT que hemos desarrollado en esta tesis ha probado ser un formalismo idóneo para interpretar y procesar la información en estructura bariónica que irá apareciendo tanto de laboratorios como de cálculos en el retículo.

Acknowledgments

Hay muchas personas a las que debo el poder llevar a buen término esta tesis doctoral. De manera especial, quiero agradecer a mis padres su sacrificio y continuo apoyo, sin los que nunca hubiera tenido esta oportunidad de dedicarme al trabajo que siempre he deseado tener. Extiendo este reconocimiento a mi hermano, cuya camaradería durante estos años ha sido extremadamente valiosa y enriquecedora. A ustedes va dedicada esta tesis.

Durante el transcurso de mi doctorado me he ido sintiendo atraído cada vez más por las aproximaciones más formales a la fenomenología de bariones. Debo a Manolo el que haya ido canalizando ese interés hacia asuntos cada vez más sugestivos y problemáticos cuya discusión componen el tema central de los resultados y métodos presentados en esta tesis. Deseo resaltar aquí su paciencia, generosidad y sabiduría, todas ellas cualidades que, además de ayudar a formarme como científico, me han hecho crecer como persona. Quiero también agradecer a Eulogio su apoyo y generosidad. Su enorme intuición física, vitalidad y gran carrera científica son un ejemplo para todos. Extiendo este agradecimiento a Juan Nieves, que me ha ayudado desde que se incorporó al grupo y cuyos consejos han sido y son muy valiosos. No me olvido de mis compañeros de doctorado Michael, Nacho y Raquel con los que he compartido despacho en la más absoluta de las armonías. También agradezco a Alberto, Javi, Luis Roca, Daniel Cabrera, Kanchan, Kenji, Murat, Sourav, Junko y Jujun su compañerismo a lo largo de estos años.

I would like to express my gratitude to my collaborators L. Alvarez-Ruso, J. M. Alarcón, T. Ledwig, J.A. Oller, V. Pascalutsa and M. Vanderhaeghen from whom I have learned many things. I reserve a special mention to Lisheng Geng with whom it has been a great luck and pleasure to collaborate. The content of this thesis has also benefited from conversations with J. Gegelia, S. Scherer, R. Young, V. Lensky, J. R. Peláez, T. Hemmert, M. Procura, T. Gail and S. Sasaki. Finally, I would like to thank N. Kaiser, W. Weise, M. Vanderhaeghen, M. Oka, J. Negele, I. Stewart and R. Young for hosting me in their Groups for relatively long stays.

Un periodo de doctorado no se puede reducir exclusivamente al trabajo. En

efecto, durante estos años he forjado un buen número de grandes amistades que espero perduren en el tiempo. Deseo resaltar aquí las de mi *Band of Brothers*, los compañeros de la *patrulla S*, Dani, Vido, Fabio, Diego, Negro, Martín, Clarilla, Esther, Conrat y muchos otros que se han ido uniendo a nuestro irresistible modo de vida. Con ustedes he disfrutado de viajes, conciertos, legendarias fiestas, sesiones de cine (raro), partidas memorables y un largo etc., que han hecho que, a final de cuentas, éstos hayan sido algunos de los mejores años de mi vida. De ello son también responsables mis camaradas *samurais*. ¡Ha sido y seguirá siendo un placer practicar con ustedes!

Quiero reservar este último párrafo de la tesis para agradecer a L.F. que se haya cruzado en mi camino en un momento crucial, tanto en el plano personal como en el profesional, pues se ha convertido en un baluarte fundamental por su apoyo incondicional, cariño y comprensión.

A todos, gracias.